ABSTRACT

Title of Dissertation:	REACTIVATION OF PLASTICITY IN THE ADULT VISUAL CORTEX BY CONTROL OF NEURONAL EXCITABILITY
Dissertation directed by:	Andrew Borrell, Doctor of Philosophy, 2018 Dr. Elizabeth Quinlan, Professor, Department of Biology, Neuroscience and Cognitive Science Program

Amblyopia is a highly prevalent form of monocular vision loss that impacts between 1-4% of the worldwide population. Amblyopia is characterized by decreased visual acuity in a single eye and is highly refractory to treatment past a “critical period” of heightened plasticity during early adolescence (>5 years of age). The time course of this critical period is due to the developmental regulation of experience-dependent synaptic plasticity in the primary visual cortex (V1). During early development, visual experience drives activity-dependent changes in NMDA-R subunit composition, refines the convergence of binocular inputs, and promotes the maturation of inhibitory circuits in V1. The transient conditions in V1 that permit the refinement of cortical circuits during the critical period also render V1 vulnerable to the detrimental impacts of amblyopia.

The expression of critical period plasticity requires visual experience: dark-rearing delays the onset and closure of the critical period and prevents the experience-

dependent change in NMDA-R subunit composition. It is now understood that visual experience in adulthood is also important for the expression of plasticity: sensory deprivation via prolonged dark exposure (DE) rejuvenates the V1 circuit to a juvenile-like state via a homeostatic increase in spontaneous excitatory in V1. Subsequent visual experience during light reintroduction (LRx) enables the expression of critical period plasticity and the functional rewiring of thalamocortical inputs to V1.

Here I asked how the homeostatic increase in spontaneous activity induced during DE is regulated by visual experience immediately following LRx (LRx_i), and during one day of subsequent day of LRx (LRx_s). I demonstrate that the homeostatic increases in spontaneous excitatory neuron activity is maintained during LRx_i and is accompanied by increased evoked excitatory neuron activity. These increases in averaged spontaneous and evoked activity returned to baseline by LRx_s. Next, I asked whether decreased spontaneous activity following one day of LRx was necessary for the reactivation of critical period plasticity. Using the mouse model of ocular dominance plasticity (ODP) and cell-type specific expression of inhibitory chemogenetic Gi-DREADD receptors in fast spiking Parvalbumin-expressing interneurons, I demonstrated that prolonged disinhibition of spontaneous V1 activity during LRx occludes the reactivation of ODP, but not the reactivation of the plasticity of acuity. These results demonstrate the differing contribution of cortical mechanisms to ocular dominance versus acuity in the regulation of the critical period plasticity, and the necessity of the decrease in average spontaneous activity for the re-expression ODP.

REACTIVATION OF PLASTICITY IN THE ADULT VISUAL CORTEX BY CONTROL OF NEURONAL EXCITABILITY

By:

Andrew Borrell

Dissertation submitted to the Faculty of the Graduate School of
the University of Maryland, College Park, in partial fulfillment
of the requirements for the degree of
Doctor of Philosophy
2023

Advisory Committee:
Dr. Elizabeth Quinlan, Chair
Dr. Jens Herberholz, Dean’s Representative
Dr. Ricardo Araneda
Dr. Melissa Caras
Dr. Quentin Gaudry

Dedication

I am truly thankful to all the people who helped and supported me over the years it took to finish this PhD. First and foremost, I must thank my advisor, Dr. Elizabeth Quinlan: her mentorship and her knowledge were crucial to my overall success. In addition to the normal responsibilities as a PhD advisor, she also helped keep me and the rest of the lab going during an unprecedented worldwide pandemic. To the members of the Quinlan Lab, I especially need to thank Dr. Crystal Lantz, who trained me the electrophysiology techniques I used in this work, as well as Dr. Clare Sengupta and Dr. Sachiko Murase, both of whom helped me with immunohistochemistry. To them and the other members of the Quinlan Lab, past and present, it did really feel like we were a little family. To my wife, Dr. Lauren Borrell, whom I met in the NACS program: thank you for calling “dibs”, and for loving and believing in me. I forgive you for taking my last name and becoming “Dr. Borrell” before me! To my friends from the NACS program: thank you all for the sense of community you provided, and for the many years of friendship still to come. You introduced me to my wife, and many of you were either at my wedding or in my wedding party! To my parents, John and Loretta Borrell, thank you for nurturing my curiosity as a strange bug-obsessed child, and for the boundless support and love you provided for me and my four siblings. To those siblings, Joey, Billy, Becky, and Johnny: thank you in advance for automatically conceding defeat in all future arguments due to my advanced degree. I know it will be hard for you. Lastly, to my dog Fitz E. Girlfriend. Thankyou for always giving me an excuse to take walks during the day, for protecting me from squirrels, and for being a constant source of joy in my life!

Table of Contents

List of Tables

List of Figures

List of Abbreviations

A1	primary auditory cortex
AC	adenylyl cyclase
AMPA	Alpha-amino-3-hydroxy-5-methyl-4-isoxazolepropionic acid
AMPA-R	AMPA receptor
BDNF	brain-derived neurotrophic factor
β-NRXN-1	beta neurexin-1
CNO	clozapine-N-oxide
contra	contralateral
CP	critical period
cre	cre recombinase
CSD	current source density map
DE	dark exposure
DREADD	designer receptors activated only by designer drugs
E/I balance	excitatory / inhibitory balance
EPSC	excitatory postsynaptic currents
ErbB4	Erb - B2 receptor tyrosine kinase 4
ERG	electro retinogram responses
FRET	fluorescence resonance energy transfer
FS	fast spiking
GABA	γ-amino-butyric acid
$GABA_A$-R	GABA receptor type A

$GABA_B$-R	GABA receptor type B
GAD65	glutamic acid decarboxylase 65
GCaMP6	green fluorescent protein-coupled calmodulin variant 6
Gi	hM4D-(Gi)-mCherry-expressing
Gi-DREADD	Gi-coupled DREADD receptor
GIRK	G-protein gated inward rectifying potassium channel
GluA1	AMPA receptor subunit type A1
GluA2	AMPA receptor subunit type A2
GluA4	AMPA receptor subunit type A4
GluN2A	NMDA receptor subunit type 2A
GluN2B	NMDA receptor subunit type 2B
HNK	(2R, 6R)-hydroxynorketamine
i.p.	intraperitoneal
IN	inhibitory interneuron
IPSC	inhibitory post synaptic currents
ipsi	ipsilateral
L2/3	Layer 2/4
L4	Layer 4
L5/6	Layer 5/6
L5/6	Layer 5/6
L6	layer 6
LFP	local field potential
LGN	lateral geniculate nucleus

LOT	lateral olfactory tract
LRx	light reintroduction
LTD	long-term depression
LTP	long-term potentiation
MD	monocular deprivation
mEPSC	miniature excitatory post synaptic current
mGluR	metabotropic glutamate receptor
MMP-9	matrix metallo-peptidase 9
NARP	neuronal-activity-regulated pentraxin
NMDA-R	N-methyl-D-aspartate receptor
NP1	neuronal pentraxin-1
NPR	neuronal pentraxin receptor
NRG1	neuregulin-1
OD	ocular dominance
ODI	ocular dominance index
ODP	ocular dominance plasticity
P28	post-natal day 28
PLC-β	phospholipase-C-beta
PTPσ	Receptor-type tyrosine-protein phosphatase sigma
PV-IN	parvalbumin-expressing inhibitory interneuron
PYR	pyramidal neuron
RS	regular spiking
s.c.	subcutaneous

S1	primary somatosensory cortex
SRP	stimulus selective response potentiation
SSRI	selective serotonin reuptake inhibitor
SST-IN	somatostatin-expressing inhibitory interneuron
STDP	spike timing-dependent plasticity
SU	single unit
TC	thalamocortical
TrkB	tropomyosin receptor kinase B
TTX	tetrodotoxin
V1	primary visual cortex
V1b	binocular primary visual cortex
VEP	visually evoked potential

Chapter 1: Introduction

1.1 Amblyopia: Impacts and Causes

Amblyopia is a form of monocular vision loss that impacts between 1-4% of the worldwide population(Hu et al. 2022). Amblyopia is characterized by decreased visual acuity in a single eye, causing a loss of depth perception, and is associated with a host of ancillary problems including employment and education difficulties, increased risk of depression and anxiety. An additional risk in older populations includes serious injury or death(Packwood et al. 1999; Rahi et al. 2002; Gunton 2013). Any monocular impairment that causes a disparity of visual quality between the eyes during early adolescence, such as a congenital cataract, strabismus (ocular misalignment) or anisometropia (unequal refractive index between the eyes) can cause amblyopia(Attebo et al. 1998; Gunton 2013). While such visual impairments can be treated with relative ease using modern medical techniques, amblyopia itself becomes increasingly refractory to treatment with age past adolescence (i.e., >5 years of age) (Holmes and Clarke 2006; Holmes et al. 2011; Gunton 2013). This difficulty in treating amblyopia arises from its true etiology: the developmentally-regulated, visual experience-dependent specification of connectivity between neurons in the visual pathway, including the primary visual cortex which are robust during the critical period and decline with age (Hou, Pettet, and Norcia 2014; D. H. Hubel and Wiesel 1964; Cynader and Mitchel 1983; von Noorden 1973). A better understanding of the neural mechanisms underlying the expression of critical period plasticity will inform more effective treatments for amblyopia in the future.

1.2 Experience-dependent synaptic plasticity

Adaptability is often thought of in terms of complex behaviors, but it also applies to the individualized calibration of the nervous system to sensory inputs. While certain aspects of brain circuitry are determined genetically, many patterns of synaptic connectivity become established through a heuristic, experience-dependent process first described by Donald Hebb (Magee and Grienberger 2020; Hensch 2005). At the circuit level, Hebbian plasticity functions by modifying the synaptic strength between coupled neurons based on patterns of pre-and postsynaptic activation; the magnitude and sign of this change depending on the relative timing of activation: when presynaptic input precedes postsynaptic spiking, the synapse strengthens; conversely, when postsynaptic spiking precedes presynaptic input, the synapse weakens(Bi and Poo 1998).

Three major types of ionotropic neurotransmitter receptors are involved in the induction and expression of Hebbian plasticity. The first two are excitatory glutamate-activated receptors: AMPA receptors (α-amino-3-hydroxy-5-methyl-4-isoxazolepropionic acid; AMPA-Rs) and NMDA receptors (N-methyl-D-aspartate; NMDA-Rs)(Durand, Kovalchuk, and Konnerth 1996; J. M. Williams et al. 2007). AMPA-Rs are tetrameric receptors composed of four subunits, and their subunit composition determines their function in the synapse; in their most abundant form (i.e., GluA2-containing isoform), AMPA-Rs are calcium impermeable ligand-gated sodium channels that mediate fast (decay time constant [τ] ~ 5 ms) excitatory postsynaptic currents (EPSCs) when activated by glutamate(Hansen et al. 2021). AMPA-Rs are responsible for most fast excitatory neurotransmission in the brain, and are critical for most neural circuits(J. D.

Shepherd and Huganir 2007). In contrast, the activation of NMDA-Rs is more complicated, requiring the binding of two ligands, glutamate and D-serine, as well as simultaneous neuronal depolarization to remove an internal magnesium which blocks the flow of ions through the NMDA-R channel. When all three conditions are met, NMDA-Rs become permeable to both sodium and calcium ions and depolarize the postsynaptic membrane(Hansen et al. 2021). NMDA-R-mediated currents are slower than AMPA-R-mediated currents (τ = 30 – 150 ms), allowing NMDA-Rs to function as both coincidence detectors, with the presence of prior depolarization acting as an indicator of ongoing neural activation, and as a critical route for extracellular calcium to enter the synapse(Markram et al. 1997; MacDermott et al. 1986; Monyer et al. 1994; Hansen et al. 2021). The third receptor is the inhibitory $GABA_A$ receptor ($GABA_A$-Rs): when activated by GABA (γ-amino-butyric acid), $GABA_A$-Rs mediate fast (τ = 5 - 9 ms), hyperpolarizing chloride currents, i.e. inhibitory post synaptic currents (IPSCs)(Ghit et al. 2021; Dixon et al. 2014). Neural inhibition can modulates the expression of Hebbian plasticity by controlling the gain and temporal precision in the spiking output of synaptically connected pyramidal neurons (Hensch and Quinlan 2018; Mitchell and Silver 2003; F Pouille and Scanziani 2001).

The interaction between AMPA-Rs and NMDA-Rs is a fundamental driving force behind Hebbian plasticity. High frequency stimulation of excitatory AMPA-R induces depolarization of the post-synaptic membrane, and subsequent activation of NMDA-Rs. Calcium influx through NMDA-Rs triggers long-term potentiation (LTP) of EPSCs by increasing the number of functional AMPA-Rs in the excitatory postsynaptic density (Hayashi et al. 2000; MacDermott et al. 1986; Bröcher, Artola, and Singer 1992;

Anggono and Huganir 2012). Conversely, low frequency stimulation of excitatory synapses induces NMDA-R and calcium-dependent AMPA-R endocytosis leading to long term depression (LTD) of EPSCs (Cummings et al. 1996; Nabavi et al. 2013; J. D. Shepherd and Huganir 2007).

The induction of Hebbian LTP/LTD can be modulated somatic feed-forward inhibition, which regulates the duration of the temporal window for integration, and by the subunit composition of NMDA-Rs, which regulates the activity threshold for the conversation of LTD to LTP (Frederic Pouille and Scanziani 2001; W. S. Chen and Bear 2007). The expression, sign and magnitude of NMDA-R dependent Hebbian plasticity can also be modified by other factors including cholinergic and adrenergic neuromodulation as well as activation of metabotropic glutamate and GABA receptors (mGluRs and $GABA_B$-Rs, respectively) in a cell-type, input, and cortical layer specific manner(Hong et al. 2019; L. Wang and Maffei 2014; Chokshi et al. 2019; Goel and Lee 2007).

1.3 Critical period plasticity characteristics, onset, and closure

The onset and duration of the critical period (CP) for ocular dominance is evolutionarily conserved and proportional to lifespan, with longer lived species exhibiting later occurring and longer CPs during which amblyopia may be induced(Berardi, Pizzorusso, and Maffei 2000). The existence of CPs is thought to allow the brain to calibrate and optimize sensory input based on individual anatomical and physiological needs (e.g., eye-spacing, neural circuit properties)(Hensch and Quinlan 2018; B.-S. Wang, Sarnaik, and Cang 2010; Prinz, Bucher, and Marder 2004). Prior to the onset of

the CP, spontaneous retinal activity (i.e., retinal waves) and a transient population of "subplate" neurons guide thalamic axons to the primary visual cortex (V1), which begin to segregate and/or converge based on ocular origin(Feller and Scanziani 2005). During this pre-CP period, excitatory pyramidal neurons (PYRs) in V1 are non-selectively activated by neighboring inputs and exhibit weak stimulus selectivity(Kuhlman, Tring, and Trachtenberg 2011; Michela Fagiolini et al. 2003; Li, Fitzpatrick, and White 2006). At the onset of the CP, the dominant isoform of NMDA-R expressed at excitatory synapses onto pyramidal neurons in the primary visual cortex contain the subunit GluN2B; these GluN2B-containing NMDA-Rs mediate ESPCs with slower decay kinetics (τ > 100 ms), providing a longer temporal window for coincidence detection via EPSC overlap(Monyer et al. 1994). Additionally, inhibitory circuitry is immature, GABA release is prone to depletion, and the number of post-synaptic $GABA_A$-Rs is comparatively low, resulting in pyramidal neuron hyper- excitability(Jiang et al. 2010; S. Huang et al. 2010). During the CP, clustered synaptic inputs sharing receptive fields and tuning properties have a high probability of coactivation, binocularly-matched tuning properties develop, acuity increases, and normal patterns of ocular dominance are strengthened (Niell and Stryker 2008; Kuhlman, Tring, and Trachtenberg 2011; Michela Fagiolini et al. 2003; Li, Fitzpatrick, and White 2006; D. Hubel and Wiesel 1959; Berardi, Pizzorusso, and Maffei 2000; Wilson et al. 2016; Iacaruso, Gasler, and Hofer 2017; B.-S. Wang, Sarnaik, and Cang 2010). As the CP progresses, visual experience drives the activity-dependent switch to GluN2A-continaing NMDA-Rs, which exhibit faster decay kinetics, thus the temporal window for coincidence detection shrinks(W. S. Chen and Bear 2007). The concomitant activity-dependent maturation of somatic inhibition

decreases excitatory neurons spiking to adult levels, shrinks the window for temporal summation of excitatory inputs, thereby resulting in the termination of the CP (Z. J. Huang et al. 1999; Frederic Pouille and Scanziani 2001).

1.4 Inhibitory gating of critical period plasticity

Changes in inhibitory circuits are proposed to both initiate and terminate the CP for ODP (Fig.1) (Hensch and Quinlan 2018). Genetic knockdown of the synaptic GABA-synthesizing enzyme GAD65 prevents the normal expression of ocular dominance plasticity (ODP, a form of CP plasticity) in response to brief MD, but does not prevent the expression of other forms of Hebbian plasticity in mice, such as rate based LTP and LTD induction paradigms (Theta burst and low frequency stimulation, respectively), nor ODP induced by monocular tetrodotoxin (TTX) injection(Hensch et al. 1998). Interestingly, GAD65-deficent mice can express rapid ocular dominance plasticity following the elevation of inhibition above a hypothetical “inhibitory threshold” following reduction of pyramidal neuron excitability with diazepam (M Fagiolini and Hensch 2000). Similar to higher mammals, dark-rearing wildtype mice retains the visual system in a perpetual pre-CP state which is characterized by retention of GluN2B containing NMDARs and hyper-excitable pyramidal neurons. Diazepam treatment in the dark leads to a precocious closure of the CP prior to visual experience (Iwai et al. 2003). Interestingly, diazepam is a positive allosteric modulator of ionotropic, α1 subunit-containing $GABA_A$-Rs, and the presence and number of these receptors on the soma of PYRs is correlated with the expression of ODP, highlighting the specific role of somatic inhibition in the time course of the CP(Katagiri, Fagiolini, and Hensch 2007).

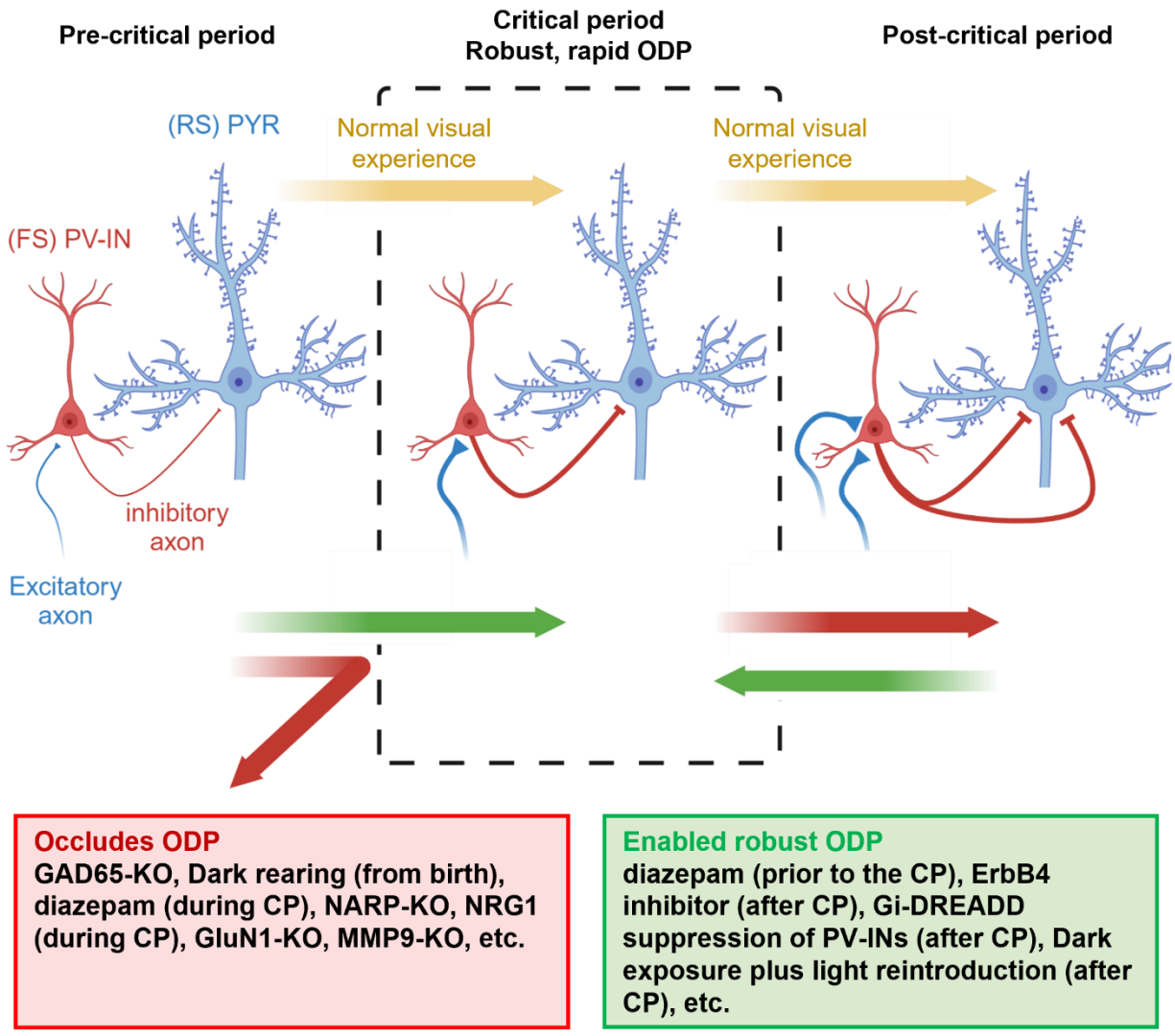

Figure 1: Inhibitory gating of critical period plasticity

Schematic diagram illustrating neural inhibitory control of ocular dominance plasticity (ODP). **(Left).** Prior to the CP, neural inhibitory output is low, as is excitatory recruitment of inhibitory interneurons, particularly fast spiking (FS) parvalbumin-expressing interneurons (PV-INs, red). Regular spiking (RS) pyramidal neurons (PYRs, blue) are therefore hyperexcitable and unable to express ODP. **(Middle)** Visual experience during normal development leads to the activity-dependent maturation of inhibitory circuitry. Cortical excitability reaches an intermediate state during the CP, allowing for the expression of the rapid and robust ocular dominance plasticity characteristic of the CP. Manipulations that prevent visual experience (e.g., dark rearing), the functional maturation of inhibition or inhibitory output (e.g., NARP-KO, GAD65-KO, respectively) prevent V1 from achieving this state of intermediate excitability. Blocking NMDA-R-dependent plasticity also prevents the expression of ODP (e.g., GluN1-KO). **(Right)** Normal visual experience during the CP eventually leads to the full maturation of inhibitory circuitry, closing the CP. Manipulations that hasten the maturation or output of inhibition cause a precocious end to the CP (e.g., NRG1 or diazepam during the CP, respectively). Manipulations that decrease inhibition in post-CP adults reactivate CP-like ODP (e.g., Gi-DREADD suppression of PV-INs, ErbB4 inhibitors, dark exposure followed by light reintroduction*).* (Created with BioRender.com)

The inhibitory interneurons (INs) that mediate the release of GABA are a heterogeneous population classified into subgroups based on morphology, physiology, and the expression of specific genetic markers(Taniguchi 2014; Wu and Sun 2015). Of particular note are fast-spiking, parvalbumin-expressing basket cell (PV-IN**)**(Y. Gu et al. 2016; Yu Gu et al. 2013; S. Huang et al. 2010)**,** which form dense “baskets” of perisomatic synapses targeting the soma of pyramidal neurons (Markram et al. 2004; Taniguchi 2014). Physiologically, PV-INs exhibit a “fast-spiking” phenotype due to their high expression of inwardly-rectifying Kv3.1 potassium channels, which allow for rapid membrane repolarization and high firing rates(Rudy and McBain 2001).

PV-INs receive excitatory synapses from multiple sources including thalamus, local pyramidal neurons, and long-range excitatory inputs(J. Lu et al. 2014). In adult V1, PV-INs receive strong TC inputs across the cortical layers, and most strongly in layer 4 (the canonical thalamo-recipient layer), allowing for rapid feedforward inhibitory responses to sensory input(Ji et al. 2016). In CP-aged mice, PV-INs are highly innervated by local PYRs (within 50 μm), and this dense innervation is developmentally regulated by experience(Severin et al. 2021; Kuhlman, Tring, and Trachtenberg 2011). Longer range connections onto PV-INs exhibit stronger short-term depression than shorter range connections (< 100 μm), allowing for rapid recruitment of PV-INs within local circuits(J. Lu et al. 2014). Additionally, PV-INs are densely interconnected via electrical gap-junction synapses, enabling their synchronous co-activation(Tamás et al. 2000). Neocortical PV-INs form dense perisomatic connections on PYRs in a wide radius (>200 μm radius); these inhibitory connections form with high probability on neighboring PYRs depending on brain region (e.g., 80% in frontal cortex L2/3 versus

40% in somatosensory cortex L2/3) (Packer and Yuste 2011). The strength of these connections can be regulated on a neuron-by-neuron basis via activity-dependent long-term potentiation of inhibition (LTPi), allowing for finer circuit control(L. Wang and Maffei 2014). Lastly, PV-INs are the most populous subgroup of interneurons, accounting for nearly 40% of all neocortical interneurons(Rudy et al. 2011). These traits allow PV-IN networks to rapidly control the spiking output in hundreds of PYRs simultaneously.

The maturation of PV-IN circuitry is experience-dependent and implicated in the initiation and termination of the CP. In V1, genetic knockdown of the AMPA-R binding protein NARP (neuronal-activity-regulated pentraxin, also known as NPTX2) results in hyper-excitable pyramidal neurons that do not express ODP(Yu Gu et al. 2013). Neuronal activity causes excitatory neurons to secrete NARP, which complexes with NP1 and NPR (neuronal pentraxin-1 and neuronal pentraxin receptor, respectively) to anchor and stabilize excitatory synapses onto PV-INs via TARP binding to the third PDZ domain of the excitatory synapse anchoring protein, PSD-95 (post-synaptic density protein 95)(S.-J. Lee et al. 2017; Sia et al. 2007; O'Brien et al. 1999; Ravi et al. 2022) (Fig.2). Strikingly, there are no changes in the number or strength of PV-IN inhibitory synapses onto PYRs in NARP-deficient mice, indicating that it is the strength of excitatory drive onto PV-Ins is an important regulatory locus for the initiation of the CP(Y. Gu et al. 2016). Another activity-dependent protein that regulates PV-IN excitability is BDNF (brain-derived neurotrophic factor); activation of TrkB receptors by BDNF on PV-INs increases the expression of the Kv3.1 channels (giving PV-INs their fast-spiking phenotype) and promotes PV-IN growth(Matsuda et al. 2021). Accelerated expression of BDNF in V1 leads to a precocious development of PV-IN circuitry and an

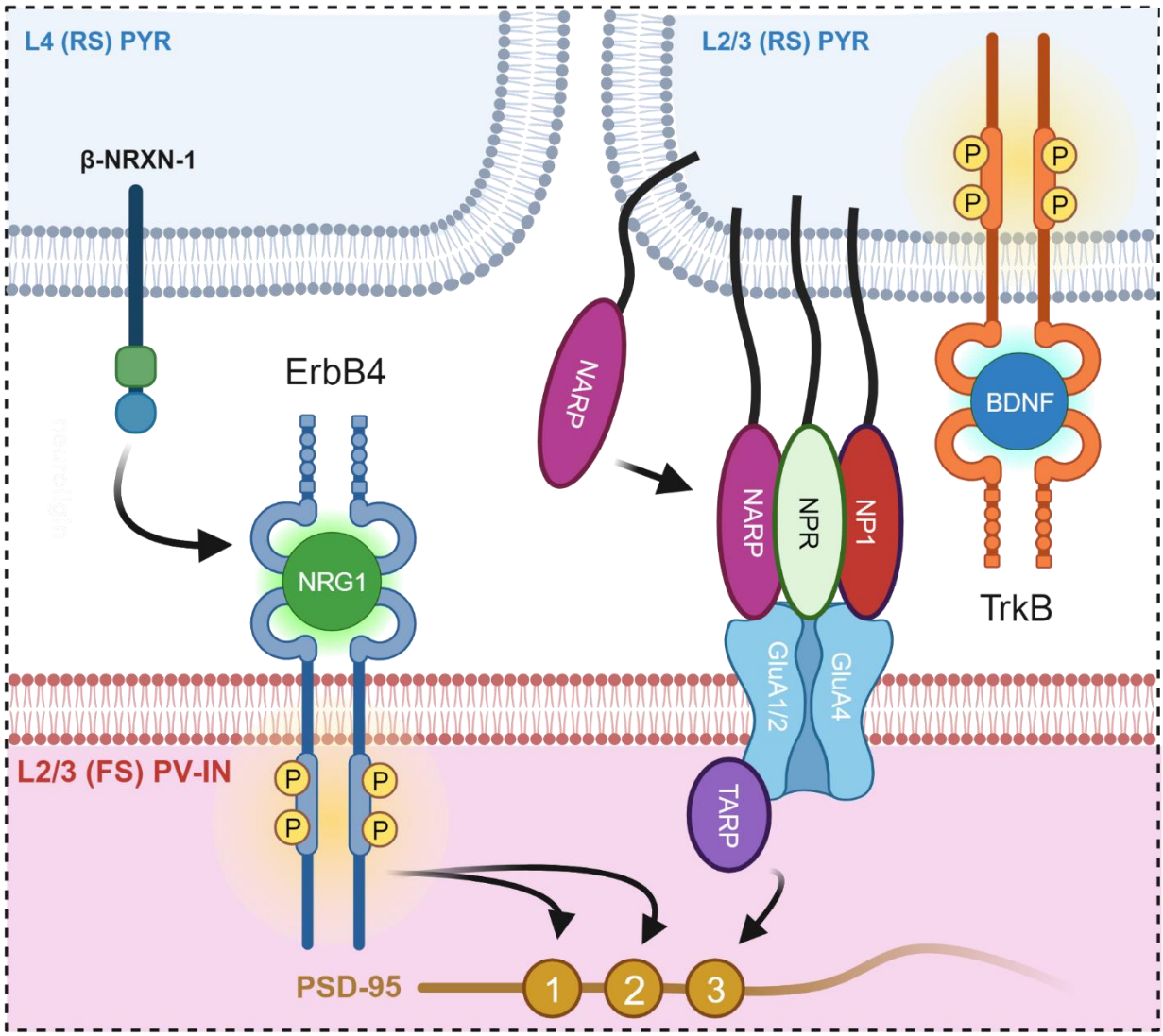

Figure 2: Endogenous activity dependent mechanisms mediating recruitment of excitatory drive onto PV expressing interneurons

Schematic diagram of two important activity-dependent metabolic pathways that enhance excitatory drive onto PV-INs. **(Left)** NRG1 binds to and activates the ErbB4 tyrosine receptor kinase, enhancing excitatory drive onto PV-INs specifically from L4 (RS) PYRs, possibly via direct interaction of presynaptic β-NRXN-1 with post-synaptic ErbB4 and PSD-95 (PDZ domains 1 or 2), thus stabilizing excitatory synapses. **(Right)** Activity-dependent secretion of NARP by pyramidal neurons leads to formation of NARP/NPR/NP1 complexes that stabilize excitatory synapses from L2/3 PYRs onto PV-INs via direct interaction of post-synaptic GluA1/2 / GluA4-containing AMPA-Rs, TARP, and PSD-95 (PDZ domain 3). NARP secretion is directly regulated by activation of TrkB by BDNF in the hippocampus and may similarly mediate the secretion of NARP in V1. (Created with BioRender.com)

accelerated onset and closure of the CP(Z. J. Huang et al. 1999). Interestingly, BDNF has also been shown to upregulate the expression of NARP in the hippocampus(Mariga et al. 2015). It is therefore possible that BDNF and NARP interact directly in the development of visual cortical inhibitory circuits. PV-IN excitability is also regulated by signaling through the ErbB4 tyrosine receptor kinase pathway (Fig.2). ErbB4 is preferentially expressed by PV-INs; genetic labeling studies indicate that the ErbB4 endogenous ligand NRG1 (neuregulin-1) is preferentially expressed by PYRs in Layer 2/3 of the somatosensory and motor cortex, whereas translating ribosome affinity purification in V1 demonstrated preferentially expression on PV-INs(Y. Gu et al. 2016; Ding et al. 2023; Sun et al. 2016). (Fukumoto et al. 2019; Sun et al. 2016). In prefrontal cortex, activation of ErbB4 enhances PV-IN excitability by anchoring and stabilizing presynaptic excitatory synapses to the ErbB4 receptor via direct and long-lasting binding with β-NRXN-1 (β-neurexin 1)(Xu et al. 2022). On the presynaptic side, ErbB4 has been shown to bind to the second and third PDZ domain of the excitatory synapse anchoring protein, PSD-95 (post-synaptic density protein 95) (Garcia, Vasudevan, and Buonanno 2000). Regardless of locus, NRG1 is upregulated by neuronal activity, and its activation of ErbB4 leads to the enhancement of excitatory drive onto PV-INs and influences the expression of ODP. Interestingly, exogenous application of NRG1 rescues ODP in NARP-deficient mice, indicating a degree of independence between these two pathways(Y. Gu et al. 2016). Indeed, NRG1 specifically increases excitatory connections from L4 PYRs onto L2/3 PV-INs, while NARP specifically mediates interlaminar connectivity between L2/3 PYRs and L2/3 PV-INs(Severin et al. 2021).

1.5 Critical periods in other sensory systems

Other sensory systems exhibit developmental CPs, and the regulation of these CPs often bear striking similarities to the regulation of CP plasticity in V1. In the primary somatosensory cortex (S1) of rodents, the region receiving input from the whiskers is known as the barrel cortex due to the cylindrical clusters of neurons that form “barrel” structures early in development, each barrel serving an individual whisker from the contralateral snout(Erzurumlu and Gaspar 2012). Like V1, unbalanced sensory input during a developmental critical period (achieved via unilateral whisker trimming) disrupts the normal development of “somatotopic maps” and barrel formation, biasing responses to the spared whiskers(Stern, Maravall, and Svoboda 2001). As with the expression of ODP, the timing of somatotopic map plasticity is different in different cortical layers, with L4 plasticity occurring earlier (before P12) and L2/3 plasticity occurring later (P12 – P14); this plasticity is NMDA-R dependent, and the timing of plasticity correlates with a developmental switch in NMDA-R subunit composition from predominantly GluN2B to GluN2A-containing NMDA-Rs(Stern, Maravall, and Svoboda 2001; H.-C. Lu, Gonzalez, and Crair 2001). While genetic knockdown of GluN2A has no impact on the timing of somatotopic map plasticity, partial knockdown of GluN2B delays the formation somatotopic maps, and pharmacological inhibition of GluN2B-containing NMDA-Rs blocks LTP in thalamocortical synapses to barrel cortex during the CP(Yamasaki et al. 2014; H.-C. Lu, Gonzalez, and Crair 2001). Like developing V1, the developing barrel cortex contains an abundance of non-functional, NMDA-R-only “silent synapses” that require activity and the insertion of AMPA-Rs to become fully functional (Rumpel, Hatt, and Gottmann 1998; Itami et al. 2003). Importantly, BDNF has been shown to be

necessary for the “unmasking” of silent synapses in the developing barrel cortex(Itami et al. 2003). Similarly, BDNF also regulates the maturation of PV-IN inhibitory circuitry in barrel cortex(Itami, Kimura, and Nakamura 2007; Z. J. Huang et al. 1999). However, unlike V1, GABA circuits in the barrel cortex undergo continual reorganization(Fuchs and Salazar 1998; Knott et al. 2002).

In the primary auditory cortex (A1), neural circuits are spatially organized into “tonotopic maps” of neurons with similar sound frequency tuning properties; the development of tonotopic maps is strongly influenced by early auditory experience: experimental exposure to pulsed or continuous pure tones early in development (P11 – 15) modifies tonotopic maps and biases the tuning properties of A1 neurons towards the experimental tone(Barkat, Polley, and Hensch 2011; L. I. Zhang, Bao, and Merzenich 2001). As with expression of ODP, the timing of the tonotopic map plasticity can be shifted via exogenous application of diazepam; similarly, tonotopic map plasticity can be reactivated in adult rodents via Gi-DREADD-mediated suppression of PV-INs (Nakamura et al. 2020; Cisneros-Franco and De Villers-Sidani 2019). BDNF also plays a role in tonotopic map plasticity: blocking BDNF signaling during the CP blocks pure tone-induced tonotopic map reorganization, whereas infusion of exogenous BDNF enhances pure tone-induced tonotopic map reorganization(Anomal et al. 2013). Interestingly, whereas in the visual system increased expression of GluN2B-containing NMDA-Rs is associated with a metaplastic shift favoring LTP, in the auditory cortex pharmacological blockade with the GluN2B antagonist Ro25-6981 enhanced thalamocortical LTP (Zeeman et al. 2021; Bridi et al. 2018; Hager et al. 2015).

Evidence of CP plasticity in the olfactory system of rodents is mixed but relies on similar pathways as those discussed previously. Olfaction is unique in that sensory inputs to the piriform (olfactory) cortex do not pass through the thalamus, rather they enter the brain first in the olfactory bulb and are routed to the cortex by projection neurons known as mitral cells. Mitral cells relay sensory inputs from the bulb to the apical dendrites of PYRs in the piriform cortex via the lateral olfactory tract (LOT); the capacity to induce NMDA-R-dependent LTP via tetanic stimulation at these LOT → piriform cortex synapses peaks at P5 and becomes virtually absent by P30, whereas top-down associational inputs remain plastic beyond P30, implying that olfactory sensory inputs to the cortex become similarly “hard-wired” early in development(Poo and Isaacson 2007). Like other sensory cortices, the developmental loss of NMDA-R dependent plasticity in LOT → piriform cortex synapses requires sensory experience (Franks and Isaacson 2005). BDNF is upregulated in the olfactory bulb and the anterior piriform cortex in response to odors; BDNF also becomes upregulated in the posterior piriform cortex and the amygdala when odors are paired with foot shocks in a fear conditioning experiment(Jones et al. 2007). PV-IN specific genetic knockdown of the BDNF receptor, TrkB, significantly reduces overall PV-IN-mediated inhibition in the anterior piriform cortex; surprisingly, decreased PV-IN activity in this brain region lead to an unexpected decrease in overall excitatory activity(Lau, Zhang, and Murthy 2022).

Similarities in developmental mechanisms of CP plasticity across different sensory systems may enable principles uncovered in the study of amblyopia in the visual system to be applied to treat non-visual plasticity-related. Conversely, similarity in

mechanisms could lead to detrimental off-target effects in pharmacological interventions that attempt to treat amblyopia.

1.6 Rejuvenating critical period plasticity

The transient conditions in V1 that allow for the refinement of cortical circuits during the CP also makes that circuit vulnerable to the irreversible impacts of amblyopia. Monocular impairment during the CP leads to LTD of impaired inputs, disrupting healthy patterns of binocularity(Sawtell et al. 2003). Interestingly, the expression of CP plasticity requires visual experience: blocking visual experience via dark-rearing delays the onset and closure of the CP and prevents the experience-dependent change in NMDA-R subunit composition(Cynader and Mitchel 1983; Iwai et al. 2003; Philpot et al. 2001). It has become apparent that visual experience in adulthood, or the lack thereof, is also important for the expression of plasticity: the Quinlan lab has shown that prolonged sensory deprivation via prolonged dark exposure (DE), initiated in adulthood, can return V1 to a highly plastic CP-like state(He, Hodos, and Quinlan 2006). Indeed, even severely amblyopic rodents (monocularly deprived from eye-opening to adulthood) exhibit a significant rejuvenation of CP plasticity following DE; harnessing this rejuvenated CP plasticity allows for the reversal of the anatomical and physiological deficits induced by amblyopia(Montey and Quinlan 2011; He et al. 2007).

The reactivation of juvenile-like plasticity by sensory deprivation has been noted in other sensory systems as well. For instance, sensory deprivation via whisker trimming can reactivate juvenile-like plasticity in thalamocortical inputs to barrel cortex,

and this plasticity coincides with the upregulation of GluN2B-containing NMDA-Rs(Chung et al. 2017). Similarly, disrupting patterned auditory input in adult post-CP rats by exposure to seven weeks of moderate intensity (65 dB) white noise (thereby "drowning out" normal environmental sounds) reactivated tonotopic map plasticity in a fashion similar to DE, including downregulation of BDNF and the upregulation of GluN2B-containing NMDA-Rs(Zhou et al. 2011; Capsoni et al. 1999; Bridi et al. 2018). Interestingly, crossmodal effects of sensory deprivation have been noted as well. It has been previously shown that DE alters synaptic connectivity in A1: lateral inputs to L2/3 A1 PYRs were weakened during DE, while the A1 feedforward thalamus → L4 → L2/3 circuit was potentiated (Emily Petrus et al. 2014; 2015). Similarly, deafening in adult, post-CP aged rodents increases LTP at thalamocortical synapses to V1, specifically at synapses onto L4 PYRs and not PV-INs (Rodríguez et al. 2018).

Sensory deprivation alone is not sufficient to drive recovery from amblyopia. In the visual system, sensory experience continues to be important following DE: while prolonged DE resets V1 to a plasticity-permissive state, the actual harnessing of plasticity requires activity-dependent proteolytic degradation of the extracellular matrix (ECM) during light reintroduction (LRx) and functional rewiring of inhibitory and excitatory circuits via visual stimulation of the impaired eye aids in the reversal of amblyopia(Montey, Eaton, and Quinlan 2013; Sachiko Murase, Lantz, and Quinlan 2017; Montey and Quinlan 2011).

1.7 Significance and Specific Aims

The expression of critical period plasticity requires visual experience: dark-rearing delays the onset and closure of the critical period and prevents the experience-dependent change in NMDA-R subunit composition. It is now understood that visual experience in adulthood is also important for the expression of plasticity: sensory deprivation via prolonged dark exposure (DE) rejuvenates the V1 circuit to a juvenile-like state via a homeostatic increase in spontaneous excitatory in V1. Subsequent visual experience during light reintroduction (LRx) enables the expression of critical period plasticity and the functional rewiring of thalamocortical inputs to V1. I was motivated to better characterize how neural circuit activity changed immediately after DE (LRx_i) and after one subsequent day of LRx (LRx_s). I originally hypothesized that spontaneous PYR activity would increase during LRx_i, then decrease to an intermediate heightened level during LRx_s. I predicted this “sweet spot” of spontaneous PYR activity, not too high and not too low, would be necessary for the re-expression of CP plasticity. I found instead that activity returned to baseline levels during LRx_s. I hypothesized that the decrease of spontaneous activity to baseline levels may be necessary for the expression of critical period plasticity. To test this hypothesis, I artificially maintained heightened spontaneous PYR activity via the use of disinhibitory chemogenetics during LRx, predicting that it would occlude the reactivation of ocular dominance plasticity. I tested these hypotheses with the following specific aims:

Specific Aim 1

I characterized the effects of dark DE and LRx on neuronal activity in mouse binocular V1 using chronically implanted extracellular electrodes. Previously published work from the Quinlan lab, as well as preliminary data from Dr. Crystal Lantz, had led me to hypothesize that spontaneous excitatory neuron activity in V1b increased during DE but decreased to an intermediate but still-elevated level following LRx. To test this hypothesis, I recorded broadband neural signals from binocular V1 of adult mice before DE, immediately during LRx (LRx_i), and after 24 hours of LRx (LRx_s) and measured changes in spontaneous and evoked activity. High pass filtering and offline spike sorting of this neuronal signal allowed me to isolate single units (SUs), representing the spiking output of single neurons, while low pass filtering allowed me to isolate local field potentials (LFPs) representing the summed output of synchronous synaptic activity. I further segregated isolated SUs into two categories: regular spiking (RS), putative pyramidal neurons and fast spiking (FS) putative interneurons. I used current source density (CSD) mapping of the visually evoked LFP (VEP) to identify the cortical laminar location of my electrode channels. Using these techniques, I was able to simultaneously measure changes in excitatory neuron firing rate and bursting activity in V1b with laminar specificity during LRx_i and LRx_s. This work identified stimulus and laminar specific changes in averaged neuronal spiking following DE that, contrary to my initial hypothesis, decreased to baseline levels during 24 hours of LRx. The result of this work is presented in Chapter 2.

Specific Aim 2

I used chemogenetic inhibitory Gi-DREADD receptors to disinhibit V1b of adult PV-cre mice. Cell-type specificity of Gi-DREADD expression was confirmed immunohistochemically via colocalization of mCherry-DREADD florescence with parvalbumin (PV)-expressing interneurons. Activity-dependent expression levels of PV in Gi-DREADD-infected cortex was compared with the uninjected cortex as an immunohistochemical readout of change in PV interneuron activity. As in Aim 1, I utilized chronically implanted electrodes in awake, head fixed mice to measure changes in evoked and spontaneous neural spiking activity and neural oscillations following intraperitoneal injection of the DREADD ligand, clozapine N-oxide. I sought to determine whether Gi-DREADD mediated disinhibition would occlude the reactivation of CP plasticity following LRx. I used monocular deprivation and measured single-eye neural responses to calculate ocular dominance before and after DE/LRx. I measured the change in visually evoked responses to stimuli of increasing spatial frequency as an electrophysiological readout of acuity. This work demonstrated cortical specificity in the expression of the CP plasticity and is presented in Chapter 3.

Chapter 2: Characterizing changes in excitability induced by dark exposure and light reintroduction

2.1 Introduction

Reactivation of ODP in adult rodents has been accomplished through a variety of means, such as pharmacological blockade of acetylcholine esterase, treatment with the antidepressant selective serotonin reuptake inhibitor (SSRI) fluoxetine, the use of ketamine or its metabolites, and even intracortical stem cell transplant (Morishita et al. 2010; Vetencourt et al. 2008; Southwell et al. 2010; S.F Grieco et al. 2016). As a non-invasive behavioral therapy, sensory deprivation via DE followed by LRx represents an attractive alternative or addendum to other such approaches.

DE induces a series of molecular and circuit level changes that rejuvenate adult V1b to a state that expresses many of the characteristics of the immature cortex: these include upregulation of GluN2B-containing NMDA-Rs, regression of inhibitory circuitry to an immature state prone to GABA depletion and decreases in the number of post-synaptic $GABA_A$-Rs. Together these result in an overall hyper-excitable phenotype in PYRs(He, Hodos, and Quinlan 2006; Jiang et al. 2010; S. Huang et al. 2010; Bridi et al. 2018). The physiological consequences of DE are cortical layer specific and depend on factors such as duration and age at DE onset. In CP-aged mice (post-natal day 21 [P21]), one day of DE fails to increase mEPSC amplitude in L2/3 PYRs, whereas two days of DE continues to increase mEPSC amplitude in L2/3 PYRs even into adulthood (>P95)(Goel and Lee 2007). Deeper layers are impacted differently by DE: while two days of DE initiated between P16 – P21 increased the average mEPSC amplitudes in L6 PYRs, two days of DE initiated between P21 – P23 does not(Emily Petrus et al.

2011). Conversely, seven days of DE initiated at P21 decreases the average mEPSC amplitude in L6 PYRs(Emily Petrus et al. 2011). Interestingly, seven days of DE does not increase mEPSC amplitude at thalamocortical (TC) synapses to L4, nor between interlaminar L4 → L2/3 synapses, whereas mEPSC amplitude does increase at lateral, intracortical L2/3 synapses(Emily Petrus et al. 2015; 2014). The lack of increased amplitude in the feedforward V1 circuit (i.e. TC → L4 → L2/3) following seven days of DE may seem to imply that prolonged DE would have little positive impact on ODP in adults, yet ten days of DE followed by reverse occlusion in amblyopic rats increases dendritic spine density (a hallmark of morphological LTP) across all V1 layers and strengthens TC synapses; which may reflect the requirement for LRx after DE to modify adult cortical circuits including TC synapses(Montey and Quinlan 2011; S. Murase et al. 2019).

The reactivation of CP plasticity by DE and LRx has two components: DE increases spontaneous activity of cortical PYR neurons, and LRx induces increased proteinase activity at the synapse. First, the loss of visually-evoked activity stimulates an upregulation of GluN2B-containing NMDA-Rs at L4 → L2/3 synapses(Bridi et al. 2018). These GluN2B-containing synapses lower the threshold for rate and voltage-dependent LTP and raise the threshold for rate and voltage-dependent LTD(Bridi et al. 2018; Guo et al. 2012). Inhibiting GluN2B with the GluN2B-specific antagonist Ro 25-6981 blocks the DE-induced increase in pyramidal neurons excitability, demonstrating that the changes in excitability is due to a Hebbian, NMDA-R-dependent mechanisms(Bridi et al. 2018; Guo et al. 2012). Similarly, pharmacologically blocking the increase in spontaneous activity by increasing GABAergic inhibition (via diazepam

or NRG1) during DE prevents changes in the LTP threshold (Bridi et al. 2018). However, it is now understood that along with the changes described above, DE also lowers the threshold for the activity-dependent activation of matrix metalloproteinase-9 (MMP-9)(Sachiko Murase et al. 2019). LRx induces an increase in perisynaptic MMP9 activity at TC synapses, which is predicted to allow plasticity of TC synapses to promote the reactivation of ODP(S. Murase et al. 2019). Importantly, this MMP-9 activity is necessary for the reactivation of ODP during LRx, as genetic knockdown or pharmacological inactivation of MMP-9 blocks the reactivation of ODP(Sachiko Murase, Lantz, and Quinlan 2017).

Interestingly, many of the circuit changes observed during DE are reversed rapidly following LRx. For instance, following two days of DE in adult (P95) mice, one day of LRx returns spontaneously potentiated L2/3 PYR → PYR connections to baseline strength via mGluR5-depednent LTD of intracortical synapse(Goel and Lee 2007; Chokshi et al. 2019). The changes noted in L6 are similarly reversed following one day of LRx(Emily Petrus et al. 2011). However, work from the Quinlan lab using *in vivo* extracellular recording electrodes demonstrates that, following ten days of DE in adult mice, increased spontaneous and evoked (RS) PYR firing rates persist following at least six hours of LRx, and ocular dominance shifts remain inducible even on the third day of LRx(Sachiko Murase, Lantz, and Quinlan 2017; He, Hodos, and Quinlan 2006). A common theme from work done in slices is that DE induces a generalized shift in bias of V1 responses to intracortical inputs during DE. The Quinlan lab has shown with FRET-based biomarkers of MMP-9 activity that MMP-9 activity is increased within a minute of visual stimulation/LRx following ten days of DE(S. Murase et al. 2019). To what extent

are the layer-specific changes in neural firing rates recapitulated using *in vivo* recordings of mice during DE? Does the near-instantaneous proteolytic degradation of TC synapses increase visually evoked activity at the initial onset of LRx (LRx_i), and how long does this increase in activity last? To answer these questions, I proposed to measure changes in V1 neural activity using the paradigm of ten days of DE followed by immediate *in vivo* extracellular recordings in awake adult mice.

2.2 Identification and validation of tools used to measure changes in V1 firing rates and bursting

I used C57bl6 mice to study the effects of DE and LRx on cortical activity. Rodents are widely used model organisms for studying the mechanisms underlying amblyopia and its potential treatment(Hooks and Chen 2020). While lacking more advanced columnar architecture like the cortices of higher mammals, mouse V1 neurons form simple functional clusters based on stimulus preference in an age-and experience-dependent fashion via Hebbian, NMDA-R-dependent mechanisms(Iacaruso, Gasler, and Hofer 2017; Jiao, Li, and Hu 2022; Kondo, Yoshida, and Ohki 2016; Jenks and Shepherd 2020; Kuhlman, Tring, and Trachtenberg 2011; Michela Fagiolini et al. 2003; Sawtell et al. 2003; B.-S. Wang, Sarnaik, and Cang 2010). Similar to humans, mice exhibit a well-defined CP for visual plasticity (peaking ~post-natal day 28 [P28]), during which time MD produces shifts in binocularity (Gordon and Stryker 1996). Strikingly, and unlike many other diseases of the brain, the etiology and outcome of monocular occlusion in mice is so similar to human amblyopia that MDed mice are often referred to directly as amblyopes(Hooks and Chen 2020).

I used chronically implanted extracellular electrode arrays to measure changes in cortical activity in V1b awake head-fixed mice. Recording from awake animals avoids the confounds of anesthesia, which can change excitatory/inhibitory balance and the stimulus preference of neurons and exert significant impacts on the expression of plasticity(Kimura and Yoshimura 2021; Afef, Rudy, and Stéphane 2022; Steven F. Grieco et al. 2021; S.F Grieco et al. 2016).

Many stimuli can be used to drive activity in V1, such as contrast modulated stochastic noise, natural scenes, but oriented gratings have long been a preferred simple parametric stimulus for studying V1 activity (Kayser, Salazar, and Konig 2003; D. Hubel and Wiesel 1959; Kaneko and Stryker 2014). Reversing gratings induce abrupt synchronous changes in TC input to V1, generating a VEP with a readily quantifiable amplitude(Heynen and Bear 2001). In this project, visual stimuli included 100% contrast, 1 Hz reversing, 30°, 60°, 120°, and 150° oriented, square wave gratings (“evoked”, 100 trials, 1 second per trial) or presentation of a 0% contrast grey screen of equal luminescence (“spontaneous”). Changes in VEP amplitude, as well as the firing rate and bursting properties isolated of RS and FS units were analyzed in response to stimuli. Orthogonal orientations were used in some experiments to avoid a contribution to VEP amplitude by stimulus-selective response potentiation (SRP). The spontaneous (0% contrast grey screen) stimulus is not expected to induce SRP, as contrast values below 12% have proven ineffective at inducing SRP in previous studies(Frenkel et al. 2006). Additionally, the Quinlan lab has extensive experience in the use of a specialized light-tight “dark room” for prolonged dark exposure experiments. This paradigm of visual stimulation has been used consistently and successfully by the Quinlan lab and others

in the study of DE's effect on V1 plasticity(Sachiko Murase, Lantz, and Quinlan 2017; Y. Gu et al. 2016; Montey and Quinlan 2011; Lantz and Quinlan 2021; He, Hodos, and Quinlan 2006).

The multichannel arrays used in this project span the depth of the implanted cortex and I use them to record broadband changes in extracellular voltage. Changes in neural activity are reflected at the population level via changes in synchronous synaptic activity and oscillatory behavior; I used low pass filtering to isolate the LFP from initially recorded broadband neural signals and current source density (CSD) analysis of visually evoked LFPs (VEPs). CSD analysis reliably identifies L4 based on the existence of a stereotypical, early occurring current sink at the site of synchronous TC input, as well as superficial (L2/3) and deep (L5/6) layers based on reversals in polarity (i.e., current sources above and below the aforementioned current sink), thus the laminar location of each recording channel can determined; changes in VEP amplitude are reliable indicators of developmental plasticity and perceptual learning(Heynen and Bear 2001; Lantz and Quinlan 2021; Frenkel et al. 2006; Frenkel and Bear 2004).

High pass filtering of the broadband signal was used to isolate multiunit activity, representing neural spiking output, which was sorted offline using Bayesian clustering and principal component analysis. PV-INs can be segregated from the broader unit population of "regular spiking" (RS) presumptive pyramidal neurons based on their waveform shape and firing rate: PV-INs exhibit a "fast-spiking" (FS) phenotype which arises from their high expression of inwardly-rectifying voltage-gated Kv3.1 potassium channels(Rudy and McBain 2001; Niell and Stryker 2008; G. V. Williams, Rao, and Goldman-Rakic 2002; Quirk et al. 2009; Lantz and Quinlan 2021). Isolated units could

be analyzed for changes in overall firing rate, as well as for changes in their bursting properties based on inter-spike interval analysis(L. Chen et al. 2009).

Mouse photoreceptors are highly insensitive to red light, therefore dark exposed mice were removed from the dark room in a light-tight container and transferred into the darkened extracellular recoding chamber under dim red-light (approximately 630 nm) illumination to limit premature visual experience during the "LRx$_i$" condition recording session(Peirson et al. 2018). LRx1 recording sessions were performed approximately 24 hours after removal from the dark room in accordance with prior studies(Goel and Lee 2007; Chokshi et al. 2019; Emily Petrus et al. 2011).

2.3 Materials and Methods

Animals

All experiments were performed at the University of Maryland, College Park, 20743 in the Bioscience Research Building, an annex of the Biology Psychology Building. Procedures utilized both male (n = 4) and female (n = 3) C57/BL6-background mice (Jackson Laboratories, Bar Harbor, ME). Subjects were housed in the Biology Psychology Building animal facility and were raised on a 12:12 hour dark/light cycle with food and water provided *ad libitum*. All procedures conformed to the guidelines of the University of Maryland Institutional Animal Care and Use Committee and in accordance with the guidelines published in the NIH Guide for the Care and Use of Laboratory Animals.

Anesthesia during survival surgeries:

Animals were anesthetized for electrode implantation using 2 – 5% isoflurane in O^2 delivered via nose cone. Surgical-plane of anesthesia was confirmed via absence of response to a strong toe-pinch administered with forceps.

Chronic electrode implantation:

Subjects Between the ages of P59 and P77 were anesthetized as described above. Once under surgical-plane anesthesia, the site of incision was sterilized with topical lidocaine, fur was removed from the scalp, and a longitudinal incision was made with a sterile scalpel. The incised skin was then retracted, and the skull was cleaned and dried with 100% acetone. A small (~4 x 2 mm) hole was drilled into the skull overlaying the visual cortex of the left hemisphere according to stereotaxic coordinates (~3 mm lateral to lambda/medial suture intersection) using a dental drill. The recording electrode was then slowly lowered to a depth of ~0.4 – 0.6 mm via digital micromanipulator. Electrodes were secured to the skull using Loctite 454 cyanoacrylate superglue and Zip kicker cyanoacrylate accelerator, and the rostral and caudal margins of the incision were sutured with sterile, 5-0 size polyglycolic acid sutures. To prevent infection, a topical triple antibiotic (neomycin, polymyxin, bacitracin) was applied to the incision site and all instruments were heat sterilized prior to use using a Germinator 500 glass bead sterilizer. Mice were allowed to recover from surgical implantation for approximately 2 to 3 weeks before extracellular recording sessions began.

Pain management and post-operative recovery:

Subjects received a subcutaneous injection of Carprofen (5mg / kg dose in 0.9% sterile saline) prior to surgical implantation. Following electrode implantation, subjects were allowed to recover on a heating pad until the righting reflex returned, then were returned to their home cage. Subjects received additional subcutaneous carprofen and once per day during subsequent post-operative monitoring (3 days). During this time, subjects were monitored for signs of infection or signs of distress (vocalizing/lethargy/weight loss/dehydration) in consultation with the attending veterinarian. Surgical procedures and post-operative monitoring were recorded on surgical forms and stored in the lab.

Dark Exposure

Implanted mice were transferred to a light-tight dark room between the ages of P100 and P101 (first dark exposure) and again at the age of P172 (second dark exposure). The dark room facility was located onsite inside the Biology Psychology Building animal facility for ten days of dark exposure. Animals were checked daily in complete darkness via the use of infrared illuminating night vision goggles. For LRx_i recordings, subject mice were removed from the dark room in a light tight container and placed in the recording setup under dim red-light illumination to limit visual stimulation prior to electrophysiological recordings under this condition.

Euthanasia:

At the cessation of experimental procedures, subjects were euthanized with excess CO^2 in the home cage at a chamber filling rate of 30 – 70% in accordance with the University

of Maryland standard operating procedure for performing carbon dioxide inhalation euthanasia. All performed euthanasia were noted in the euthanasia logbook and carcasses were frozen and stored for subsequent disposal by veterinary staff.

Electrodes:

Premade 16-channel omnetics core tungsten microwire electrodes were purchased from Tucker Davis Technologies (TDT). Microwires were 33 μm in diameter and cut to specification with a 45° tip angle resulting in an input resistance of approximately 20 – 30 kΩ.

Data Acquisition and Analysis

A TDT RZ5-2 Bioamp real-time processor, plus an optically isolated, battery-powered Medusa 16-channel preamplifier were used for recording *in vivo* broadband extracellular voltage. Proprietary TDT OpenEx software was used for experimental design and control of data acquisition. Broadband signals were filtered between 10 Hz and 300 Hz (high pass / lowpass) to isolate LFPs, and between 300 Hz and 5 kHz (high pass / lowpass) to isolate multiunit activity. A 60 Hz notch filter was employed to filter out potential contamination from electrical sources. Multiunit data were sorted into single units offline using Bayesian clustering and principal component analysis with proprietary TDT OpenSorter software. Custom MATLAB routines were used to analyze recorded data, calculating single unit waveform, firing rate, and bursting properties, as well as to calculate VEP amplitude and perform CSD analysis. Bursting threshold was determined

via the mean inter-spike interval (MISI) method (L. Chen et al. 2009). Visual stimuli were presented on a black-and-white Clinton Medical CRT monitor and were generated via custom MATLAB routines and Psychtoolbox extensions (Pyschtoolbox.org). Data were averaged by trial, with visual stimuli consisting of 100, 1 second duration trials.

Statistical Analysis

Data normality was evaluated with a one sample Kolmogorov-Smirnov test. When comparing two distributions of data, a two-sample Kolmogorov-Smirnov test was used. Data were fit with logarithmic trendlines for visualization; statistics were performed on data averaged by animal or as distributions of all single unit data. Nonparametric tests were used to determine significance in non-normally distributed data. To determine significance between paired samples, a Wilcoxon signed-rank test was used. When samples were unpaired, a Wilcoxon rank sum test was used. A Bonferroni *post hoc* correction was used for multiple comparisons.

2.4 Results and Discussion

2.4.1 Current source density mapping of averaged VEPs reveals laminar location of electrode channels.

To enable layer-specific analysis of evoked and spontaneous visual cortical activity in adult (P59 – P77) mice, I implanted 16 channel vertical electrode arrays into the left hemisphere of V1b using stereotaxic coordinates. Following a recovery period of approximately 2 to 3 weeks, implanted mice were placed in the recording chamber and shown visual stimuli consisting of 1 Hz reversing square wave gratings (100 1 second trials, 100% contrast, 0.05 cycles per degree, 30° orientation). Current source density analysis of the averaged VEP identifies current sources and sinks across in the dimensions of distance (the length of the electrode) and time (the duration of the recording). A current sink may represent the flow of positive ions into a cell, or negatively charged ions out of a cell. In V1, an early sharp sink is considered indicative of synchronous thalamocortical input to L4 (Fig.1A)(Niell and Stryker 2008; Senzai, Fernandez-Ruiz, and Buzsáki 2019). The L4 sink is characteristically accompanied by early sources in extra-granular layers, followed by later latency sinks in L2/3 and L5/6. Computational modeling predicts that these later sources and sinks may be due to feedback from higher visual areas and recurrent synapses from within V1(Rimehaug et al. 2022). Similar CSD profiles can be generated following direct electrical stimulation of the visual thalamus as well as photic stimulation of the retina(Heynen and Bear 2001). Once laminar location was determined, VEPs were averaged by layer (Fig.1B).

The fast oscillation superimposed on the L4 VEP (Fig.1B, cyan) may be the result of gamma oscillations, and similar oscillations have been noted in the L4 VEP previously(Niell and Stryker 2008).

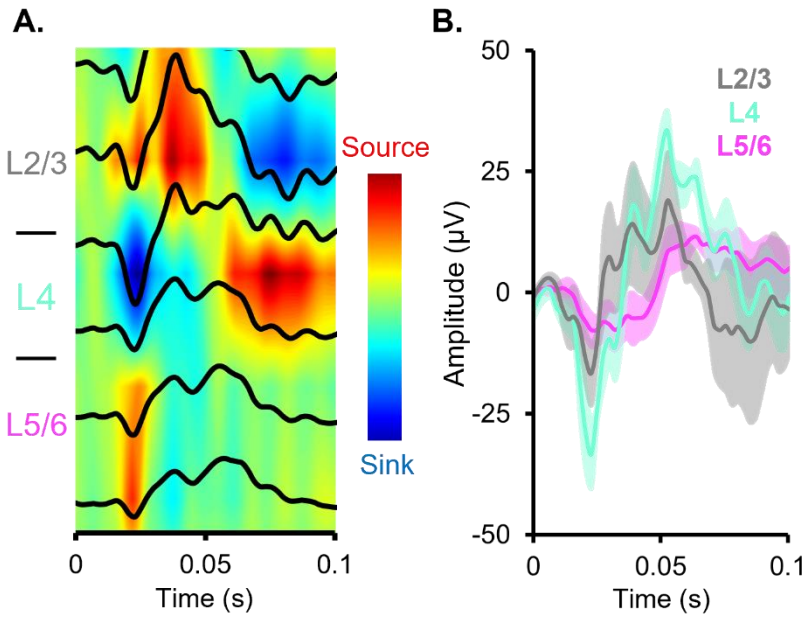

Figure 1: Identification of laminar location of electrode channels

A. Current source density (CSD) map calculated from trial averaged visually evoked local field potentials (VEPs; black line overlay). Current sources are depicted in red, and current sinks are depicted in blue. The early sharp current sink in layer 4 represents feed-forward input from thalamus. Current sources above and below layer 4 represent feed-forward input to superficial layers 2/3 and deep layers 5/6 (respectively). **B.** Layer-averaged VEP waveforms +/- SEM collected from 7 mice. VEPs are generated in response to a 1 Hz reversing square-wave grating. stimulus onset is at zero seconds. Note the differences in amplitude between the layer 4 VEP (cyan) versus the layer 2/3 and layer 5/6 VEPs (grey and magenta, respectively; this coloring convention will continue throughout thesis unless noted otherwise).

2.4.2 DE and LRx$_i$ induce layer-specific increases in spontaneous and evoked firing rates

To measure changes in excitatory PYR and inhibitory PV-IN firing rates, I first classified isolated single units by waveform shape and spike rate (Fig.2). “Fast-spiking” (FS) PV-INs (red, n = 21, 7 mice) exhibit the expected characteristic narrow spike waveform (trough to peak time, Fig 2.C), high peak to trough ratio (Fig.2B), and steeper Endslope (Fig.2B – D) versus “regular-spiking” (RS) PYRs (blue, n = 103, 7 mice) (Rudy and McBain 2001; Niell and Stryker 2008). In addition to waveform shape, high firing rate has also been shown to be a reliable indicator of interneurons; in particular, PV-INs have been shown to maintain high firing rates (up to 60 Hz), thus rate is also a reliable parameter for unit classification (Fig2.D)(Quirk et al. 2009). Isolated FS units comprised approximately 17% of all recorded units across both conditions (ctrl and LRx$_i$), which corresponds to the expected proportion of inhibitory interneurons (inhibitory INs or PVs?) detected immunohistochemically in mouse neocortex (19.5%) (Tamamaki et al. 2003; Niell and Stryker 2008). The fast-spiking phenotype of PV-INs is attributed to their expression of voltage-gated inward rectifying Kv3.1 channels. Genetic knockdown of Kv3.1 in mice broadens the action potentials of PV-INs and reduces their maximal firing rate. Interestingly, this reduction in PV-IN firing rate lengthened the duration of MD required to drive deprived-eye depression, from three days typically required in wildtype mice to five days required in the Kv3.1 KO mice(Matsuda et al. 2021). It is worth noting that visual experience also regulates the expression of the related voltage-gated potassium channel Kv3.2: five days of DE initiated between the ages of P25 to P30 increases expression of Kv3.2 potassium channels in L2/3 PV-INs

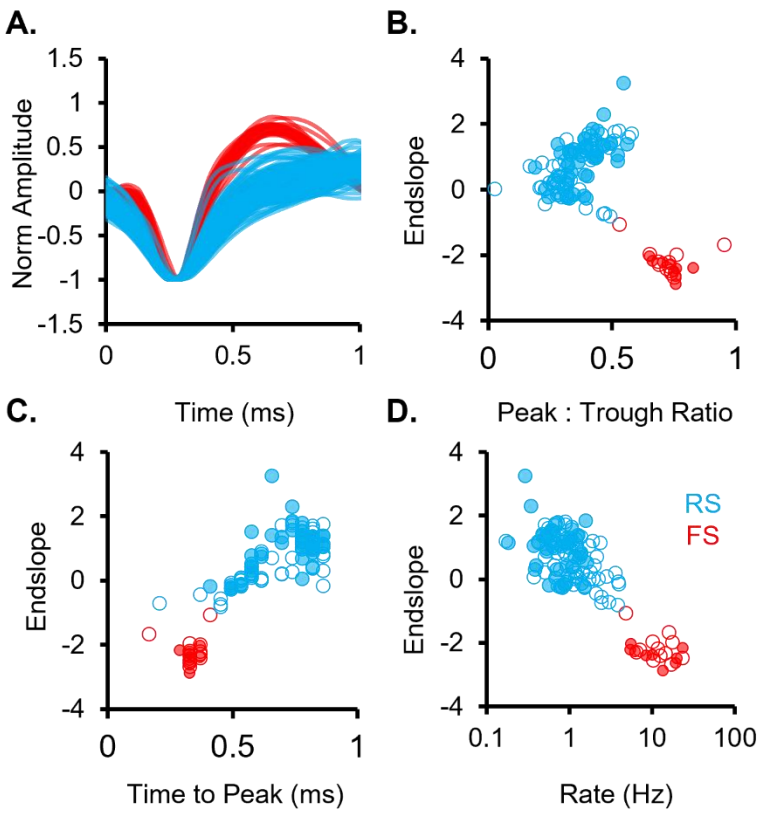

Figure 2: Classification of single units by waveform and rate

A. Average waveforms of regular spiking (RS, blue, presumptive pyramidal neurons, n = 103 units, 7 subjects) and fast spiking (FS, red, presumptive PV+ interneurons, n = 21 units, 7 subjects) single units collected during the control condition ("ctrl", prior to DE, unfilled circles) and during initial LRx ("LRx_i", immediately following DE, filled circles) during spontaneous stimulation (luminescent grey screen). Evoked (reversing gratings) stimuli were performed immediately after spontaneous stimuli. Spontaneous and evoked units recorded during a given session were sorted and classified as RS or FS together and did not differ between stimuli. **B – D.** Scatter plots of single unit characteristics used as criteria for classification. Endslope is measured at the point 0.5 ms after the initial waveform trough. Time to peak is measured from time of the initial trough. Units from all implanted subjects (n=7) were pooled and classified using k-means clustering. Only units that clustered reliably using all three parameters were analyzed. Note that FS units exhibit steeper endslopes, larger peak to trough ratios, faster time to peaks, and higher firing rates versus RS units.

(Grabert and Wahle 2009). Increased Kv3.2 during DE could shift the endslope used as a metric of (FS) PV-In classifications. However, the noted upregulation of Kv3.2 occurs only in L2/3, and all FS units recorded in my experiments were from L4 and L5/6; this may explain the lack of noticeable shift is detectable in the SU scatterplots (Fig.2B – D)(Grabert and Wahle 2009).

Previously we have shown that spontaneous RS firing rates are increased in adult V1b following brief (three day) DE and this increase is necessary for DE-induced metaplasticity (Bridi et al. 2018). Increased mEPSC amplitude following DE is well-attested in L2/3 in CP-aged mice (P21) and on to adulthood (>P90), however in acute slice experiments, increases in mEPSC frequency is absent following DE(Goel and Lee 2007; Bridi et al. 2018). The severing of thalamic axons which occurs during cortical slice preparation may impact the readout of the effect of DE. Severed thalamic axons in cat V1 exhibit high release probability are highly refractory to ongoing electrical stimulation, exhibiting an increased failure rate at stimulation intervals below 50 ms(Stratford et al. 1996). This could mean that the assessment of increased spontaneous firing rates following DE may only be possible in an intact brain. Conversely, it could indicate the increase in firing rate is a delayed effect that requires sensory input during LRx, as we have previously shown that rapidly induced MMP-9 activity at thalamocortical synapses during LRx increased spontaneous firing rate which persists for at least six hours(Sachiko Murase, Lantz, and Quinlan 2017). To test the hypothesis that spontaneous firing rates are indeed elevated during the initial reintroduction to light (LRx_i), I recorded from V1b of awake head-fixed mice prior to DE and immediately after DE. Extra care was taken to control light exposure prior to

electrophysiological recordings before LRx_i. Subject mice were shown a static luminescent grey screen; the neuronal response to this stimulus is considered spontaneous activity as V1 (RS) PYRs are driven most strongly by high contrast patterned, oriented stimuli of low spatial frequency(Niell and Stryker 2008; Frenkel et al. 2006).

Here I demonstrate that DE plus LRx_i causes a significant increase in average spontaneous RS firing rates in L4, but not in L2/3 or L5/6(Fig.3A). These results were unexpected, given that previous reports have indicated that both TC → L4 and L4 → L2/3 feedforward mEPSC amplitude were unaltered following DE, implies that L4 activity should not be the locus of increased activity (Emily Petrus et al. 2015; 2014). This result is particularly unexpected given that plasticity at TC → L4 synapses is limited to early postnatal development: LTP and LTD induction at TC → L4 induced via white-matter stimulation is only observed during the first week after eye-opening (~P20 LTP). Similarly, LTD exhibits a more gradual decline, and is lost by ~P30)(Jiang, Treviño, and Kirkwood Alfredo 2007). Even dark-rearing from birth, which delays the onset and closure of the CP and prevents experience-dependent change in NMDA-R subunit composition, does not change the developmental time course for loss of LTP and LTD in L4(Cynader and Mitchel 1983; Philpot et al. 2001; Jiang, Treviño, and Kirkwood Alfredo 2007). The developmental loss of LTP and LTD in L4 is also independent of neural inhibition, as induction of LTP and LTD was not rescued by intracellular blockade of inhibitory chloride channels via DNDS(4,4'-dinitro-stilbene-2,2'-disulphonic acid)(Jiang, Treviño, and Kirkwood Alfredo 2007; Dudek and Friedlander 1996), therefore decreased (FS) PV-In activity during DE isn't expected to increase L4 RS spontaneous activity.

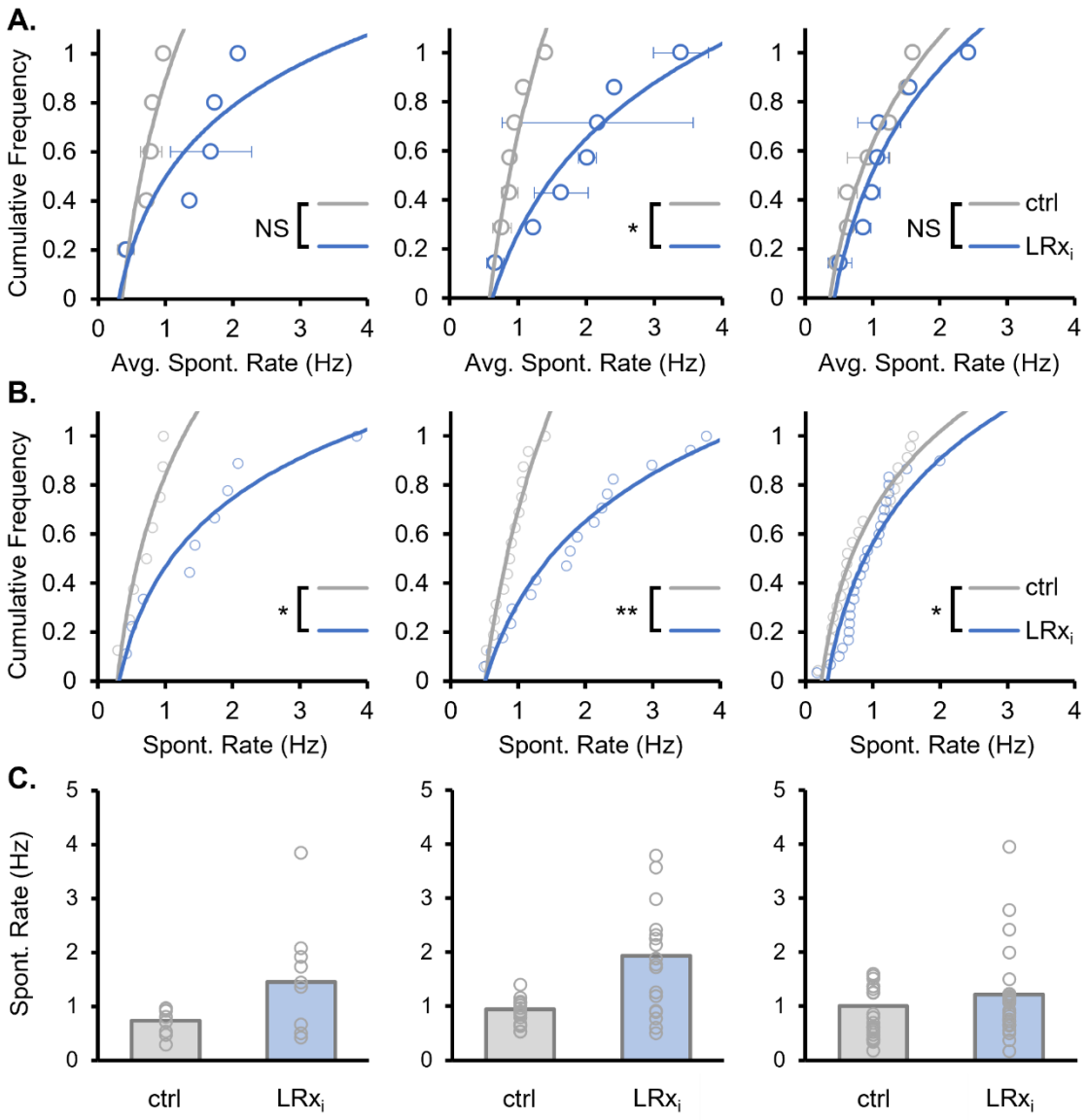

Figure 3: DE plus LRx$_i$ induces Layer-specific changes in spontaneous RS firing rates

A. Cumulative distribution of spontaneous RS firing rates averaged by mouse and layer. LRx$_i$ caused a significant rightward shift in the distribution of averaged spontaneous RS firing rates in L4, but not in L2/3 or L5/6. (Wilcoxon sign ranked test [ctrl vs. LRx$_i$] * $p < 0.05$) **B.** Cumulative distribution of all spontaneous RS units. LRx$_i$ caused a significant rightward shift in the distribution of spontaneous RS firing rates in L2/3, L4, and L5/6 (Kolmogorov-Smirnov test [ctrl vs. LRx$_i$] [L2/3] *$p < 0.05$; [L4] **$p < 0.005$; [L5/6]] *$p < 0.05$). **C.** Averaged histograms of data points presented in B. ([ctrl] (mice, units): [L2/3] n = 5, 8; [L4] n = 7, 16; [L5/6] n = 7, 23); [LRx$_i$] (mice, units): [L2/3] n = 5, 9; [L4] n = 7, 17; [L5/6] n = 7, 30).

Additionally, while five days of MD in juvenile cats reduces soma size in the lateral geniculate nucleus (LGN, the visual thalamus), MD following ten days of DE produced no such effect in adult cats, indicating that the thalamus is not directly impacted by DE in adulthood and arguing against a purely TC origin of the increased spontaneous activity noted in L4 (Duffy et al. 2016).

My experiments did not reveal an increase in spontaneous RS activity in L2/3 when averaged by animal despite previous work demonstrating significant effects following DE in this cortical layer (Bridi et al. 2018; Goel and Lee 2007). Previously examination of the impact of DE on layer 6 PYRs in P21 mice demonstrated that although two days of DE failed to change the average mEPSC amplitude, the distribution of mEPSC amplitudes was significantly different. More specifically, high and low amplitude mEPSCs became more prevalent while intermediate amplitude mEPSCs became rarer, but the changes balanced out to a net-zero change in the average mEPSC amplitude(Emily Petrus et al. 2011). It is possible a similar shift in the distribution of spontaneous and evoked SU firing rates was obscured by averaging in my experiments. To test this hypothesis, I plotted the cumulative distribution of all unit firing rates per layer (Fig.3B). There was a significant rightward shift in the distribution of spontaneous RS firing rates in L2/3 and L4, and L5/6 (Fig.3B). One possible interpretation of these distributions is that in L2/3, approximately 40% of the RS exhibited no apparent shift versus control, whereas the upper 60% increase in firing rate. This suggests that the expected enhancement of spontaneous RS firing rates did indeed occur in a subset of L2/3 PYRs. A sampling bias may have contributed to this

result, as one subject accounts for 3 of 8 units in the control condition, and one subject accounts for 5 of 9 units in the LRx_i condition.

The significant increase in spontaneous RS activity was consistent between measurement in L4. Interestingly, in rat V1 during the CP (P28), approximately one third of V1 L4 PYRs that share TC input form recurrent synaptic connections(L. Wang et al. 2013). Optogenetically evoked TC-EPSCs onto L4 PYRs were weakened by 3 days of MD initiated at P24, while recurrent EPSCs between L4 PYRs were not affected(L. Wang et al. 2013). In younger rats MDed between P14 and P17, spontaneous PYR firing rates increased; this increase was attributed to a decrease in feedback, but not feedforward inhibition, and an increase in the relative proportion of recurrently connected L4 PYRs from 10.6% to 18.9% in the deprived hemisphere (Maffei, Nelson, and Turrigiano 2004). It is intriguing to consider that the increased spontaneous RS firing rates in L4 reflect an enhancement in recurrent connectivity in L4. However, following one day of LRx, MMP-9 activity does not co-localize with VGlut1, a marker of intracortical excitatory synapses. Like many of the changes induced in cortical circuitry by visual deprivation, these changes in spontaneous activity noted in L4 reversed within two days of eye-reopening, and possibly sooner(Sachiko Murase, Lantz, and Quinlan 2017; Maffei, Nelson, and Turrigiano 2004).

While TC inputs to L4 aren't strengthened during DE, we have previously noted that MMP-9 activity at TC synapses is rapidly activated within seconds of visual stimulation following DE(Emily Petrus et al. 2014; Sachiko Murase et al. 2019). Spontaneous and evoked (RS) PYR firing rates are elevated following six hours of LRx; given the rapidity of MMP-9 activity, I predicted that evoked RS activity would also be

increased during LRx_i. To test this hypothesis, I recorded evoked activity in response to 1 Hz reversing square wave gratings (100 1 second trials, 100% contrast, 0.05 cycles per degree, 30° orientation). Consistent with these previous results, I detected a significant increase in evoked RS spike rates in LRx_i. These changes were observed in L4, but not in L2/3 or L5/6 (Fig.4A) (Sachiko Murase, Lantz, and Quinlan 2017). Interestingly, unlike spontaneous activity, there was no significant shift in the distribution of evoked RS firing rates in L2/3 or L5/6 (Fig.4B). This agrees with the observation that DE does not strengthen feed-forward connectivity between L4 and L2/3 PYRs, such that an increase in activity is due to spontaneously activity(Emily Petrus et al. 2015).

In my experiments, RS units from L5/6 were binned, but there are differences in the function and characteristics of neurons in these deep layers. For instance, PYRs in L6 project primarily to the ipsilateral thalamus, while L5 PYRs project to a variety of locations including other cortical regions, the brainstem, and the striatum(Harris and Shepherd 2015). In L5 of mouse V1, two subclasses of excitatory neurons have been shown to exhibit different plasticity properties in response to MD and DE (initiated P26 – P31). Cortico-cortical projecting “RS” PYRs first exhibited synaptic depression during the first twelve hours of DE, followed by TNF-α-dependent return to baseline in approximately three days. Conversely, “intrinsic bursting” (IB) PYRs underwent αCaMKII-dependent LTP that peaked at three days of DE, and slowly returned to baseline by the tenth day(Pandey, Hardingham, and Fox 2022). The opposing sign in plasticity exhibited by these two subgroups of L5 PYRs cancel each other out largely until the third or fifth day of DE, after which there is an apparent net effect of potentiation that returns to baseline by the tenth day(Pandey, Hardingham, and Fox 2022).

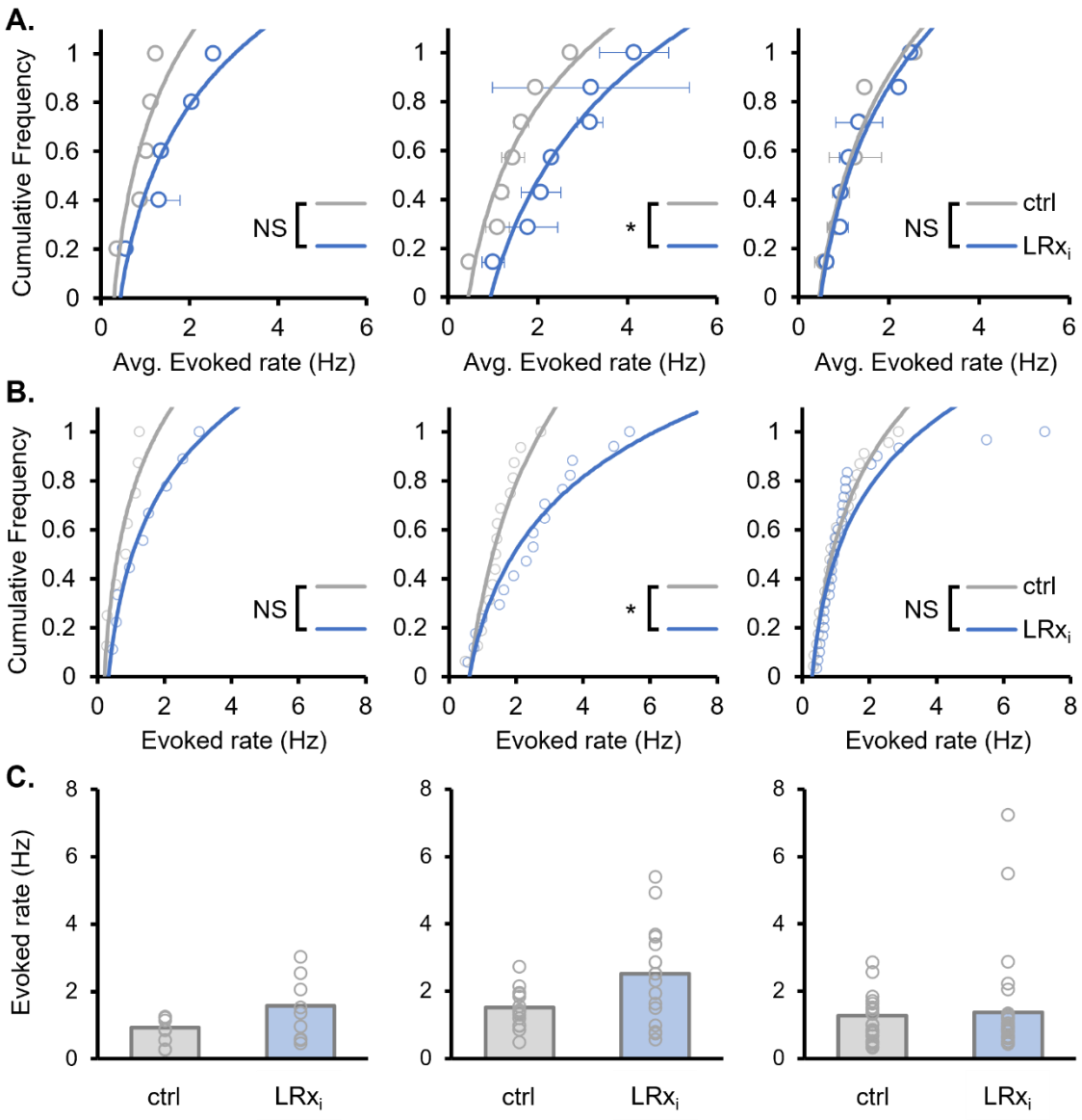

Figure 4: DE plus LRx$_i$ induces Layer-specific changes in evoked RS firing rate

A. Cumulative distribution of spontaneous RS firing rates averaged by mouse and layer. LRx$_i$ caused a significant rightward shift in the distribution of averaged evoked RS firing rates in L4, but not in L2/3 or L5/6. (Wilcoxon sign ranked test [ctrl vs. LRx$_i$] * $p < 0.05$) **B.** Cumulative distribution of all evoked RS units. LRx$_i$ caused a significant rightward shift in the distribution of evoked RS firing rates L4 (Kolmogorov-Smirnov test [ctrl vs. LRx$_i$] [L2/3] NS; [L4] *$p < 0.05$; [L5/6] NS). **C.** Averaged histograms of data presented in **B.** ([ctrl] (mice, units): [L2/3] n = 5, 8; [L4] n = 7, 16; [L5/6] n = 7, 23); [LRx$_i$] (mice, units): [L2/3] n = 5, 9; [L4] n = 7, 17; [L5/6] n = 7, 30).

Interestingly, two days of DE increased mEPSC amplitude in L6 between P16 – P21, while two days of DE had no effect between P21 – P23. Conversely, seven days of DE decreased mEPSC amplitude in L6; it is possible that PYRs in L6 similarly exhibit DE-duration dependent rebound plasticity on the timescale of days(Emily Petrus et al. 2011). Given the noted heterogeneity of responses in L5/6 it is difficult to draw strong conclusions from the lack of effect seen in Figs.3-4, however I did see changes in my cumulative distributions in spontaneous activity in L5/6, suggesting that a subset of L5/6 PYRs were impacted by LRx_i (Fig.3B). In the future, it may be worthwhile to develop new SU classification techniques to distinguish IB from cortico-cortical projecting PYRs in L5. Lastly, it is worth noting that these evoked responses were averaged over an entire one second trial of a reversing grating stimulus, but these evoked responses are most apparent in the first 100 ms immediately following grating reversal (Fig.4 supplement 1). Averaging over an entire second has blunted the difference between the evoked and spontaneous conditions, however z-scores of control evoked single unit firing rates normalized to the within-animal spontaneous firing rate are significantly elevated (one-sample Wilcoxon signed rank test), and the distribution of normalized evoked z-scores is significantly different from the distribution of spontaneous firing rate z-scores (Fig.4 Supplement 2A). Interestingly, during LRx_i, normalized evoked z scores are no longer significantly elevated, while the evoked and spontaneous distributions are still significantly different, possibly reflecting the enhanced excitability that enables ODP after LRx (Fig.4 Supplement 2B).

Figure 4 Supplement 1: Evoked response to reversing stimuli is most elevated immediately following grating reversal

A. Cumulative distribution of evoked and spontaneous RS firing spikes times from L4 of one representative test subject. Note the significant leftward shift in the distribution of spike times during the first 0.1 s following evoked grating reversal versus spontaneous stimulation (Kolmogorov-Smirnov test [spont. Vs. evoked] [ctrl] $p^* < 0.05$; [Lrx_i] $p^{***} < 0.0005$). **B.** Peri-stimulus time histogram of evoked spike times from A. presented as mean +/- SEM. D. Peri-stimulus time histogram of spontaneous spike times from A. presented as mean +/- SEM. ([ctrl] (mice, units): 1, 3; [LRx_i] (mice, units): 1,3).

Figure 4 Supplement 2: evoked firing rates significantly elevated vs. spontaneous firing rates

Cumulative distribution of z-scores normalized to within-animal spontaneous firing rate averages and standard deviations calculated using the entire one second trial duration. **A.** Normalized z-scores of RS activity were significantly elevated in the control condition. Normalized evoked z-scores were significantly shifted versus spontaneous normalized z-scores. (one-sample Wilcoxon signed rank test, [evoked RS] $^{**}p < 0.0025$; Kolmogorov Smirnoff test [evoked RS vs. spont. RS] $^{*}p < 0.025$; Bonferroni corrected for 2 comparisons; n = 7 mice, 47 units). **B.** Normalized z-scores of RS activity were no longer significantly elevated during LRx_i. Normalized evoked z-scores were still significantly shifted versus spontaneous normalized z-scores. (one-sample Wilcoxon signed rank test, [evoked RS] NS; Kolmogorov Smirnoff test [evoked RS vs. spont. RS] $^{*}p < 0.025$; Bonferroni corrected for 2 comparisons; n = 7 mice, 56 units).

Figure 4 Supplement 1: Evoked response to reversing stimuli is most elevated immediately following grating reversal

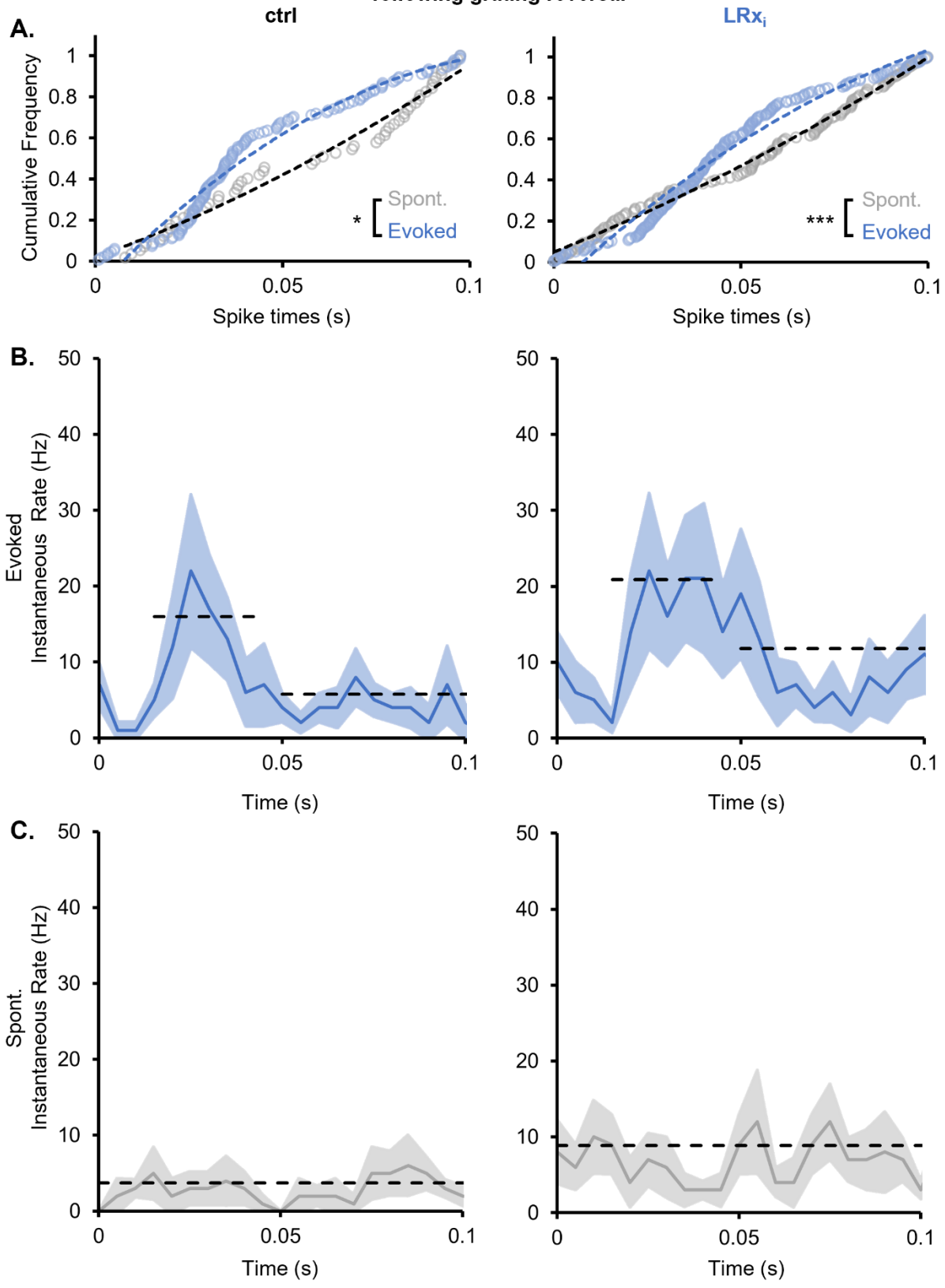

Figure 4 Supplement 2: evoked firing rates significantly elevated vs. spontaneous firing rates

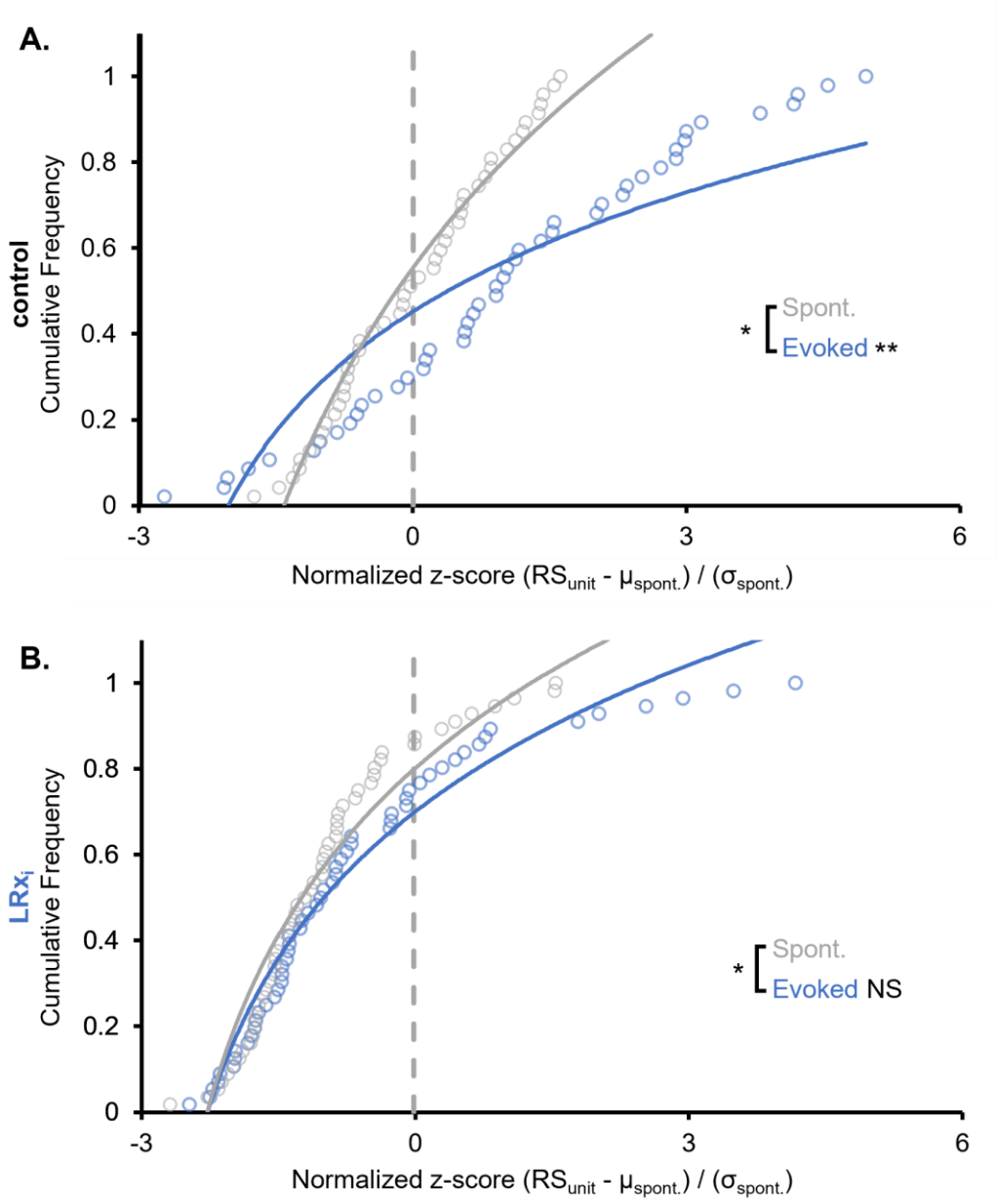

2.4.3 DE and LRx$_i$ induce layer-specific increases in evoked excitatory/inhibitory balance

Prolonged DE removes the feed-forward input to cortical interneurons and decreases cortical inhibition. The decrease in inhibition is proposed to contribute to the increase in spontaneous RS activity that is necessary for DE-induced metaplasticity (Y. Gu et al. 2016; Bridi et al. 2018). To test the hypothesis that PV-IN firing rates are decreased during LRx, I measured changes in evoked and spontaneous FS firing rates in V1. Because inhibitory interneurons only make up approximately ~20% of all cortical neurons, I binned (FS) PV-INS across all layers to achieve sufficient statistical power(Tamamaki et al. 2003). Surprisingly, I detected no significant difference in either spontaneous or evoked average FS firings rates during LRx$_i$ (Fig.5A – B; Fig.6A - B). Comparing changes in RS to FS demonstrate a significant shift in evoked excitatory / inhibitory balance (Fig.6D). This result may be due to sampling bias, FS units were not present during every recording session. Of the seven mice used in this experiment, one exhibited no FS units, a second exhibited FS units only during the ctrl condition, and a fourth exhibited a FS unit only during LRx$_i$. Evoked E/I balance increased by (~150 – 300%) in three of four subjects with matched recordings and decreased by (~95%) in one. Overall, the result is due to the lack of concurrent increase of evoked FS firing rates with RS firing rates, indicating an inability of (FS) PV-INs to scale their activity with neighboring (RS) PYRs. Alternatively, LRx$_i$ may be insufficient visual stimulation to drive decreases in FS firing rates, as we have recently shown that (FS) PV-IN firing rates are decreased following six hours of LRx(Sachiko Murase, Lantz, and Quinlan 2017).

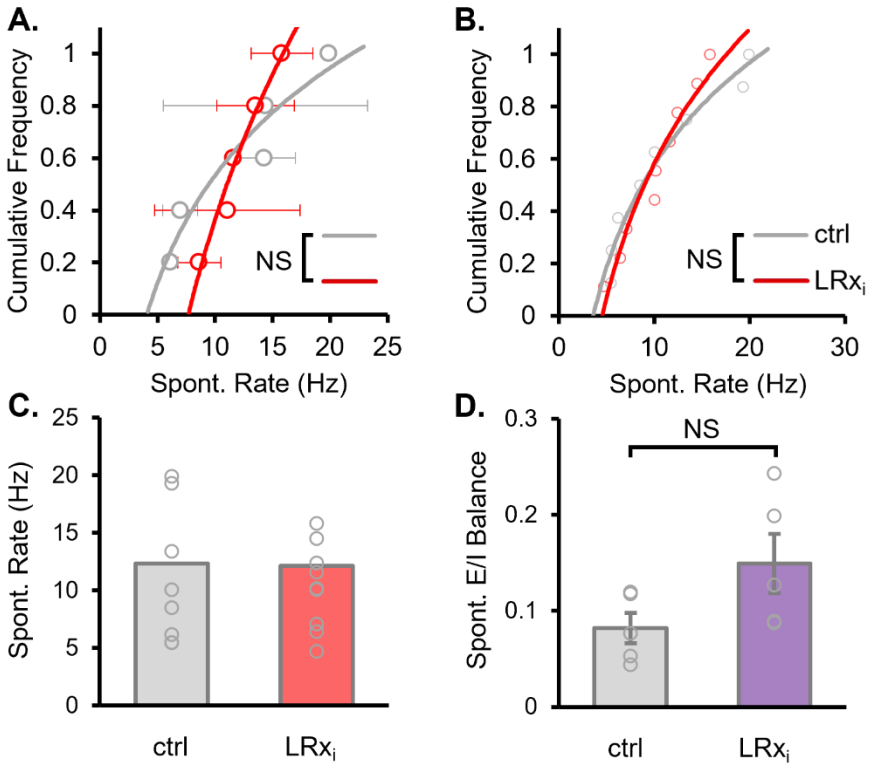

Figure 5: DE plus LRx$_i$ had no effect on spontaneous FS firing rate and E/I balance

A. Cumulative distribution of spontaneous FS firing rates averaged by mouse across all layers. No significant change was detected following LRx$_i$. (Wilcoxon rank sum test [ctrl vs. LRx$_i$] [spont. rate] NS). **B.** Cumulative distribution of all spontaneous FS units. No significant shift was detected in the distribution of spontaneous FS units. (Kolmogorov-Smirnov test [ctrl vs. LRx$_i$] NS). **C**. Averaged histograms of data presented in B. ([ctrl] (mice, units): 7, 9; [LRx$_i$] (mice, units): 7,12). **D.** Histogram of average spontaneous excitatory / inhibitory balance presented as mean +/- SEM. No significant change was detected following LRx$_i$ (Wilcoxon rank sum test [E/I ratio] NS.)

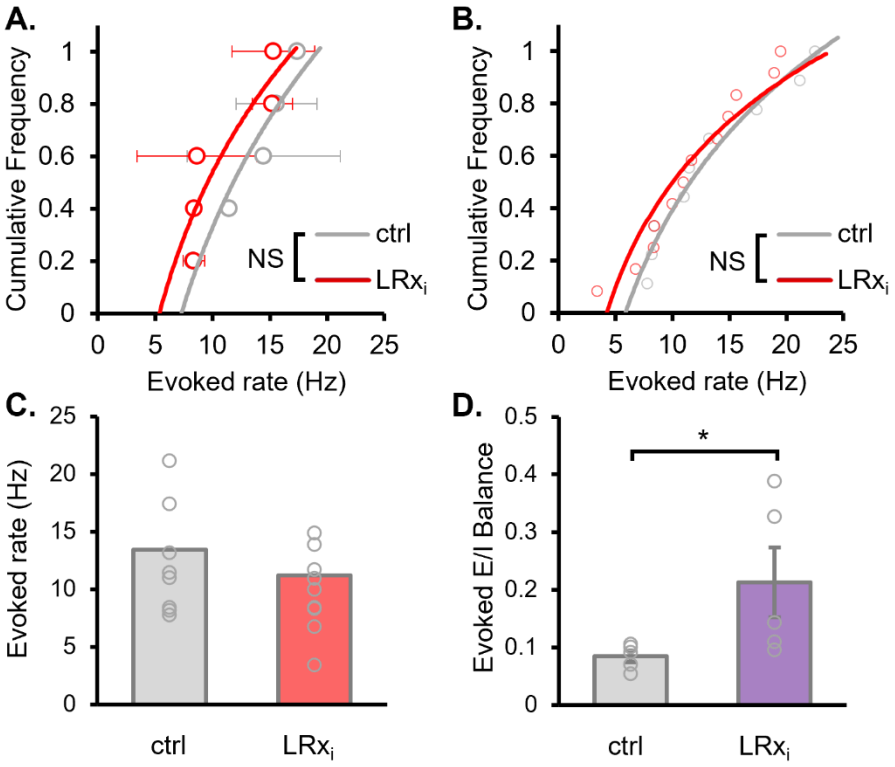

Figure 6: DE plus LRx$_i$ increases Evoked E/I balance

A. Cumulative distribution of FS firing rates averaged by mouse across all layers. No significant change was detected following LRx$_i$. (Wilcoxon rank sum test [ctrl vs. LRx$_i$] [Evoked rate] NS). **B.** Cumulative distribution of all evoked FS units. No significant shift was detected in the distribution of evoked FS units. (Kolmogorov-Smirnov test [ctrl vs. LRx$_i$] NS). **C.** Averaged histograms of data presented in B. ([ctrl] (mice, units): 7, 9; [LRx$_i$] (mice, units): 7,12). **D.** Histogram of average evoked excitatory / inhibitory balance presented as mean +/- SEM. Evoked E/I balance significantly increased following LRx$_i$ (Wilcoxon rank sum test [E/I ratio] *$p < 0.05$.)

In contrast to the stability of thalamic input to PYRs, MD causes a rapid loss of TC inputs onto PV-INs that occurs within hours(Quast et al. 2023). Following DE and LRx, we have shown that Vglut2 puncta surrounding PV-INS significantly colocalizes with MMP-9 biomarker activity, predicting that structural and functional plasticity is robustly activated at these synapses(Sachiko Murase, Lantz, and Quinlan 2017). Interestingly, thalamo-cortical synapses may PV-INs contain NMDARs, while cortical cortico-cortical synapses do not. This suggests the intriguing possibility that decreased firing rates of (FS) PV-IN firing rates observed following six hours of LRx may be due to LTD of TC inputs enabled by LRx(Lewis et al. 2022). If so, L4 PV-INs would not be likely to contribute to this effect as they do not exhibit NMDA-Rs at TC inputs, however PV-INs in other cortical layers do receive TC input and may be regulated in this fashion(Kloc and Maffei 2014).

2.4.4 DE and LRx$_i$ induce layer-specific increases in spontaneous and evoked bursting.

Previously, we showed that DE induced both an increase in spontaneous RS firing rates and an increase in spontaneous RS bursting (Bridi et al. 2018). Neuronal bursting is important to the function of cortical circuits and can enhance the fidelity of synaptic transmission by overcoming low probability of release in facilitating synapses(Krahe and Gabbiani 2004). To determine if spontaneous bursting activity is elevated during LRx$_i$, I utilized mean inter-spike interval (MISI) burst detection, an auto-adaptive process that calculates burst thresholds based on the firing parameters of an isolated units rather than an arbitrary interspike interval threshold(L. Chen et al. 2009). Here I found that LRx$_i$ caused a significant increase in averaged L4 spontaneous RS

burst rates and durations in L4, but not in L2/3 or L5/6 (Fig.7A). The increase in averaged L4 spontaneous burst rate was accompanied by a significant shift in the distribution of L4 spontaneous RS burst rates (Fig.7B). No significant changes were detected in the parameter of spontaneous RS burst duration (Fig.8), however there was a significant rightward shift in the spike content of spontaneous RS bursts in L2/3 (Fig.9B). No changes were detected in spontaneous FS burst rate, burst duration, nor spikes per burst (Fig.10).

When the same analysis was applied to evoked RS bursting activity, I found a significant increase in averaged evoked RS burst rate in L4, but not in L2/3 or L5/6 (Fig.11A). The increase in averaged RS evoked burst rate in L4 was not accompanied by a shift in the distribution of evoked L4 RS burst rates (Fig.11B). Burst duration was unaffected during LRx_i, however I did detect a significant rightward shift in the distribution of evoked RS burst spike content in L5/6 (Fig.13B). No significant changes were detected in evoked FS bursting properties (Fig.14).

Bursting is a common feature of thalamic neurons, which typically switch between modes of tonic firing and bursting activity. SU recordings from anesthetized cats have recently demonstrated that bursting in LGN neurons increases with stimulus contrast(Sanchez et al. 2023; Krahe and Gabbiani 2004). If the spontaneous bursting detected in L4 RS PYRs reflected thalamic bursting, it would likely be more elevated during high contrast evoked stimulation. The simultaneous increase in evoked and spontaneous L4 RS burst rate may indicate that the overall contrast sensitivity has decreased during prolonged DE. Alternatively, it may be that increased bursting in cortical neurons is a homeostatic mechanism that mimics bursting input from the

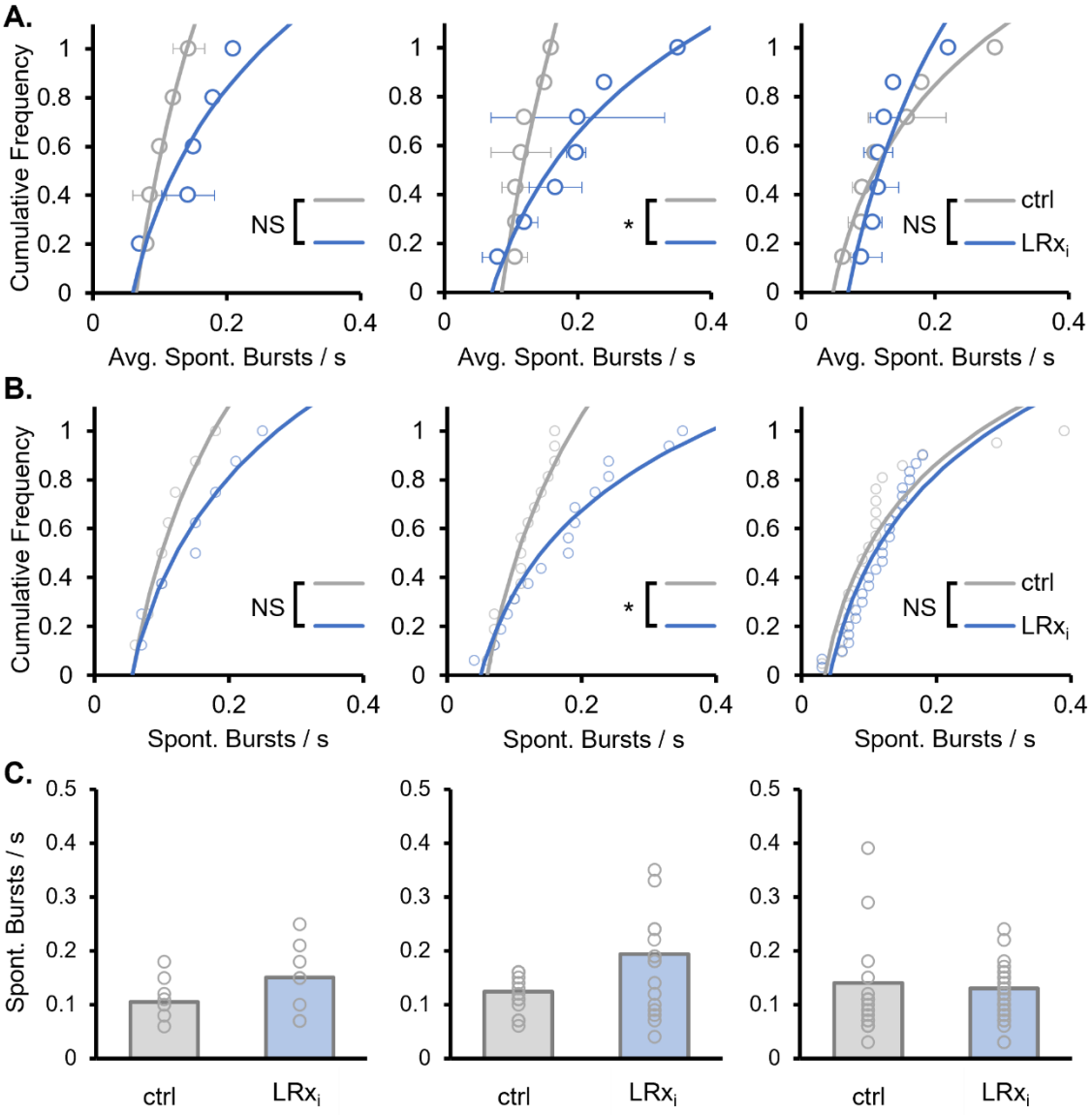

Figure 7: DE plus LRx$_i$ induces Layer-specific changes in spontaneous RS burst rate

A. Cumulative distribution of spontaneous RS burst rate averaged by mouse and layer. LRx$_i$ caused a significant rightward shift in the distribution of averaged spontaneous RS burst rate in L4, but not in L2/3 or L5/6. (Wilcoxon sign ranked test [ctrl vs. LRx$_i$] [L2/3] NS; [L4] *p < 0.05; [L5/6]] NS) **B.** Cumulative distribution of all spontaneous RS bursting units. LRx$_i$ caused a significant rightward shift in the distribution of spontaneous RS burst in L4, but not in L2/3 or L5/6 (Kolmogorov-Smirnov test [ctrl vs. LRx$_i$] [L2/3] NS; [L4] *p < 0.05; [L5/6]] NS). **C.** Averaged histograms of data points presented in B. ([ctrl] (mice, units): [L2/3] n = 5, 8; [L4] n = 7, 16; [L5/6] n = 7, 23); [LRx$_i$] (mice, units): [L2/3] n = 5, 9; [L4] n = 7, 17; [L5/6] n = 7, 30).

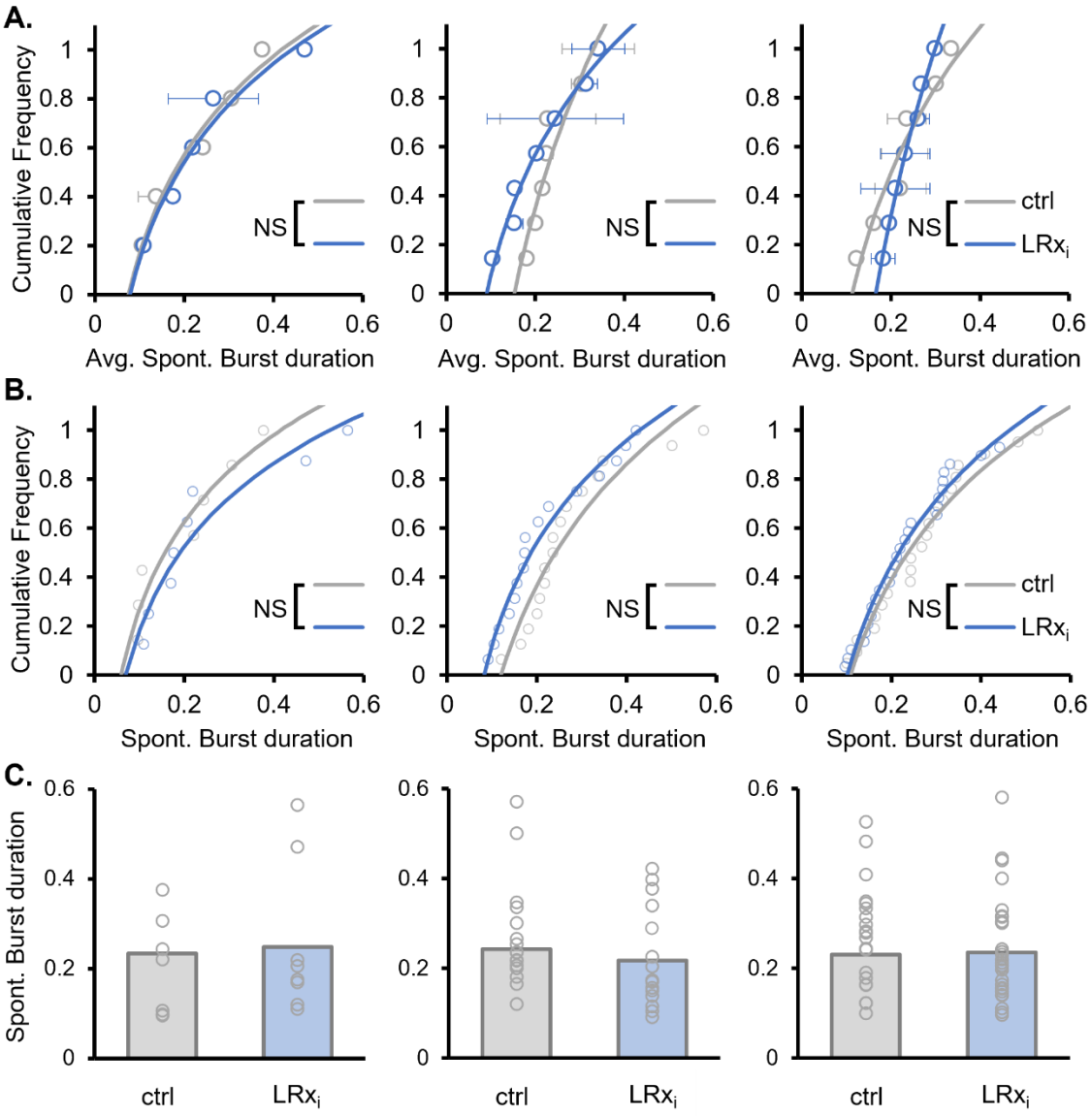

Figure 8: DE plus LRx$_i$ does not change spontaneous RS burst duration

A. Cumulative distribution of spontaneous RS burst duration averaged by mouse and layer. LRx$_i$ had no effect on the distribution of averaged spontaneous RS burst durations in any layer. (Wilcoxon sign ranked test [ctrl vs. LRx$_i$] NS) **B.** Cumulative distribution of all spontaneous RS units' burst duration. LRx$_i$ had no effect on the distribution of spontaneous RS burst durations in any layer (Kolmogorov-Smirnov test [ctrl vs. LRx$_i$] NS). **C.** Averaged histograms of data points presented in B. ([ctrl] (mice, units): [L2/3] n = 5, 8; [L4] n = 7, 16; [L5/6] n = 7, 23); [LRx$_i$] (mice, units): [L2/3] n = 5, 9; [L4] n = 7, 17; [L5/6] n = 7, 30).

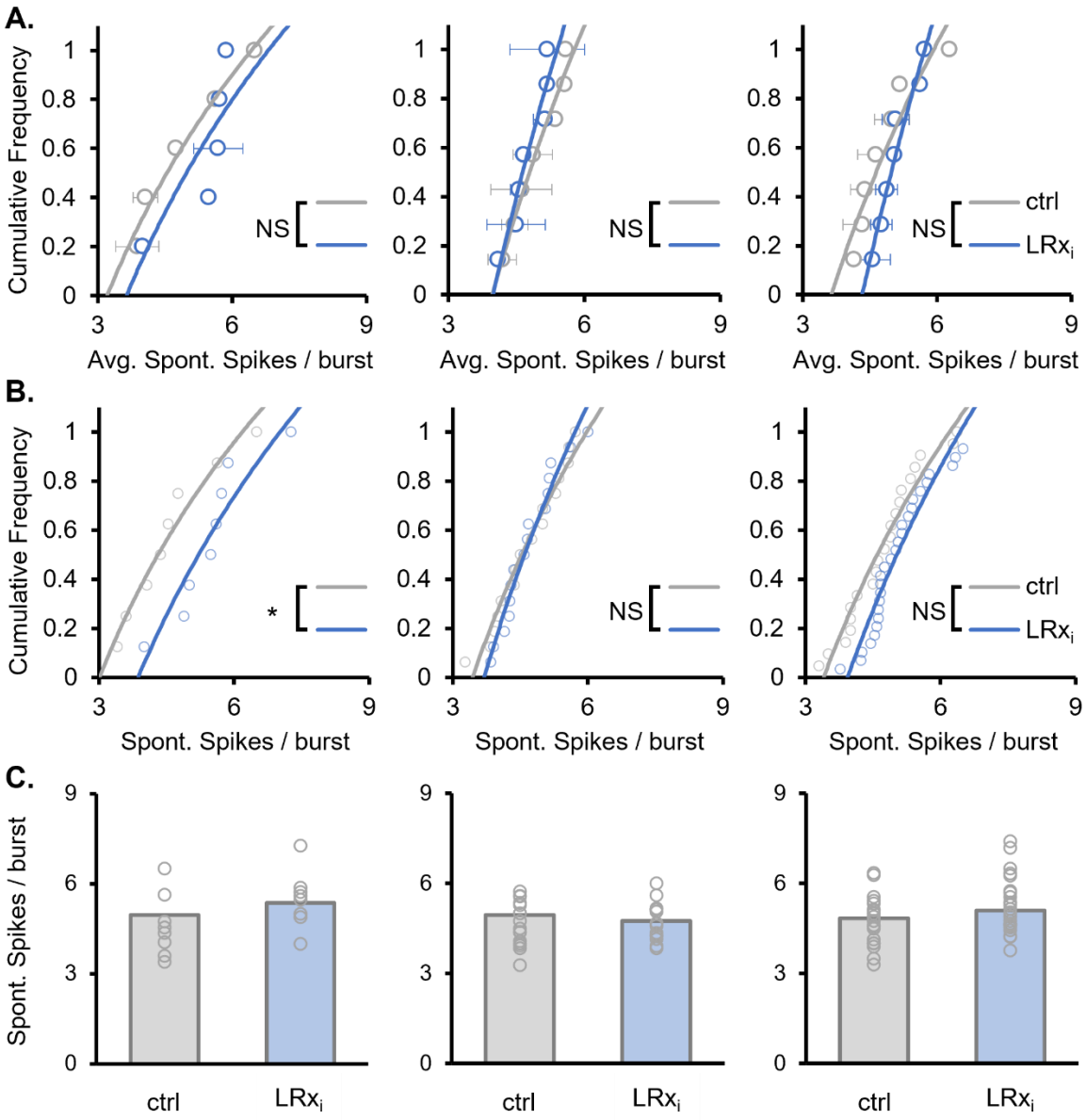

Figure 9: DE plus LRx$_i$ induces layer specific changes in spontaneous RS burst spike content

A. Cumulative distribution of spontaneous RS burst spike content averaged by mouse and layer. LRx$_i$ had no effect on the distribution of averaged spontaneous RS burst spike contents in any layer. (Wilcoxon sign ranked test [ctrl vs. LRx$_i$] NS) **B.** Cumulative distribution of all spontaneous RS units' burst spike content. LRx$_i$ caused a significant rightward shift in the distribution of spontaneous burst spike content in L2/3, but not in L4 or L5/6 (Kolmogorov-Smirnov test [ctrl vs. LRx$_i$] [L2/3] *p < 0.05; [L4] NS; [L5/6]] NS)). **C.** Averaged histograms of data points presented in B. ([ctrl] (mice, units): [L2/3] n = 5, 8; [L4] n = 7, 16; [L5/6] n = 7, 23); [LRx$_i$] (mice, units): [L2/3] n = 5, 9; [L4] n = 7, 17; [L5/6] n = 7, 30).

thalamus. Bursting inputs more reliably drive facilitating inputs onto Martinotti-type somatostatin-expressing interneurons (SST-INs) that target top-down inputs onto apical dendrites(Ji et al. 2016; Gentet et al. 2012). Increased bursting may recruit SST-INs to compensate for increased cortico-cortical connectivity induced by DE(E. Petrus et al. 2015). The noted significant shift in evoked burst spike content without an increase in averaged burst spike content in L5/6 may reflect the differing responses of L5/6 PYR subpopulations to DE (Pandey, Hardingham, and Fox 2022). Bursting input is an effective means to induce LTP or LTD in synapses. For instance, intracellular tetanization of L2/3 PYRs in A1 cortical slices generates bursts of action potentials that increase intracellular calcium and drive heterosynaptic plasticity. However, the sign of the change depends on the synaptic release probability: synapses with low release probability potentiate, while synapses with high release probability depress(C. M. Lee et al. 2012). Computational models have suggested that this form of heterosynaptic

Figure 10: DE plus LRx_i does not change spontaneous FS burst properties

A. (right) Cumulative distribution of spontaneous FS burst rate averaged by mouse across all layers. LRx_i had no effect on the distribution of averaged FS burst rate. (Wilcoxon rank sum test [ctrl vs. LRx_i] NS) (middle) Cumulative distribution of all spontaneous FS units' burst rates. LRx_i had no effect on the distribution of FS burst rate (Kolmogorov-Smirnov test [ctrl vs. LRx_i] NS). (left) Averaged histograms of data presented in A (middle). ([ctrl] (mice, units): 7, 9; [LRx_i] (mice, units): 7,12). **B. (right)** Cumulative distribution of spontaneous FS burst duration averaged by mouse across all layers. LRx_i had no effect on the distribution of averaged FS burst duration. (Wilcoxon rank sum test [ctrl vs. LRx_i] NS) **(middle) Cumulative** distribution of all spontaneous FS units' burst duration. LRx_i had no effect on the distribution of FS burst duration (Kolmogorov-Smirnov test [ctrl vs. LRx_i] NS). (left) Averaged histograms of data presented in B (middle). ([ctrl] (mice, units): 7, 9; [LRx_i] (mice, units): 7,12). **C.** (right) Cumulative distribution of spontaneous FS burst spike contest averaged by mouse across all layers. LRx_i had no effect on the distribution of averaged FS burst spike content. (Wilcoxon rank sum test [ctrl vs. LRx_i] NS) (middle) Cumulative distribution of all spontaneous FS units' burst spike content. LRx_i had no effect on the distribution of FS burst content (Kolmogorov-Smirnov test [ctrl vs. LRx_i] NS). (left) Averaged histograms of data presented in B (middle). ([ctrl] (mice, units): 7, 9; [LRx_i] (mice, units): 7,12).

Figure 10: DE plus LRx$_i$ does not change spontaneous FS burst properties

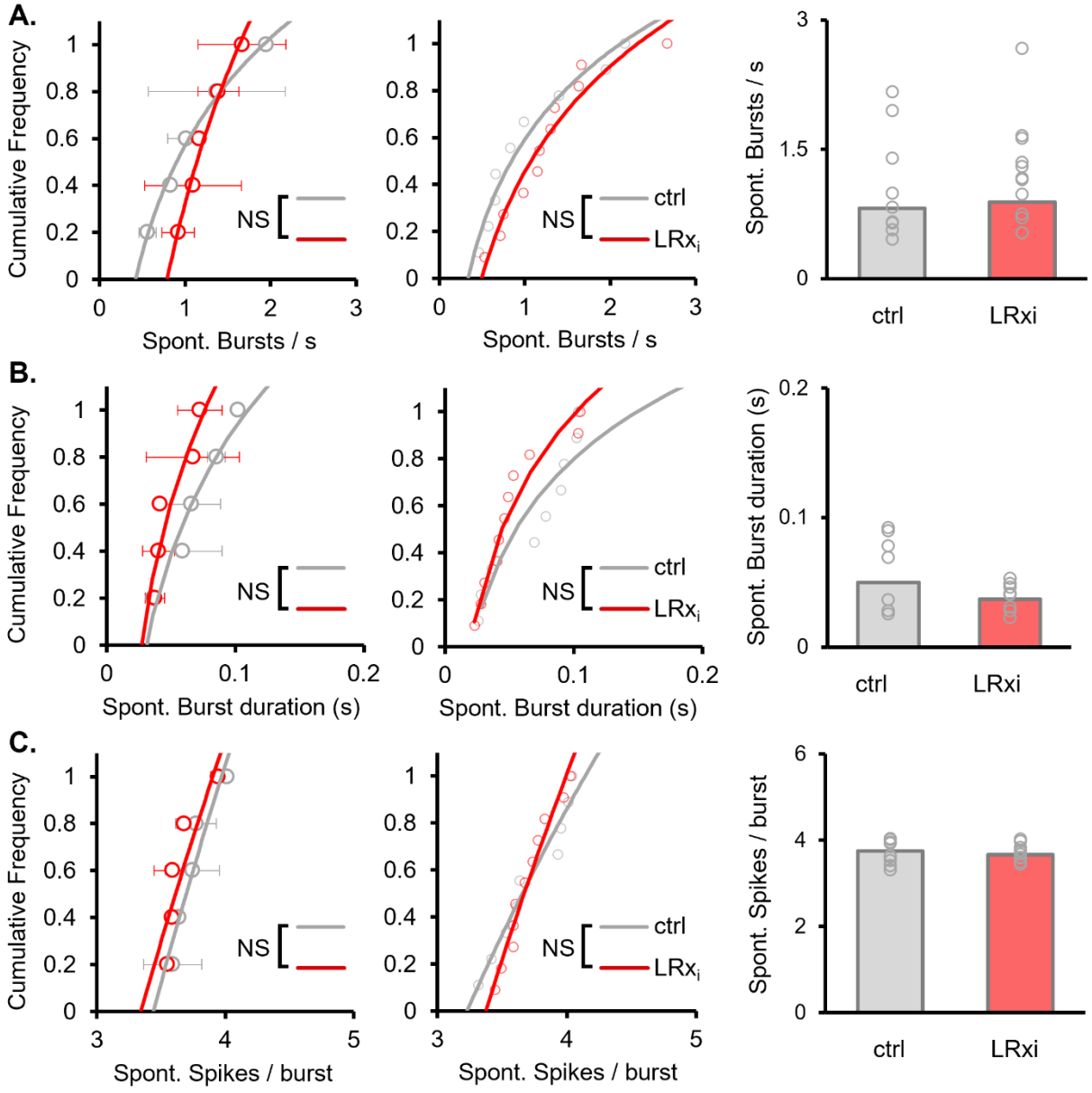

plasticity coupled with homosynaptic spike timing dependent plasticity (STDP), can prevent the saturation of LTP and LTD, preventing “runaway dynamics”(J. Chen, Lonjers, and Lee 2013). Furthermore, Hebbian plasticity is boosted by neuromodulation. Work in acute slices in mouse V1 has demonstrated that adrenergic agonists “prime” L2/3 synapses for STDP (β-adrenergic agonist isoproterenol for LTP, and α-adrenergic agonist methoxamine for LTD), and two days of DE extends the integration window for

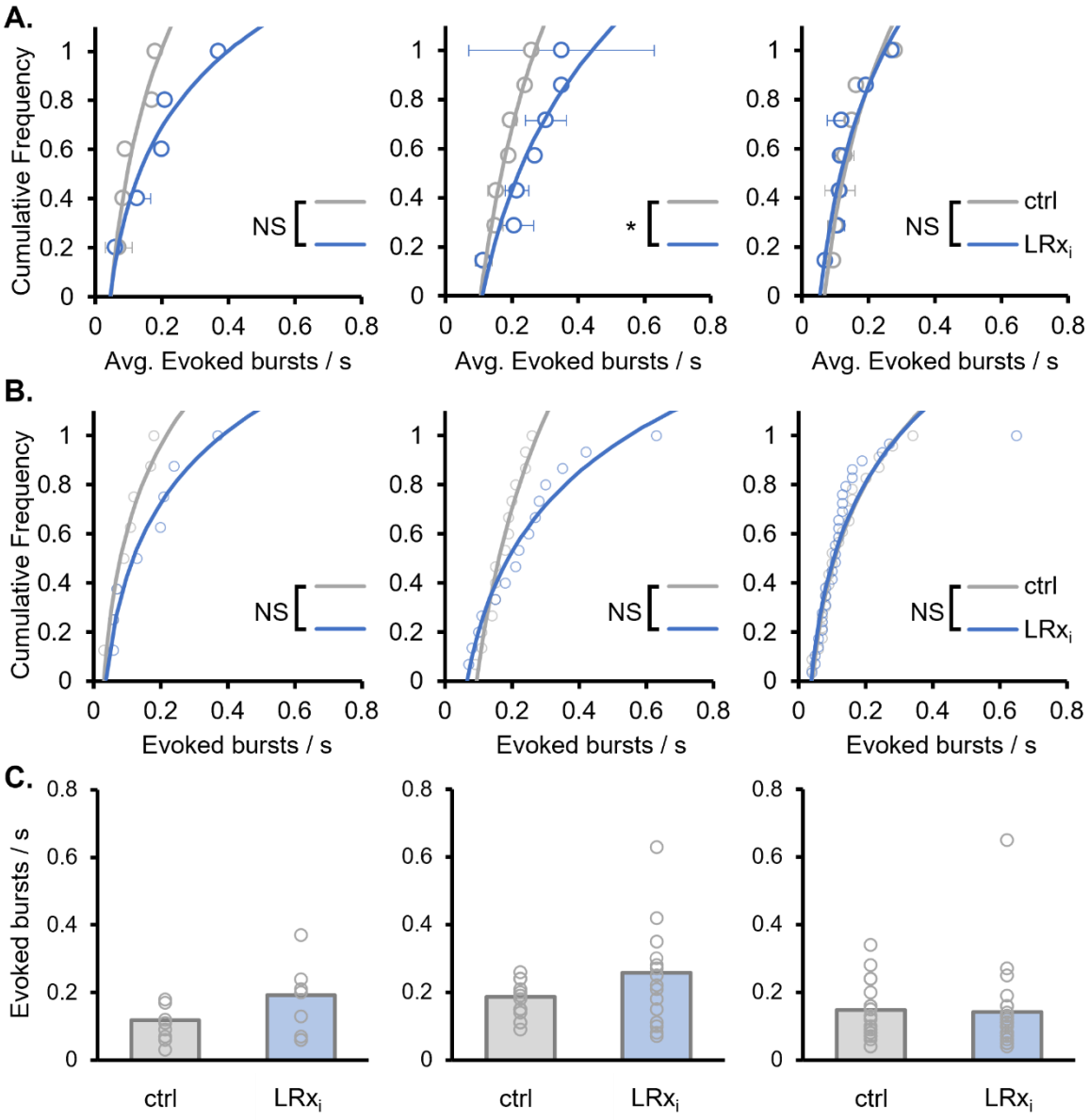

Figure 11: DE plus LRx$_i$ induces Layer-specific changes in evoked RS burst rate

A. Cumulative distribution of evoked RS burst rate averaged by mouse and layer. LRx$_i$ caused a significant rightward shift in the distribution of averaged evoked RS burst rates in L4, but not in L2/3 or L5/6. (Wilcoxon sign ranked test [ctrl vs. LRx$_i$] [L2/3] NS; [L4] *p < 0.05; [L5/6]] NS) **B.** Cumulative distribution of all evoked RS bursting units. LRx$_i$ had no effect on the distribution of evoked RS burst in any layer (Kolmogorov-Smirnov test [ctrl vs. LRx$_i$] NS). **C.** Averaged histograms of data points presented in B. ([ctrl] (mice, units): [L2/3] n = 5, 8; [L4] n = 7, 16; [L5/6] n = 7, 23); [LRx$_i$] (mice, units): [L2/3] n = 5, 9; [L4] n = 7, 17; [L5/6] n = 7, 30).

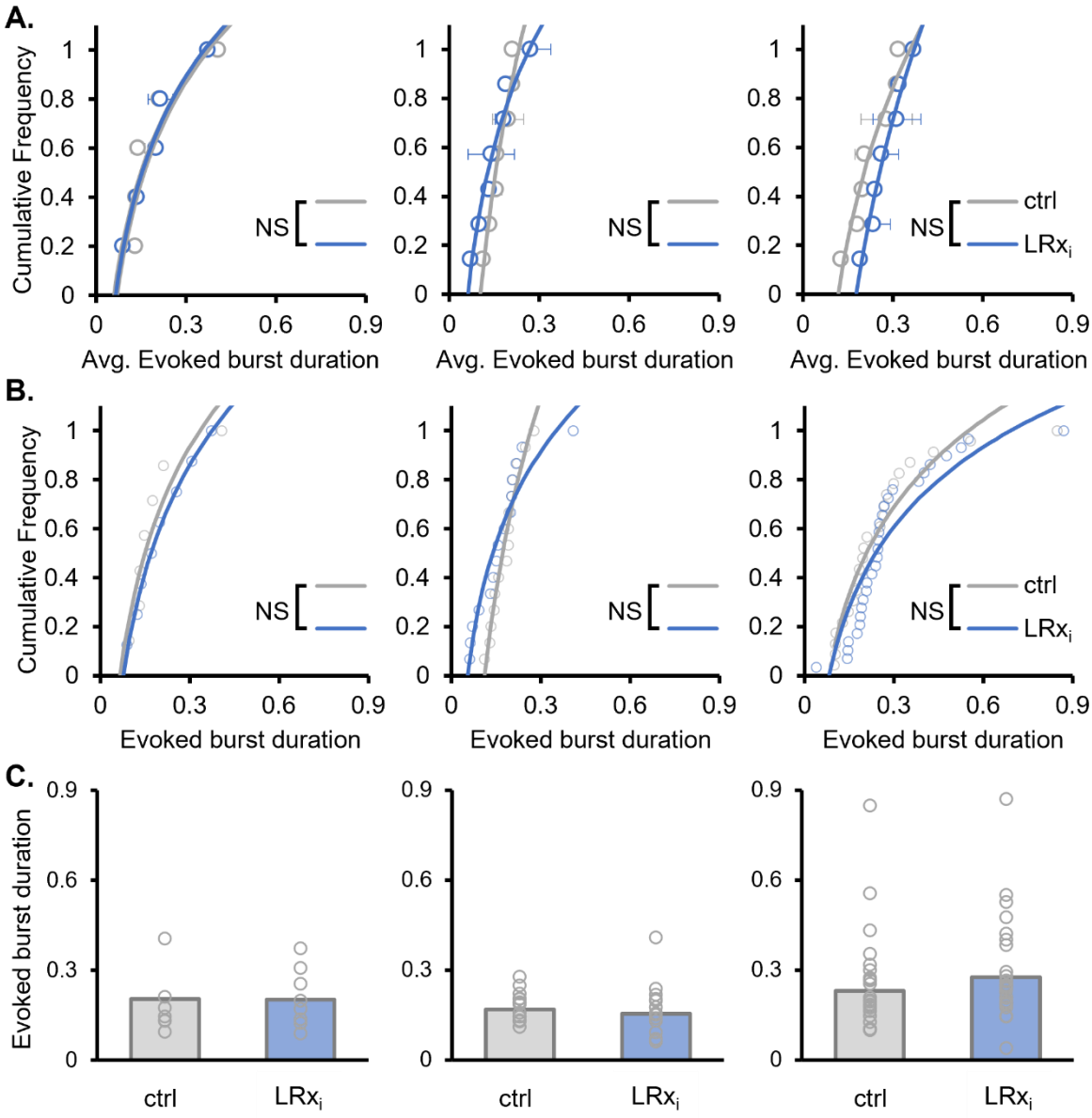

Figure 12: DE plus LRx$_i$ does not change evoked RS burst duration

A. Cumulative distribution of evoked RS burst duration averaged by mouse and layer. LRx$_i$ had no effect on the distribution of averaged evoked RS burst durations in any layer. (Wilcoxon sign ranked test [ctrl vs. LRx$_i$] NS) **B.** Cumulative distribution of all evoked RS units' burst duration. LRx$_i$ had no effect on the distribution of evoked RS burst durations in any layer (Kolmogorov-Smirnov test [ctrl vs. LRx$_i$] NS). **C.** Averaged histograms of data points presented in B. ([ctrl] (mice, units): [L2/3] n = 5, 8; [L4] n = 7, 16; [L5/6] n = 7, 23); [LRx$_i$] (mice, units): [L2/3] n = 5, 9; [L4] n = 7, 17; [L5/6] n = 7, 30).

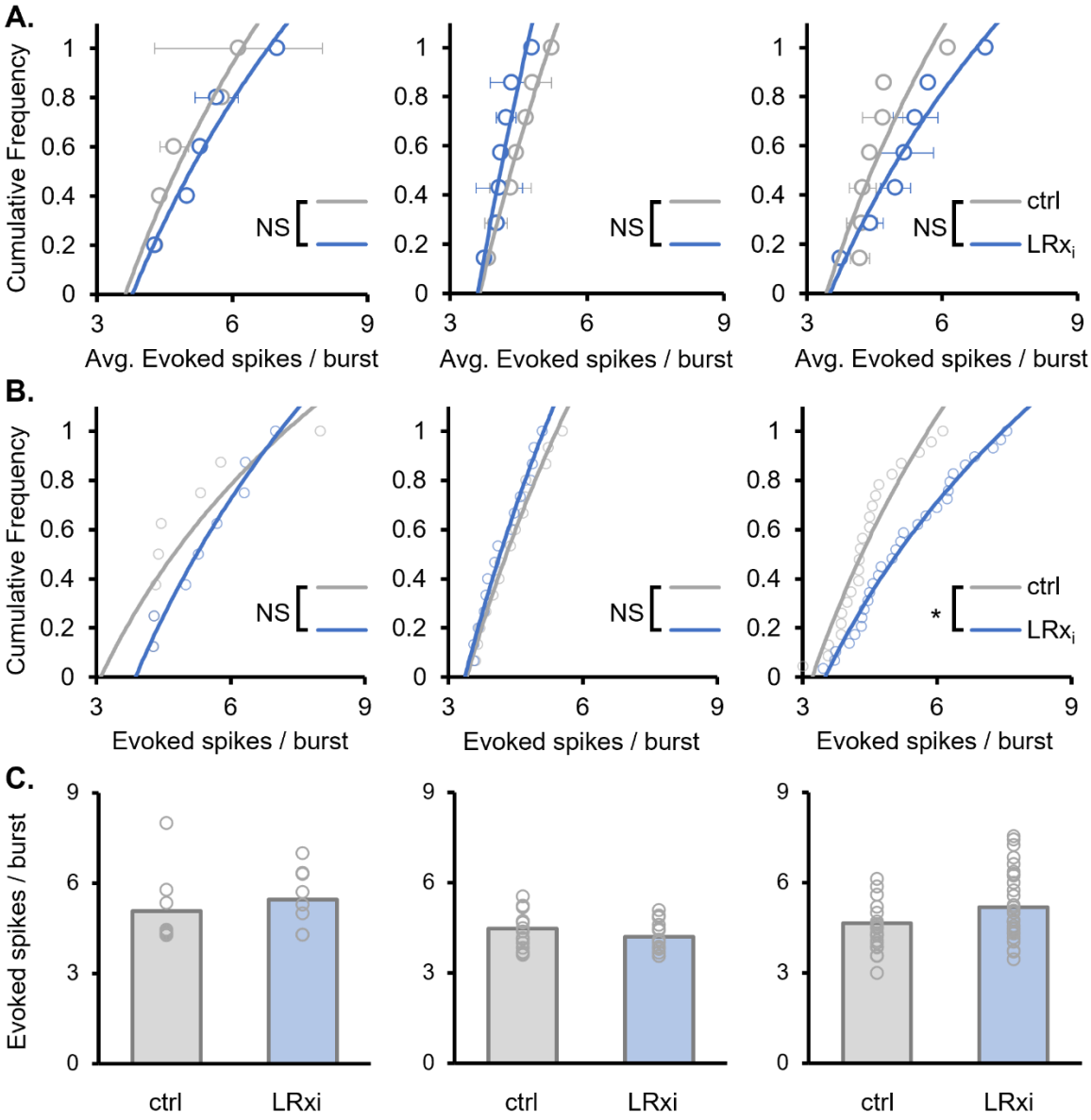

Figure 13: DE plus LRx$_i$ induces layer specific changes in evoked RS burst spike content

A. Cumulative distribution of evoked RS burst spike content averaged by mouse and layer. LRx$_i$ had no effect on the distribution of averaged evoked RS burst spike contents in any layer. (Wilcoxon sign ranked test [ctrl vs. LRx$_i$] NS) **B.** Cumulative distribution of all evoked RS units' burst spike content. LRx$_i$ caused a significant rightward shift in the distribution of evoked burst spike content in L5/6, but not in L2/3 or L4 (Kolmogorov-Smirnov test [ctrl vs. LRx$_i$] [L2/3] NS; [L4] NS; [L5/6]] *p < 0.05). **C.** Averaged histograms of data points presented in B. ([ctrl] (mice, units): [L2/3] n = 5, 8; [L4] n = 7, 16; [L5/6] n = 7, 23); [LRx$_i$] (mice, units): [L2/3] n = 5, 9; [L4] n = 7, 17; [L5/6] n = 7, 30).

Figure 14: DE plus LRx$_i$ does not change evoked FS burst properties

A. (right) Cumulative distribution of evoked FS burst rate averaged by mouse across all layers. LRx$_i$ had no effect on the distribution of averaged evoked FS burst rate. (Wilcoxon rank sum test [ctrl vs. LRx$_i$] NS) **(middle)** Cumulative distribution of all evoked FS units' burst rates. LRx$_i$ had no effect on the distribution of evoked FS burst rate (Kolmogorov-Smirnov test [ctrl vs. LRx$_i$] NS). **(left)** Averaged histograms of data presented in A **(middle).** ([ctrl] (mice, units): 7, 9; [LRx$_i$] (mice, units): 7,12). **B. (right)** Cumulative distribution of evoked FS burst duration averaged by mouse across all layers. LRx$_i$ had no effect on the distribution of averaged evoked FS burst duration. (Wilcoxon rank sum test [ctrl vs. LRx$_i$] NS) (middle) Cumulative distribution of all evoked FS units' burst duration. LRx$_i$ had no effect on the distribution of evoked FS burst duration (Kolmogorov-Smirnov test [ctrl vs. LRx$_i$] NS). **(left)** Averaged histograms of data presented in B (middle). ([ctrl] (mice, units): 7, 9; [LRx$_i$] (mice, units): 7,12). **C. (right)** Cumulative distribution of evoked FS burst spike contest averaged by mouse across all layers. LRx$_i$ had no effect on the distribution of averaged evoked FS burst spike content. (Wilcoxon rank sum test [ctrl vs. LRx$_i$] NS) **(middle)** Cumulative distribution of all evoked FS units' burst spike content. LRx$_i$ had no effect on the distribution of evoked FS burst content (Kolmogorov-Smirnov test [ctrl vs. LRx$_i$] NS). **(left)** Averaged histograms of data presented in B (middle). ([ctrl] (mice, units): 7, 9; [LRx$_i$] (mice, units): 7,12).

timing-dependent LTD from less than 100 ms to greater than 150 ms(Guo et al. 2012). Once caveat is that these plasticity effects were studied in L2/3, which unlike layer 4, retains plasticity past early development(Jiang, Treviño, and Kirkwood Alfredo 2007; Desai et al. 2002). Nonetheless, it is reasonable to predict that LRx$_i$ induces plasticity at thalamo-cortical synapses. In addition to my own data demonstrating changes in PYR neuron activity in L4 following LRx$_i$, DE followed by LRx increases MMP-9 activity at thalamocortical synapses. Similarly, LRx followed by reverse occlusion enabled rapid changes in dendritic spine density in layer 4 excitatory neurons, an anatomical correlate of synaptic plasticity(Sachiko Murase, Lantz, and Quinlan 2017; Montey and Quinlan 2011). In the absence of plasticity at synapses onto L4 PYRs, the increased bursting I observe would allow L4 PYRs to drive postsynaptic partners more reliably.

Figure 14: DE plus LRx$_i$ does not change evoked FS burst properties

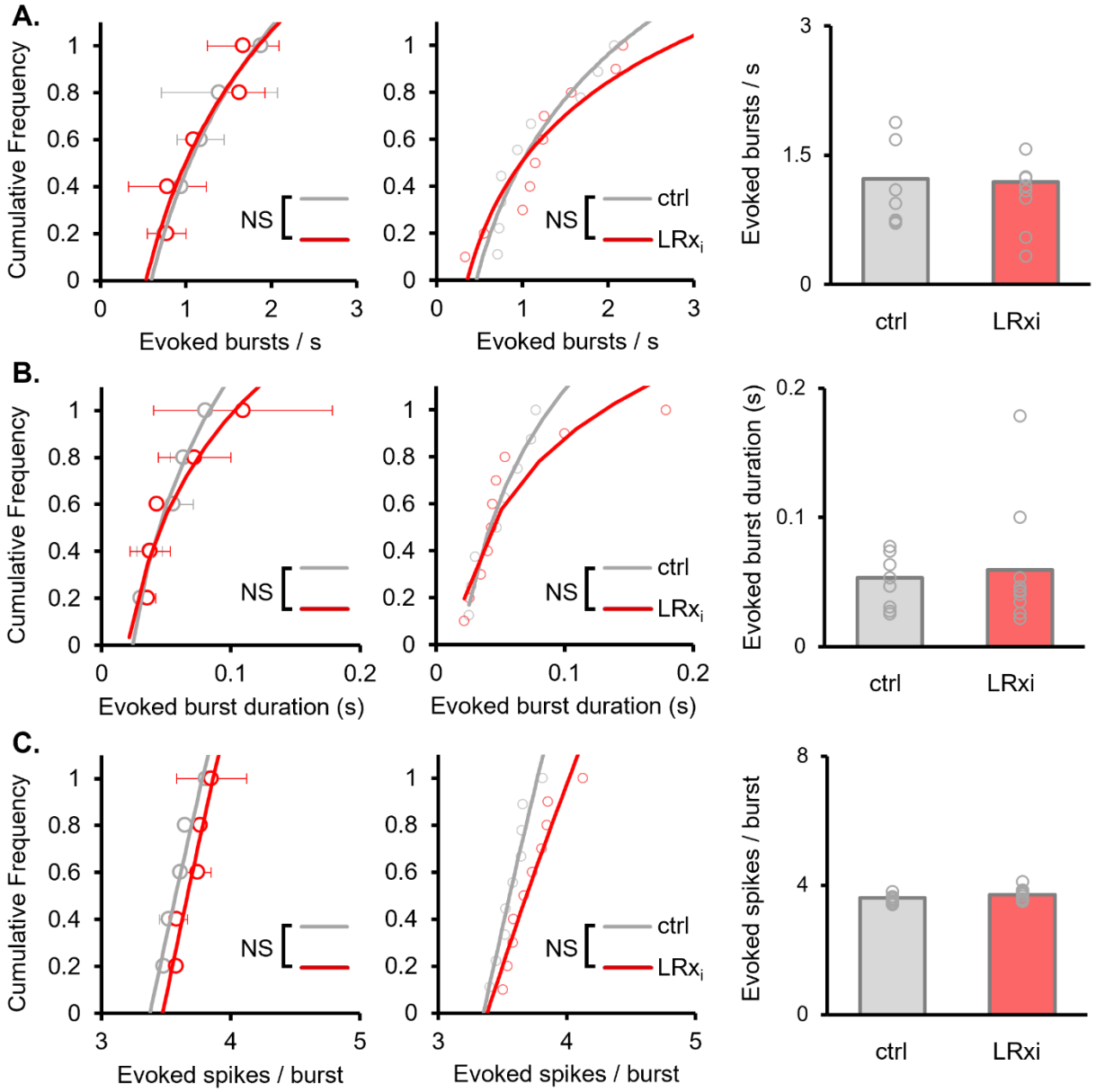

2.4.5 Layer specific potentiation during LRx$_i$

Other forms of NMDAR-dependent Hebbian plasticity could be impacted by metaplasticity induced by DE. Of particular interest is the phenomenon of stimulus-selective response potentiation (SRP). SRP is thought to induce some of the synaptic changes that are engaged by perceptual learning and is a convenient, tractable

paradigm. to study. Repeated presentation of a visual stimulus, typically a 1 Hz, reversing oriented grating, can induce robust SRP, expressed as a significant (>150%) and long-lasting increase in VEP amplitude that is selective for the characteristics of the inducing stimulus. The magnitude of the SRP also correlates with behavioral habituation to the potentiating stimulus(Frenkel et al. 2006; Montgomery et al. 2022). SRP was originally believed to be induced via LTP of TC synapses onto L4 PYRs, however genetic knockdown of the NMDA-R subunit GluN1 in L4 PYRS does not block the expression of SRP(Fong et al. 2020). It is now also appreciated that SRP requires functional NMDA-Rs on TC synapses to PV-INS(Kaplan et al. 2016). Although a full description of the identity of the synapses that are strengthened during SRP is unknown, SRP is highly sensitive to both stimulus orientation and contrast. As V1 neurons typically exhibit contrast invariant tuning to orientation, this indicates a role for contrast sensitive neurons of the LGN in SRP which is proposed to require feedback from L6 corticothalamic projections (Priebe and Ferster 2008; Niell and Stryker 2008; Montgomery et al. 2022).

In these experiments, my goal was to run a comprehensive battery of stimulus orientations to measure changes in stimulus selectivity before and after DE. However, since a wide range of stimulus parameters were used, I had no truly naïve stimuli available for a post-hoc analysis of the contribution of SRP to observed changes in evoked neuronal responses. To test for the induction of SRP during LRx_i, I compared VEP amplitudes from the control condition and from LRx_i. I detected a significant increase in the amplitude of the L4 VEP during LRx_i. L4-specific increases in VEP amplitude are a hallmark of SRP, and may be induced with as little as one round of

repetitive visual stimulation, and can last for weeks if not longer(Fig.15)(Frenkel et al. 2006; Montgomery et al. 2022). While increased VEP amplitude can be attributed to dark adaptation, which potentiates electro retinogram responses (ERGs) and increases the amplitude of VEPs to flashing stimuli, it has also been argued that rapidly reversing stimuli (such as a 1 Hz reversing grating) can rapidly light adapt a previously dark adapted mouse(Walz 2013; Ridder and Nusinowitz 2006). It is worth noting, however, that SRPs is absent at low contrast (below 12%), and spontaneous recordings that are the main focus of this project were performed at 0% contrast (Frenkel et al. 2006). It is possible but unlikely that SRP is responsible for the increased evoked RS firing rate described in section 2.5.2, as SRP only increase reversing grating-evoked firing rates at peak latency of the negative going VEP, with little impact on averaged firing rates(Montgomery et al. 2022). It is interesting to note however, that if PV-IN NMDA-R function is necessary for SRP, that DE-induced changed to V1 function do not somehow occlude synaptic changes that mediate the SRP effect at these synapses.

2.4.6 One day of subsequent LRx reverses layer-specific changes in V1 activity.

Previously, we have observed increased spontaneous and evoked activity as late as six hours after LRx(Sachiko Murase, Lantz, and Quinlan 2017). However, changes in mEPSC amplitude induced via sensory deprivation have been shown to reverse within 24 hours (Goel and Lee 2007; Chokshi et al. 2019; Emily Petrus et al. 2011). It is possible that differences between that the intact brain of an awake mouse responds is more capable of maintaining increased spontaneous activity during LRx. Alternatively, decreased spontaneous activity during LRx may function as a homeostatic mechanism not unlike the homeostatic increase noted during DE, and may require more than six

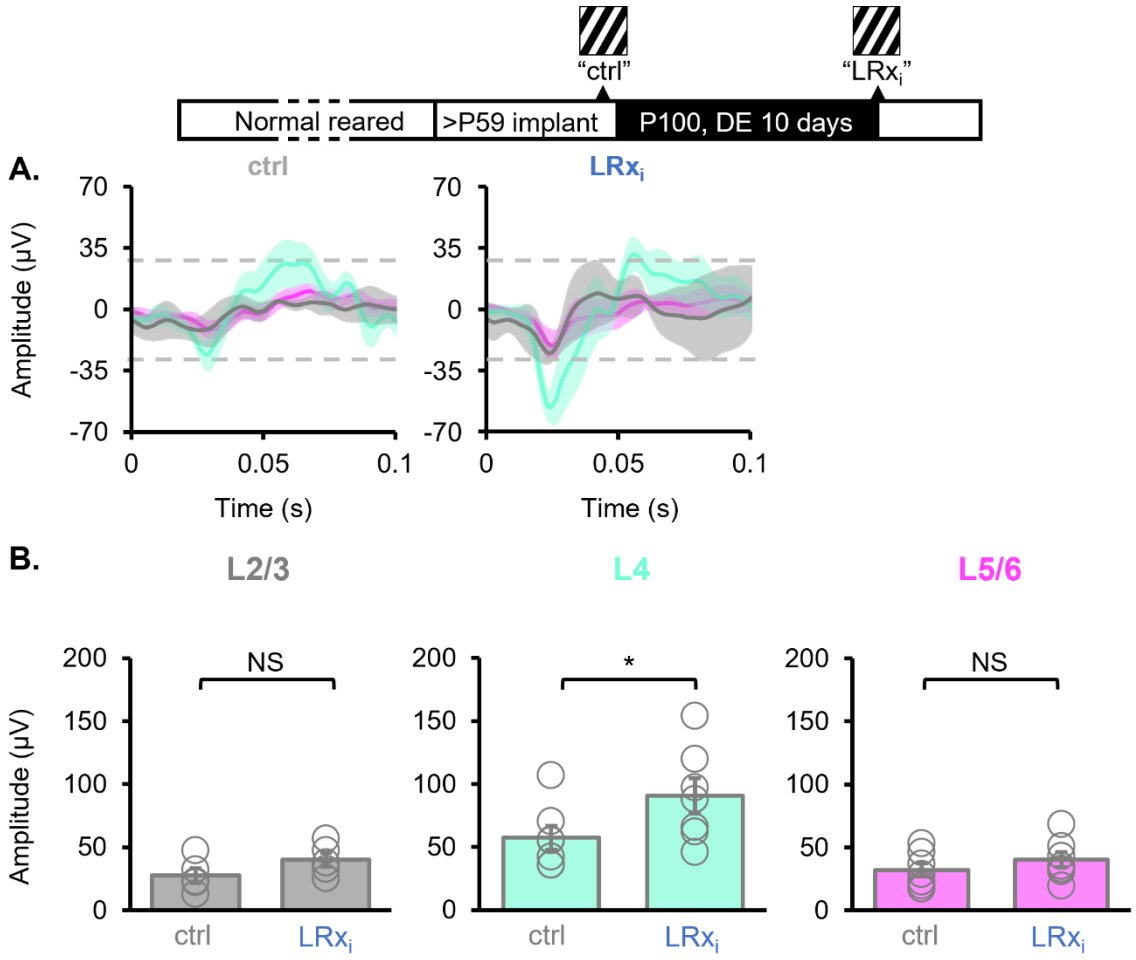

Figure 15: Layer 4 VEP potentiated following LRx_i

(top) Experimental timeline. **A.** Layer-averaged VEPs +/- SEM recorded before DE and during LRx_i. The horizontal grey dashed line indicates the original amplitude of the L4 VEP. **B.** Quantification of VEP amplitude by condition (mean +/- SEM). L4 VEPs significantly potentiated during LRx_i. (Wilcoxon sign ranked test [ctrl vs. LRx_i] L4 *$p < 0.05$). (n = 7 mice).

hours to manifest. To test the hypothesis that a subsequent day of LRx reduces spontaneous and evoked activity versus LRx_i *in vivo*, Subjects were given a second session of dark, and I recorded spontaneous and evoked activity prior to DE, and after one subsequent day of LRx (LRx_s). In normal reared mice, there is a refractory period for rejuvenation of plasticity via DE and LRx that begins at P45(S. Huang et al. 2010).

Since it is not known if a similar refractory period may exist for a second session of DE, I erred on the side of caution and waited 70 days before initiating the second DE session.

I also changed the visual stimulus parameters, and orthogonal orientations were used in some experiments to avoid a contribution by SRP although I cannot rule out the persistence of SRP from the earlier phase of this experiment (Frenkel et al. 2006). I detected no significant change in VEP amplitude following LRx_i and LRx_s in any cortical layer (Fig.16). The lack of further potentiation is not likely due to saturation of the VEP response (Frenkel et al. 2006). Overall, this result suggests that the increase in VEP amplitude following the first DE was not due to dark adaptation, but due to SRP.

Next, I measured changes in evoked and spontaneous RS firing rates during LRx_s. No significant difference was detected between averaged spontaneous RS rates nor the distribution of spontaneous RS rates (Fig.17). This result aligns well with previously observed findings in acute brain slices demonstrating the rapid reversal of circuit changes induced during DE, including reversal of potentiated mEPSC amplitude (Goel and Lee 2007; Chokshi et al. 2019; Emily Petrus et al. 2011; Pandey, Hardingham, and Fox 2022). Interestingly, while no significant change was detected in averaged evoked RS firing rates, there was a significant leftward shift in the distribution of L2/3 and L5/6 firing rates (Fig.18B). Again, the discrepancy between distribution and averages in L5/6 may be attributable to the distinct subpopulations of PYRs in that cortical region (Pandey, Hardingham, and Fox 2022). It should be noted that only two of the five subject mice used in this part of the study had stable L2/3 units during the control condition, so this shift in L2/3 distribution may be due to sampling bias. No

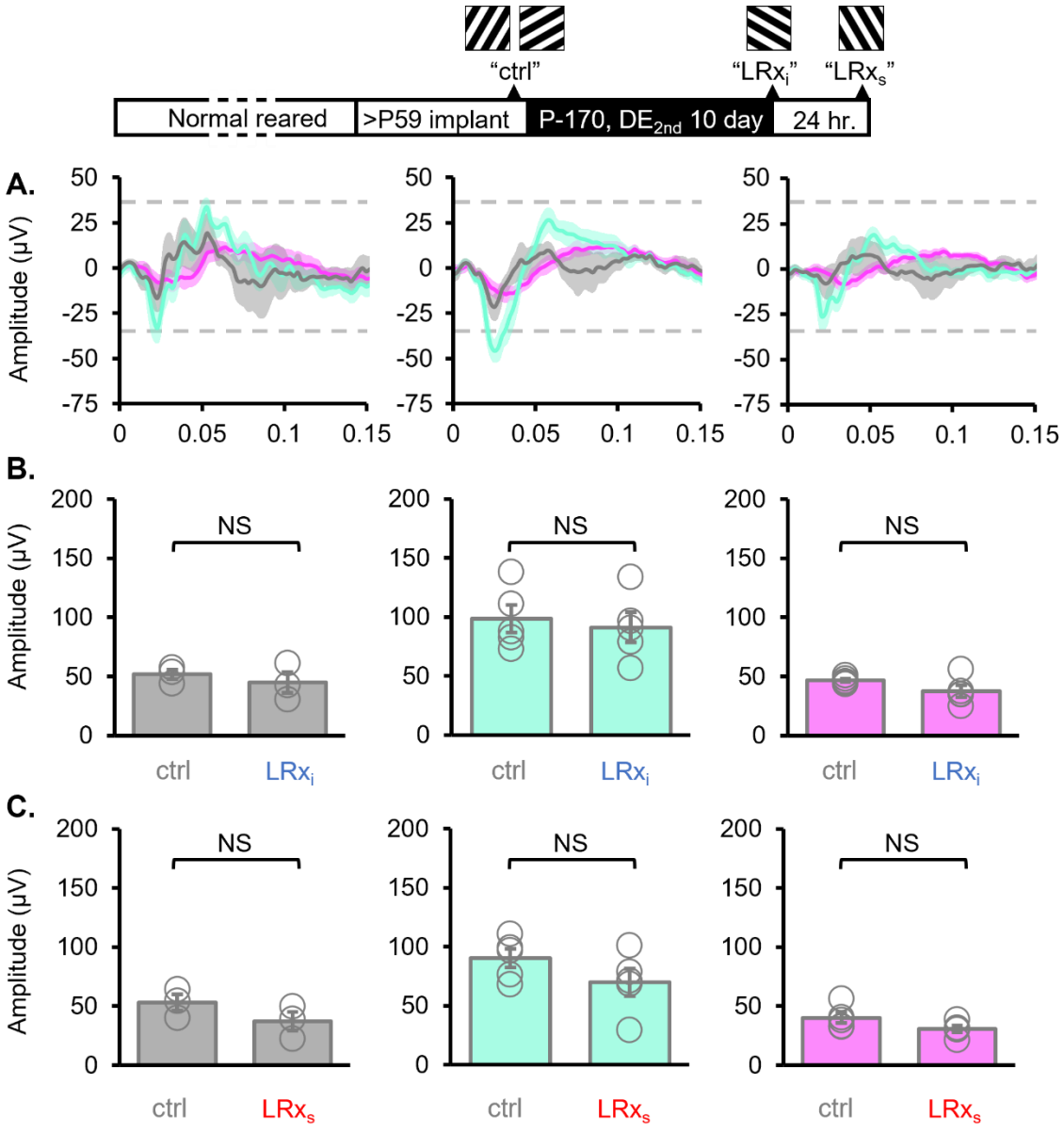

Figure 16: VEP amplitudes are not directly changed by LRx$_i$ or LRx$_s$

(top) experimental timeline. **A.** Layer-averaged VEPs +/- SEM before DE$_{2nd}$ and during LRx$_i$ and LRx$_s$. The horizontal grey dashed line indicates the amplitude of the L4 VEP prior to DE$_{2nd}$. **B.** Quantification of VEP amplitude by condition (mean +/- SEM). VEP amplitudes were not significantly different during LRx$_i$. (Wilcoxon signed rank test). **C.** VEP amplitudes were not significantly different during LRx$_s$. (Wilcoxon signed rank test). (n = 5 mice)

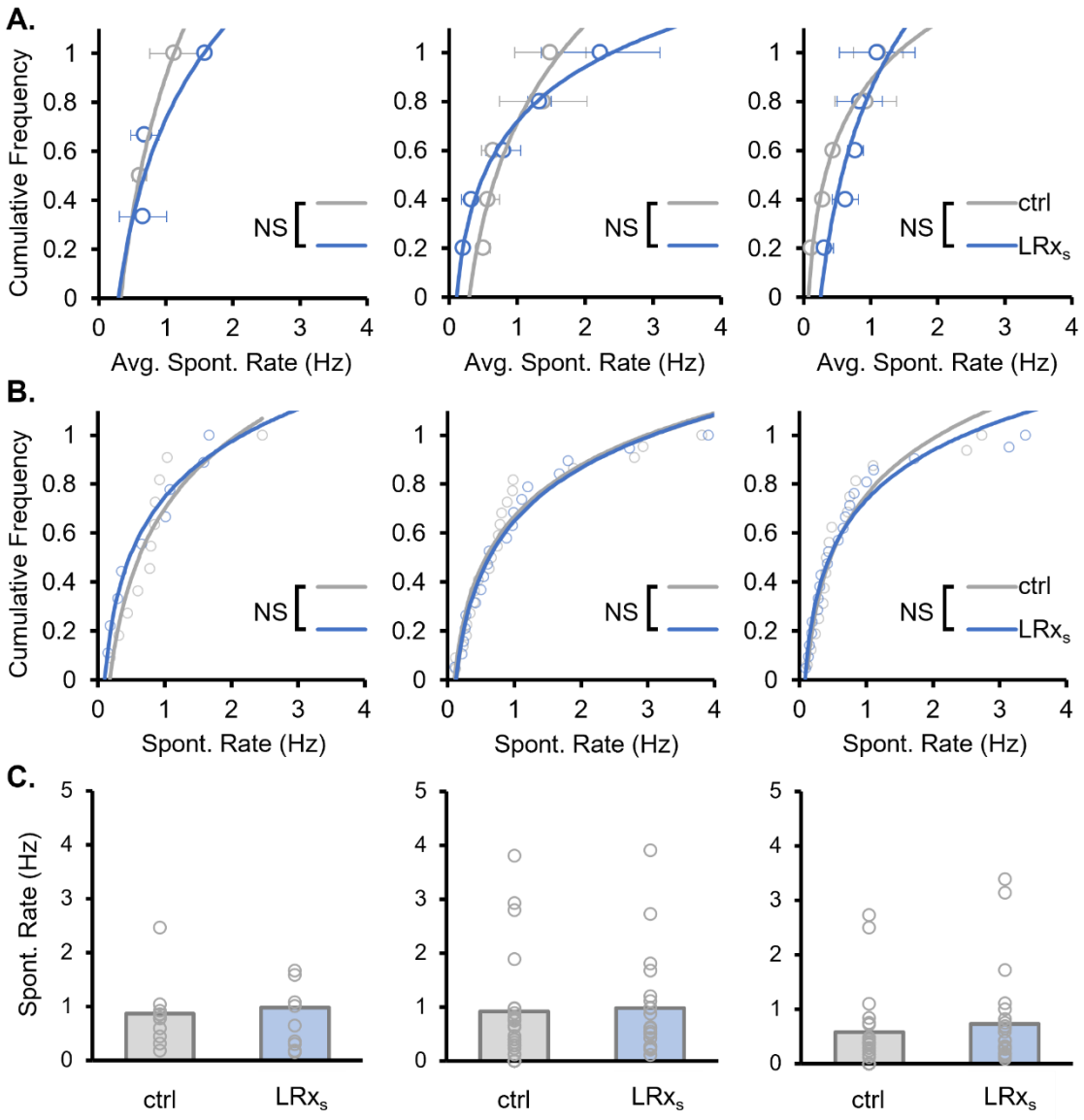

Figure 17: Spontaneous RS firing rate returns to baseline following one subsequent day of LRx

A. Cumulative distribution of spontaneous RS firing rates averaged by mouse and layer. No significant shift in the distribution of averaged spontaneous RS firing rates was detected following one subsequent day of LRx. (Wilcoxon sign ranked test [ctrl vs. LRx_s] NS) **B.** Cumulative distribution of all spontaneous RS units. No significant shift was detected in the distribution of spontaneous RS units following one subsequent day of LRx (Kolmogorov-Smirnov test [ctrl vs. LRxs] NS). **C.** Averaged histograms of data points presented in B. ([ctrl] (mice, units): [L2/3] n = 2, 11; [L4] n = 5, 31; [L5/6] n =5, 23); [LRx_i] (mice, units): [L2/3] n = 2, 11; [L4] n = 5, 19; [L5/6] n = 5, 21).

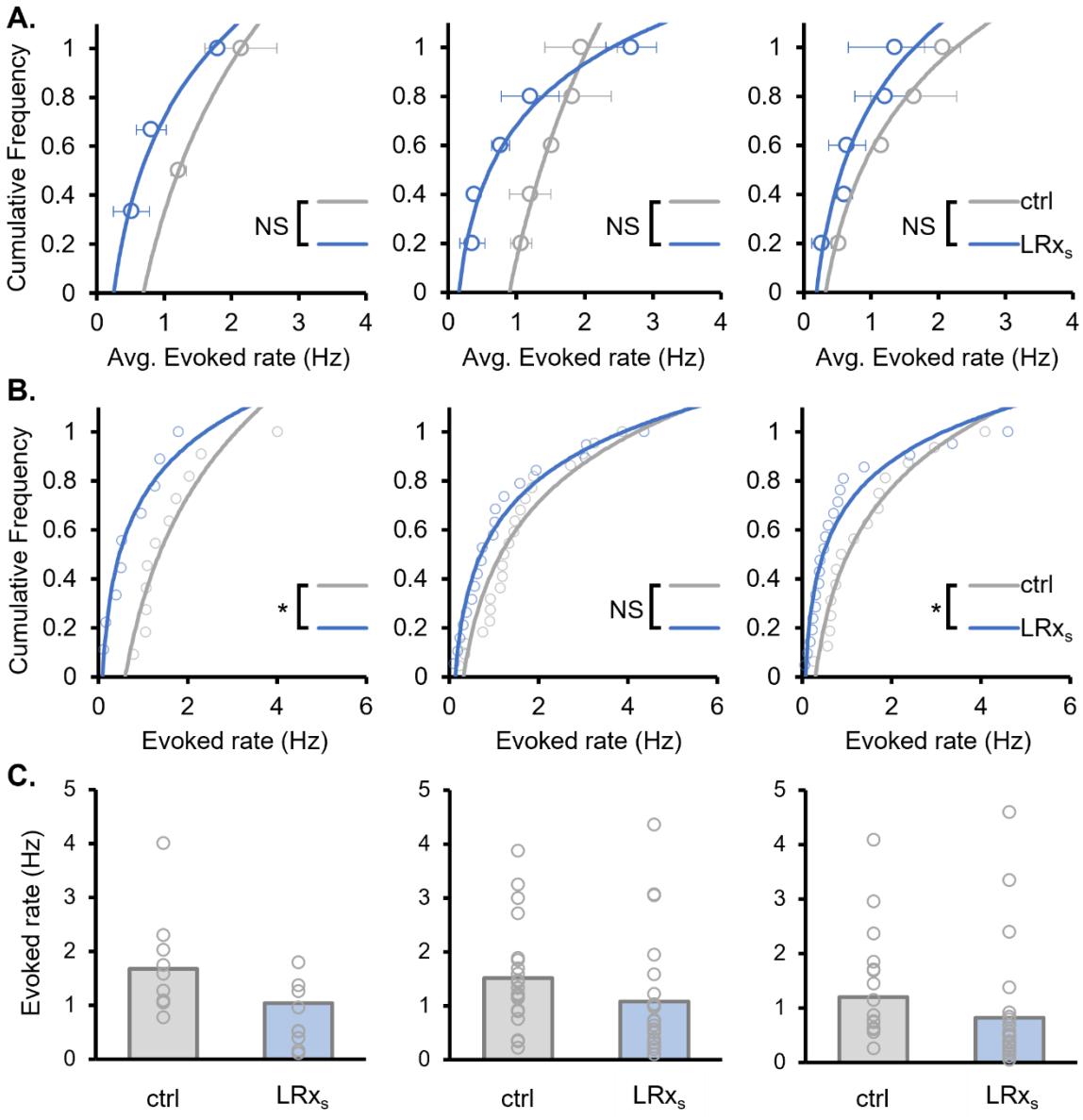

Figure 18: LRx$_s$ induced layer-specific shift in evoked RS firing rates

A. Cumulative distribution of evoked RS firing rates averaged by mouse and layer. No significant shift in the distribution of averaged evoked RS firing rates was detected following one subsequent day of LRx. (Wilcoxon sign ranked test [ctrl vs. LRx$_s$] NS) **B.** Cumulative distribution of all evoked RS units. One day of LRx$_s$ caused a significant leftward shift in the distribution of evoked RS units in L2/3 and l5/6, but not in L4 (Kolmogorov-Smirnov test [ctrl vs. LRx$_s$] [L2/3] *p < 0.05; [L4] NS; [L5/6]] *p < 0.05). **C.** Averaged histograms of data points presented in B. ([ctrl] (mice, units): [L2/3] n = 2, 11; [L4] n = 5, 31; [L5/6] n =5, 23); [LRx$_s$] (mice, units): [L2/3] n = 2, 11; [L4] n = 5, 19; [L5/6] n = 5, 21).

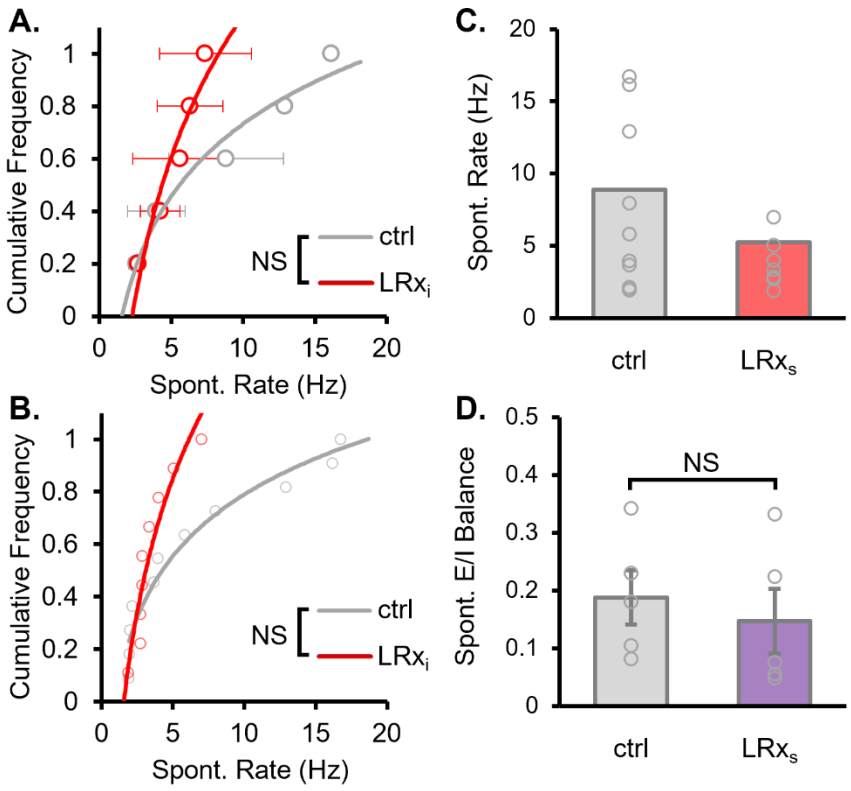

Figure 19: Spontaneous FS firing rate and E/I balance return to baseline following one subsequent day of LRx

A. Cumulative distribution of spontaneous FS firing rates averaged by mouse across all layers following one subsequent day of LRx. No significant change was detected following LRx_s. (Wilcoxon rank sum test [ctrl vs. LRx_s] [spont. rate] NS). **B.** Cumulative distribution of all spontaneous FS units. No significant shift was detected in the distribution of spontaneous FS units. (Kolmogorov-Smirnov test [ctrl vs. LRx_s] NS). **C.** Averaged histograms of data presented in B. ([ctrl] (mice, units): 5, 10; [LRxs] (mice, units): 5,9). **D.** Histogram of average spontaneous excitatory / inhibitory balance presented as mean +/- SEM. No significant change was detected following LRx_s (Wilcoxon rank sum test [E/I ratio] NS.)

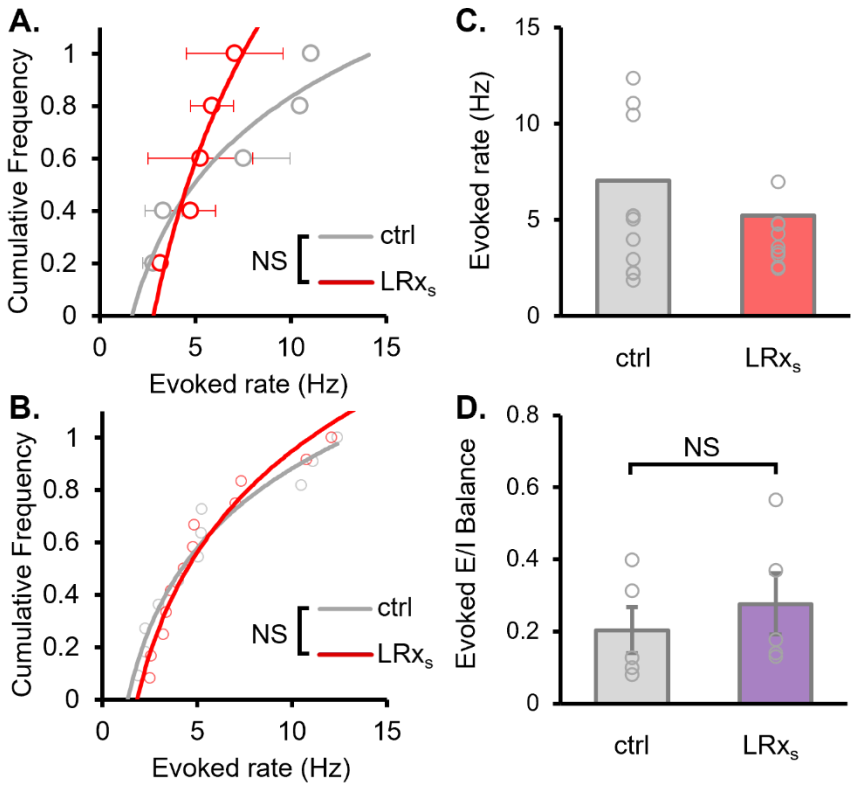

Figure 20: Evoked FS firing rate and E/I balance return to baseline following one subsequent day of LRx

A. Cumulative distribution of evoked FS firing rates averaged by mouse across all layers following one subsequent day of LRx. No significant change was detected following LRx_s. (Wilcoxon rank sum test [ctrl vs. LRx_s] [spont. rate] NS). **B.** Cumulative distribution of all evoked FS units. No significant shift was detected in the distribution of evoked FS units. (Kolmogorov-Smirnov test [ctrl vs. LRx_s] NS). **C.** Histogram of average evoked excitatory / inhibitory balance presented as mean +/- SEM. No significant change was detected following LRx_s (Wilcoxon rank sum test [E/I ratio] NS.) D. Averaged histograms of data presented in B. ([ctrl] (mice, units): 5, 10; [LRx_s] (mice, units): 5,9).

change was detected in evoked or spontaneous FS firing rate, and E/I balance (Fig. 18 – 20). Previously, the Quinlan lab has shown that following ten days of DE, sensitivity to monocular deprivation remains elevated after as many as three days of LRx(He, Hodos, and Quinlan 2006). This raises the intriguing possibility that decreased excitability following one day of LRx is a necessary component of the reactivation of ODP during LRx. I will be exploring this possibility in Chapter 3.

Chapter 3: The effect of prolonged hyperexcitability on the reactivation of ocular dominance plasticity during light reintroduction

3.1 Introduction

PV-INs play a major role in the initiation of the CP for ocular dominance plasticity by controlling the excitability of V1 pyramidal neurons. Early in postnatal development, prior to the CP, pyramidal neurons are hyper-excitable and unable to express ODP; activity-dependent expression of BDNF by PYRs during early visual experience enhances excitatory drive onto PV-INs, possibly via upregulation of the immediate early gene NARP, thereby increasing inhibitory tone, decreasing neuronal excitability, and enabling the expression of ODP(Z. J. Huang et al. 1999; Matsuda et al. 2021; Mariga et al. 2015). In support of this model, manipulations that decrease the recruitment of PV-INs early in development, such as constitutive knockdown of NARP, renders V1 hyper-excitable and unable to express ODP, whereas increasing PV-IN recruitment during the CP pharmacologically with NRG1 decreases V1 excitability, accelerating the time course of the CP and causing its precocious closure(Yu Gu et al. 2013; Y. Gu et al. 2016). Conversely, blocking PV-IN recruitment in adult mice via pharmacological inhibition of the NRG1 receptor ErbB4, increases pyramidal neurons excitability and enables the expression of ODP well past the CP(Y. Gu et al. 2016).

Interestingly, the same pathways that modify the time course of the CP for the induction of ODP via PV-IN recruitment also mediate V1 circuit changes in response to MD. More specifically, MD and DE both decrease excitatory drive onto PV-INs: following one day of contralateral MD, single eye-evoked responses of L2/3 PYRs are unexpectedly elevated despite the loss of patterned contralateral visual input, while

binocularly evoked L2/3 PV-IN firing rates are decreased by half(Kuhlman et al. 2013). This work in acute V1b brain slices demonstrated a decrease in EPSC amplitude onto L2/3 PV-INs by glutamate uncaging in L4 and L5a following one day of MD, but not in L2/3(Kuhlman et al. 2013). The decrease in PV-IN firing rate is transient and eye specific: by the third day, PV-IN recruitment via stimulation of the non-deprived (ipsilateral) eye return to normal while stimulation of the deprived (contralateral) eye remains decreased (Kuhlman et al. 2013). The transient reduction in PV-IN-mediated inhibition during one day of MD permits the expression of ODP: increasing inhibition with diazepam during MD blocked ODP in CP-aged mice, whereas targeted chemogenetic suppression of PV-IN inhibition in post-CP aged mice (P35) with Gi-DREADD (discussed later in this chapter) reactivated ODP(Kuhlman et al. 2013).

We have recently proposed a mechanism for the MD-induced reduction in PV-IN firing rate. MD induces the transient disconnection of short range (<25μm) intralaminar (i.e., within L2/3) excitatory connections onto PV-INs(Severin et al. 2021). The decrease in intralaminar L2/3 PYR → L2/3 PV-IN excitatory connectivity was blocked by overexpression of NARP but not by exogenous application of NRG1(Severin et al. 2021). Interestingly, the UV-laser glutamate uncaging paradigm used by Kuhlman et al. (2013) to stimulate V1b has a spatial resolution of ~ 50 to 100μm in L2/3, and closer to 100μm in other cortical layers, and therefore would not detect short range disconnections of L2/3 PYR → L2/3 PV-INs(Kuhlman et al. 2013; G. M. G. Shepherd, Pologruto, and Svoboda 2003). Previously, Kuhlman et al. (2013) also showed a decrease in L4 and L5a recruitment of L2/3 PV-INs during MD, as did Sun et al. (2016) using the same technique. Conversely, work from the McGee lab using glutamate

uncaging detected most synaptic input to PV INs from L4, and very little in L2/3 or L5/6 (mice aged P35 – P38)(Stephany et al. 2014). Severin et al. (2021) casts doubt on the impact of changes in L4 PYR excitation onto L2/3 PV-INs in the response to MD: following one day of MD, no decrease was detected in L4 PYR → L2/3 PV-IN connection strength assessed via electrical or optogenetic stimulation in L4 (via Scnn1a-cre, aka L4-cre) of V1m. The MD-induced disconnection of L2/3 PYR → L2/3 PV-IN was observed in both V1b and V1m(Severin et al. 2021). It is possible this discrepancy is due to cortical region, and that disconnection between L4 PYRs and L2/3 PV-INs is more pronounced in V1b. Alternatively, in experiments utilizing UV uncaged glutamate, activation of apical dendrites on PYRs is more sensitive to the focal plane of the UV laser than PYR somas, and the apical dendrites of L5 PYRs were sensitive to uncaged glutamate as far as 75μm from the soma. This raises the possibility that activation patterns induced by glutamate uncaging in L2/3 of V1 are due to activation of apical dendrites on L4 PYRs(Kötter et al. 2005). Interestingly, delivery of NRG1 increases excitatory connections between L4 PYRs and L2/3 PV-INs in both V1b and V1m, and this effect is peaks after one day of MD(Severin et al. 2021; Sun et al. 2016). Thus different signaling pathways regulate intra and interlaminar excitatory input onto L2/3 PV-INs, and are differentially recruited by MD(Severin et al. 2021). Strikingly, both the NARP and NRG1/Erbb4 pathways are activity-dependent, NMDA-R-independent, and impact only intracortical PV-IN connectivity(Severin et al. 2021; Sun et al. 2016).

In adult mouse prefrontal cortex, excitatory TC connections onto PV-INs are the only inputs that exhibit NMDA-R currents(Lewis et al. 2022). Alternatively, Slice experiments in V1 of CP-aged (P25) mice detected no evidence of NMDA-R in FS

interneurons in L4(Kloc and Maffei 2014). Genetic knockdown of NMDA-R function in V1 PV-INs blocks the expression of SRP, indicating that a third route by which PV-IN recruitment is regulated by sensory input via traditional Hebbian mechanisms, although it may be specific to PV-INs in L5/6(Kaplan et al. 2016; Montgomery et al. 2022)(Lewis et al. 2022). Interestingly, knock-out of NMDARs in PV-INs blocks the expression of ODP, but not SRP (Kaplan et al. 2016). Conversely, genetic knockdown of NARP blocked ODP and the induction of SRP via 5 Hz visual stimulation, but not 10 Hz visual stimulation(Yu Gu et al. 2013).

The work described above utilizes genetic or pharmacological manipulations of excitatory input onto PV-INs to investigate their role in ODP described. Manipulation of PV-IN output can also be investigated by Cell-type specific expression of inhibitory chemogenetic Gi-DREADD receptors (Designer Receptors Exclusively Activated by Designer Drugs). Gi-DREADD, a mutant G protein-coupled muscarinic M4 receptor activate an internal metabolic signaling cascade mediated by intracellular G protein effectors $G_{\alpha}i$ and $G_{\beta\gamma}$ when bound by the otherwise inert (see section 3.3) DREADD ligand clozapine-N-oxide (CNO) (Roth 2016). The functional consequence of Gi-DREADD activation includes suppression of neuronal activity via $G_{\beta\gamma}$-mediated activation of hyperpolarizing G protein-couped inward rectifying potassium channels (GIRKs) as well as $G_{\alpha}i/G_{\beta\gamma}$ -mediated inhibition of presynaptic release(Armbruster et al. 2007; Stachniak, Ghosh, and Sternson 2014; Wettschureck and Offermanns 2005). In *ex vivo* acute V1 slices, activation of Gi-DREADD via bath application of CNO significantly reduces current-evoked firing rates of infected PV-INs, and *in* vivo extracellular recordings show that the decreased excitability of PV-INs following Gi-

DREADD activation disinhibits V1, causing significant increases in VEP amplitude and evoked (RS) PYR firing rates and (Kaplan et al. 2016). In Kuhlman et al., 2013, Gi-DREADD activation in PV-INs decreased visually evoked calcium responses in infected PV-INs; in post-CP (P35) mice, three days of MD coupled with Gi-DREADD activation in PV-INs decreased the amplitude of deprived (contralateral) eye calcium responses, indicating suppression of PV-IN inhibition with Gi-DREADD is sufficient to reactivate ODP in post-CP mice(Kuhlman et al. 2013). Similarly, targeted suppression of PV-INs output with Gi-DREADD has also been used in primary auditory cortex (A1) of adult rats to reactivate CP plasticity and enable the plasticity of tonotopic maps in response to passive tone exposure, a type of receptive field plasticity that shares some features of ODP (Cisneros-Franco and De Villers-Sidani 2019).

Prolonged DE in adulthood also disinhibits V1, likely via activity dependent decreases in the recruitment of PV-INs. Following DE, (FS) PV-INs firing rates are reduced versus control, and this effect is reversed by increasing excitatory drive onto PV-INs with treatment by NRG1(Y. Gu et al. 2016). DE-induced metaplasticity is blocked by increasing excitatory drive onto PV-INs with NRG1, or enhancing inhibition with the benzodiazepine, implying that decreased inhibition enables the subsequent increase in spontaneous (RS) PYR firing rates necessary for DE-induced metaplasticity(S. Huang et al. 2015; 2010; Bridi et al. 2018).

The homeostatic increase in V1 pyramidal neurons induced by brief DE can by reversed following one day of LRx: one day of LRx reverses the DE-induced increase in intra-L2/3 synaptic strength via mGluR5-depednent LTD(Chokshi et al. 2019). While the most abundant form of AMPA-R contains at least one GluA2, rendering it calcium

impermeable, homomeric GluA1-only AMPA-Rs are inward-rectifying calcium-permeable receptors that have been implicated in the induction of LTP(Hansen et al. 2021; Park et al. 2018). In four-week-old rats, seven days of DE increased the ratio of GluA1 to GluA2-containing AMPA-Rs in L2/3, and this change was likewise reversed following two days of LRx(Goel et al. 2006). Similar effects have been noted in deep cortical layers: two days of LRx reverses the increase in L6 EPSC amplitudes induced following two days of DE (Emily Petrus et al. 2011). Bidirectional effects also occur in PV-INs: while inward-rectifying potassium channels expressed at the soma give PV-INs their fast spiking phenotype, Kv3.2/Kv3.1 expression at inhibitory terminals can also limit spike-evoked calcium influx and GABA release and can modify the efficiency of neural inhibition(Goldberg et al. 2005). Five days of DE initiated between the ages of P25 to P30 increases expression of inward rectifying Kv3.2 potassium channels in L2/3 PV-INs, and this increase is reversed following five Days of LRx(Grabert and Wahle 2009).

Previously we have shown that, following ten days of DE, ODP remains inducible after as many as three days of LRx(He, Hodos, and Quinlan 2006). The persistence of ODP on the third day of LRx implies that the changes in excitability induced during DE and reversed following brief (one to two day) LRx are not necessary for the expression of ODP. Conversely, other changes induced during LRx are necessary for the reactivation of ODP. For instance, the Quinlan lab has previously demonstrated that the reactivation of ODP by LRx following DE requires activity-dependent proteolytic degradation at TC synapses(Sachiko Murase, Lantz, and Quinlan 2017). Genetic knockdown of MMP-9 results in a hyper-excitable V1 that did not express LRx-mediated

changes in (RS) PYR excitability and did not express the reactivation of ODP by DE/LRx(Sachiko Murase, Lantz, and Quinlan 2017). Conversely, degradation of the ECM in MMP-9 knockout mice with the enzyme hyaluronidase rescued the reactivation of plasticity by DE/LRx but did not change (RS) PYR firing rates(Sachiko Murase, Lantz, and Quinlan 2017). In chapter 2, I demonstrated that increases in spontaneous and evoked (RS) PYR activity is significantly elevated during $LRx_{i,}$ but returns to baseline following a subsequent day of LRx (LRx). This begs the question, is the decrease in excitability a necessary component of reactivated ODP following LRx, or can the changes induced by visual experience during LRx reactivate plasticity in the absence of decreased pyramidal neuron excitability? To answer this question, I used PV-IN specific expression of Gi-DREADDs to disinhibit pyramidal neurons in adult V1 during DE/LRx.

3.2 Identification and Validation of tools used to disinhibit V1 during LRx

The response to brief MD is the canonical model of receptive field plasticity confined to an early postnatal critical period. In mice, binocular visual experience during development allows the unequal convergence of contralateral retinal inputs via the thalamus to V1 to create a ~2:1 bias in response amplitude to contralateral inputs (Fig.1A) (Coleman, Law, and Bear 2009; Feller and Scanziani 2005; McCurry et al. 2010). Initiating MD during the CP depresses impaired eye inputs and potentiates open-eye inputs, causing an ocular dominance shift that decreases contralateral bias (Fig.1C) (Frenkel and Bear 2004). As with humans, MD initiated during the CP also causes perceptual deficits in acuity (Prusky and Douglas 2003). MD-induced deficits in acuity may also be measured physiologically, as VEP amplitude covaries with the spatial

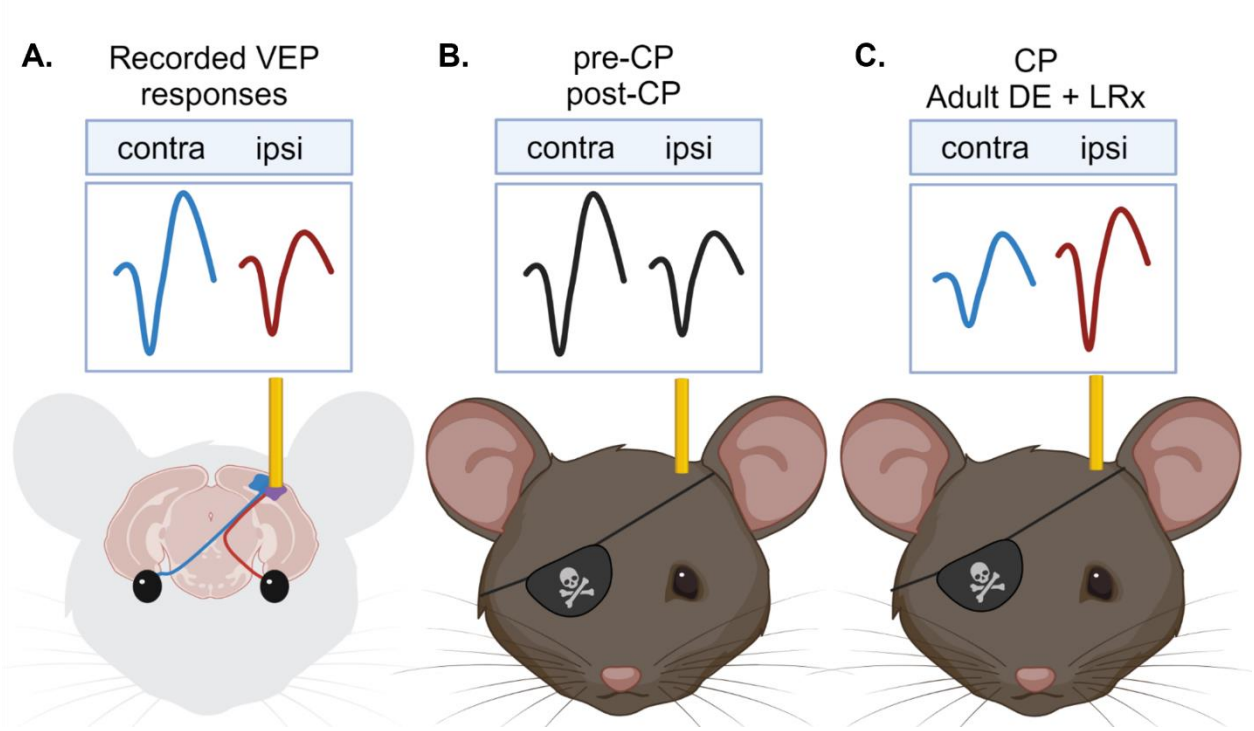

Figure 1: Mouse model of ocular dominance plasticity

Schematic diagram of mouse ODP model. **A.** In this cartoon, the recording electrode is implanted in the left hemisphere of V1b. Under normal binocular rearing conditions, VEPs recorded in response to stimulation of the eye contralateral to the recording electrode (in this case, the right eye, shown in blue) are roughly twice the magnitude of VEPs recorded in response to stimulation of the eye ipsilateral to the recording electrode (left eye, shown in red). This stereotypical relationship is known as “contralateral bias”. **B.** Monocular deprivation (here represented as an eyepatch) initiated prior to or after the CP does not disrupt the normal pattern of contralateral bias. **C.** Monocular deprivation initiated during the CP causes rapid shifts in ocular dominance, causes depression of the contralateral VEP response (blue) and potentiation of the ipsilateral VEP response (red), thus disrupting normal contralateral bias. (Created with BioRender.com)

frequency of a reversing grating stimulus(Montey, Eaton, and Quinlan 2013; He et al. 2007).

In this project, I used PV-cre mice of the same genetic background as the mice used in Chapter 2 (i.e., C57/BL6-background mice [Jackson Laboratories, Bar Harbor, ME]). As previously mentioned, Gi-DREADD suppression of PV-INs has been used to reactivate ODP in adult mice as well as tonotopic map plasticity in adult rat A1(Cisneros-Franco and De Villers-Sidani 2019; Kuhlman et al. 2013).

Gi-DREADD can suppress neural activity via $G_{\beta\gamma}$-mediated activation of G-protein gated inward rectifying potassium channels (GIRKs), hyperpolarizing infected neurons (Anderson et al. 2021; Roth 2016; Wettschureck and Offermanns 2005). In V1, Gi-DREADD activation has been shown to nearly abolish current-evoked firing rates of infected PV-INs(Kaplan et al. 2016). *In vivo* extracellular recordings demonstrate that Gi-DREADD-mediated disinhibition significantly increases VEP amplitude and evoked RS firing rates(Kaplan et al. 2016). Interestingly, while Gi-DREADD-mediated suppression of PV-INs increased VEP amplitude in this study, the relative contribution of contralateral and ipsilateral inputs was unaffected, thus contralateral bias is not occluded by suppression of PV-INs under normal circumstances(Kaplan et al. 2016). Additionally in L2/3 cortical neurons, Gi-DREADD activation not only hyperpolarized infected neurons, it also significantly decreased presynaptic release probability, likely via inhibitory modulation of voltage gated calcium channels in the presynaptic terminal by $G_{\beta\gamma}$ (Fig.2) (Wettschureck and Offermanns 2005; Stachniak, Ghosh, and Sternson 2014). Importantly, activation of DREADDs via a single dose of CNO can exhibit long lasting effects on infected neurons(~9-12 hours), facilitating long term experiments(Alexander et al. 2009).

It is important to note that the DREADD ligand CNO, while itself originally considered inert and unable to exert pharmacological effects on non-DREADD receptors, has been shown to undergo metabolism to bioactive compounds such as clozapine and N-desmythclozapine, which may cause off-target behavioral and physiological changes, particularly in rats(MacLaren et al. 2016). The metabolism of CNO to bioactive compounds also occurs in mice, but the behavioral effects of CNO

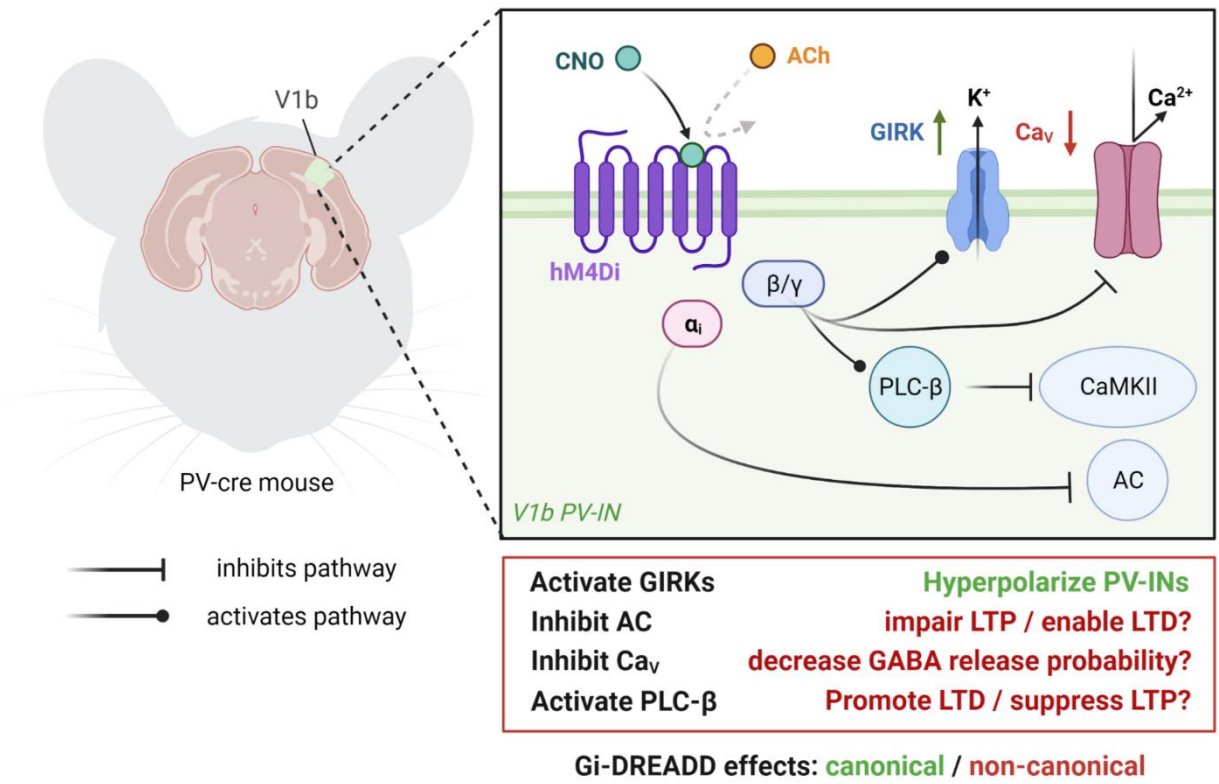

Figure 2: Gi-DREADD mechanism

(left) hM4Di-mCherry-(Gi)-DREADD expression was restricted to PV-INs via cell-type specific expression of cre-recombinase in PV-INs of PV-cre mice. (right) Schematic diagram of Gi-DREADD mechanisms. Circular arrow caps indicate activation of metabolic pathways, and flat arrow caps indicate inhibition of metabolic pathways. Canonically, activation of the hM4Di-(Gi)-DREADD receptor by CNO suppresses neuronal activity via $G_{\beta/\gamma}$ subunit-mediated activation of GIRKs, which leads to efflux of potassium ions and hyperpolarization of infected neurons. Activation of endogenous Gi-coupled GCPRs has a wide range of additional effects including activation of phospholipase-C (PLC; which inhibits downstream CaMKII, which can promote LTD and suppress LTP), inhibition of voltage-gated calcium channels (which may silence presynaptic release of GABA), and the inhibition of adenylyl cyclase (AC; decreases cAMP production and may impair LTP and enable LTD). The impact of these non-canonical Gi-DREADD effects are not as well-attested as GIRK activation but cannot be ruled out. (Created with BioRender.com)

metabolism occurred predominantly at doses an order of magnitude higher than used in this project (i.e., 0.5 mg/kg versus 5 mg/kg), and others have noted that even 10 mg/kg doses in mice fail to metabolize to levels of clozapine sufficient to drive clozapine-specific effects, and clozapine itself effectively activates DREADD receptors(Manvich et al. 2018; Mahler and Aston-Jones 2018). There has been a report that CNO itself does not cross the blood brain barrier, and may actually require metabolism into clozapine to enter nervous tissue *in vivo*, conflicting with earlier reports(Bender, Holschbach, and Stöcklin 1994; Gomez et al. 2017). With these considerations in mind, CNO-injected PV-cre controls were used in all of the following experiments to account for possible off-target effects.

3.3 Materials and Methods

Animals

All experiments were performed at the University of Maryland, College Park, 20743 in the Bioscience Research Building. Procedures utilized both male (n = 17) and female (n = 16) C57/BL6-background PV-cre mice (Jackson Laboratories, Bar Harbor, ME). Subjects were housed in the Biology Psychology Building animal facility and were raised on a 12:12 hour dark/light cycle with food and water provided *ad libitum*. During the summer of 2019 (June to July), when roof renovations in the Biology Psychology Building necessitated housing dark exposed mice in dark room facilities in the Chemistry Building. The University of Maryland Institutional Animal Care and Use Committee confirmed that all experiments were in accordance with the guidelines published in the NIH Guide for the Care and Use of Laboratory Animals.

Viral vector injection and electrode implantation:

For electrophysiological recordings, I fabricated 16-channel platinum-iridium electrode arrays which span cortical layers 1-6 (1.2 mm long, 0.2 mm wide, 15 - 20 kΩ). Surgeries were performed on subjects between the ages of P30 and P80 under surgical plane of anesthesia and received post-operative pain management and observation as described in section 2.3. Experiments utilized both males ([Gi-DREADD, PV-cre control]n = 8, 9) and females ([Gi-DREADD, PV-cre ctrl], n = 9,7)Viral infection and electrode implantation were performed concurrently during the same surgery to limit discomfort to the animals, and because long term healing of the craniotomy following viral injection decreased the efficiency with which electrode headstages could be

secured to the scalp with super glue. As in Chapter 2, the site of incision was sterilized with topical lidocaine, fur was removed from the scalp, and a longitudinal incision was made with a sterile scalpel. The incised skin was then retracted, and the skull was cleaned and dried with 100% acetone. Two small (~2 mm) holes were drilled into the skull overlaying the visual cortex of the left hemisphere according to stereotaxic coordinates, one hole for the electrode (~3 mm lateral to lambda/medial suture intersection), and one hole rostral to the electrode hole (<0.5 mm) to limit damage to the brain region being recorded from. First, a 33-gauge Hamilton syringe was slowly lowered to a depth of ~0.5 mm, and the viral vector was injected (300 nL, 50 nL/min; AAV-hsyn-FLEX-hM4D-(Gi)-mCherry, UNC Vectorcore). Following retraction of the syringe, the recording electrode was then slowly lowered to a depth of ~1 mm via digital micromanipulator. Electrodes were secured to the skull using Loctite 454 cyanoacrylate superglue and Zip kicker cyanoacrylate accelerator, and the rostral and caudal margins of the incision were sutured with sterile, 5-0 size polyglycolic acid sutures. To prevent infection, a topical triple antibiotic (neomycin, polymyxin, bacitracin) was applied to the incision site and all instruments were heat sterilized prior to use using a Germinator 500 glass bead sterilizer. Mice were allowed to recover from surgical implantation for approximately 2 to 3 weeks before extracellular recording sessions began.

Data Acquisition and Analysis

Data were acquired and analyzed as described in Chapter 2, with the following addition: ocular dominance indices (ODI) were calculated by recording VEPs in response to stimulation from the right (contralateral) eye and the left (ipsilateral eye) individually, and

taking the ratio of the responses using the following formula: ([Contra – Ipsi]/[Contra + Ipsi])(Y. Gu et al. 2016). Monocular visual spatial acuity was estimated physiologically via VEP amplitude, which covaries with the spatial frequency of the visual stimulus(Montey, Eaton, and Quinlan 2013; He et al. 2007).

Dark Exposure

Darkroom experiments utilized mice implanted in adulthood (P53 – P80; males [Gi-DREADD, PV-cre ctrl] n = 5,5; females [Gi-DREADD, PV-cre ctrl] n = 6, 5). Implanted mice were transferred to a light-tight dark room at age P90 – P97 for ten days. The dark room facility was located onsite inside the Biology Psychology Building animal facility, or in the Chemistry Building (as described above). Mice were transferred between buildings in an air-conditioned van built to purpose and maintained by the University of Maryland Central Animal Resource Facility (CARF). Animals were checked daily in complete darkness via the use of infrared illuminating night vision goggles.

Monocular deprivation (MD):

Monocular deprivation was performed to occlude the subject's visual input through the right eye. Surgeries were performed under surgical plane of anesthesia and subjects received post-operative pain management and observation as described in section 2.3. The margins of the upper and lower eyelids (Approximately 0.5 mm deep along the length) of the right eye were trimmed, and the lids were sutured together with 3 - 4 continuous "box stitches" using 5-0 size polyglycolic acid sutures.

Eye opening:

Eye opening was performed to open the subject's previously deprived right eye following brief (three day) monocular deprivation. Surgeries were performed under surgical plane of anesthesia and subjects received post-operative pain management and observation as described in Chapter 2. To separate the top and bottom eyelids, surgical scissors were used to carefully cut away eye sutures and the lids were gently re-opened with blunt forceps, then e flushed 3X with sterile saline.

Transcardial perfusion (terminal procedure):

Under surgical plane of isoflurane anesthesia, the ventral body wall was cut open below the diaphragm and the rib cage was opened to expose the heart. A small hole was cut in the left ventricle and a cannula was inserted into the aorta and clamped. The subject was perfused transcardially with fresh 4% paraformaldehyde. Subjects were then decapitated, and the brain quickly removed, post-fixed for 24 hours in (4% paraformaldehyde), and cryoprotected in 30% sucrose for 24 hours. Coronal sections (20 microns) were cut on a freezing sliding microtome (Leica SM 200R) and stored in cryoprotectant solution (0.58 M sucrose, 30% (v/v) ethylene glycol, 3 mM sodium azide, 0.64 M sodium phosphate, pH 7.4) at -20° C until antibody incubation/plating for immunohistochemistry. Sections were blocked using 4% normal goat serum for one hour, followed by antibody incubation and appropriate secondaries.

Antibodies

The following antibodies were used: To quantify hM4D-(Gi)-mCherry expression, Rabbit-anti RFP (abcam; ab62341) was amplified with goat anti-rabbit (Thermofisher Scientific, Alexa 488; A11008). To quantify Parvalbumin immunofluorescence, Guinea Pig anti-Parvalbumin primary antibodies (Synaptic Systems, Cat No. 195 004) amplified with Goat anti-guineapig secondaries (Life Technologies Corp.; Alexa Fluor 647; A21450) were used.

Imaging and Immunohistochemistry

A Lecia LSM 710 confocal microscope equipped with a 405 diode, an Argon laser (458, 476, 488, 496, and 514nm) and a white light laser (470-670nm in 1 nm increments) was used for quantitative immunofluorescence and fluorescent co-localization. DREADD and Parvalbumin immunofluorescence was visualized in a single z-section and acquired with a 5x, 10x, and 40x objective. Co-localization of somatic DREADD expression and Parvalbumin was determined in a single plane using FIJI and the JACoP Plugin (NIH); data were thresholded by maximum pixel intensity (5% upper bound) and masked with size exclusion based on PV-IN soma size to calculate DREADD:Parvalbumin somatic co-localization using Mander's correlation coefficient.

Statistical Analysis

Data normality was evaluated with a one sample Kolmogorov-Smirnov test. When comparing two distributions of data, a two-sample Kolmogorov-Smirnov test was used. Data were fit with logarithmic trendlines for visualization; statistics were performed on

data averaged by animal or as distributions of all single unit data. Nonparametric tests were used to determine significance in non-normally distributed data. To determine significance between paired samples, a Wilcoxon signed-rank test was used. When samples were unpaired, a Wilcoxon rank sum test was used. A Bonferroni *post hoc* correction was used for multiple comparisons. For samples with more than two measures within the same subjects, a Friedman's test followed by a Dunn-Sidak multiple comparisons test was used.

3.4 Results and discussion

3.4.1 Cell-type specific expression of Gi-DREADD in PV-cre mice.

To drive cre-dependent expression of Gi-DREADD, I injected an adeno-associated viral (AAV) vector encoding floxed Gi-DREADD (AAV-hsyn-FLEX-hM4D-mcherry, UNC Vectorcore) into V1b (300 nL undiluted virus, 3 mm lateral to lambda/medial suture intersection, left hemisphere) of PV-cre transgenic mice (Jackson Labs). I evaluated efficacy and spread of Gi-DREADD expression by quantifying colocalization of immunolabeled mCherry-DREADD and parvalbumin (PV) in the Gi-DREADD-injected hemisphere (Fig.3A), utilizing the uninjected hemisphere as a within-animal control (n = 3 mice, uninjected hemisphere not shown) following delivery of the DREADD ligand, CNO (0.5 mg/kg mouse weight, i.p.). I used Mander's correlation coefficient to quantify co-localization; the co-localization of mCherry-DREADD with PV was specific to the injected hemisphere and absent in control hemisphere (Fig.3C). Because PV expression is activity-dependent and can be used as a readout of activity in this class of interneurons, I also compared the distribution of the mCherry-DREADD/PV ratio. This analysis revealed a significant rightward shift in mCherry-DREADD/PV ratio, indicating that high expression of Gi-DREADD was correlated with lower levels of PV expression (Fig.3C) (Cisneros-Franco and De Villers-Sidani 2019).

For electrophysiological recordings, I fabricated 16-channel platinum-iridium electrode arrays which can be used to survey activity across the full cortical depth. Electrode arrays were implanted under surgical plane of anesthesia as in Chapter 2, during the same surgical session and the delivery of AAV-Gi-DREADD. Following a

Figure 3: Extracellular Recordings and targeted expression of Gi-DREADD in PV-cre mice

A. Background subtracted, maximum intensity projection of mCherry-Gi-DREADD infected V1b at 10x magnification. **B. (right)** Layer-averaged VEP waveforms +/- SEM collected from 21 mice (Gi-DREADD infected + PV-cre control). VEPs are generated in response to a 1 Hz reversing square-wave grating; stimulus onset is at zero seconds. Note the differences in amplitude between the layer 4 VEP (cyan) versus the layer 2/3 and layer 5/6 VEPs (grey and magenta, respectively; this coloring convention will continue throughout thesis unless noted otherwise). (left) Average waveforms of regular spiking (RS, blue, presumptive pyramidal neurons, n = 142 units, 21 subjects) and fast spiking (FS, red, presumptive PV+ interneurons, n = 34 units, 20 subjects) single units collected during evoked stimulation (luminescent grey screen) from Gi-DREADD infected (n = 10 mice) and PV-cre control mice (n = 11) **C.** Average quantification of PV and mCherry-DREADD co-localization (n=3 mice; Mander's coefficient [[mCherry/PV]) two-way paired t-test, *p = 0.036). **D.** Scatter plots of single unit characteristics used as criteria for classification. Endslope is measured at the point 0.5 ms after the initial waveform trough. Time to peak is measured from time of the initial trough. Units from all implanted subjects (n=21) were pooled and classified using k-means clustering. Only units that clustered reliably using all three parameters were analyzed. Note that FS units exhibit steeper endslopes, larger peak to trough ratios, faster time to peaks, and higher firing rates versus RS units. (Closed circles = Gi-DREADD, open circles = PV-cre control) **E.** Cumulative probability function of background-subtracted mCherry-DREADD to PV intensity ratio in injected (green) versus uninjected (grey, control) hemisphere (n = 3 mice, Kolmogorov-Smirnov test, †p = 2.10e-57). PV expression is activity-dependent, therefore decreased PV-immunoreactivity suggests decreased PV+ interneuron (PV-IN) activity.

recovery period of 2 - 3 weeks, implanted mice were placed in the recording chamber and shown visual stimuli consisting of 1 Hz reversing square wave gratings (50 trials 1 second per trial, 100% contrast, 0.05 cycles per degree, 30° - 180° orientations). As in Chapter 2, current source density analysis of the averaged VEP was used to identify laminar location of electrode channels (Fig.4)(Niell and Stryker 2008; Senzai, Fernandez-Ruiz, and Buzsáki 2019). The fabricated electrodes used in this project differ in shape from those used in Chapter 2 in that they are a linear array of sixteen channels (approximately 70 μm vertical spacing), rather than two rows of eight channels, allowing for more recording channels per layer (Fig.4). Once laminar location was determined, VEPs were averaged by layer (Fig.3B). As in chapter 2, isolated single units were classified by waveform shape and rate (Fig.3D; red = FS, blue = RS, filled versus unfilled circles = Gi-DREADD versus PV-cre ctrl, respectively). Spike sorting was done offline in Opensorter software (Tucker Davis Technologies) in concatenated

Figure 3: Extracellular Recordings and targeted expression of Gi-DREADD in PV-cre mice

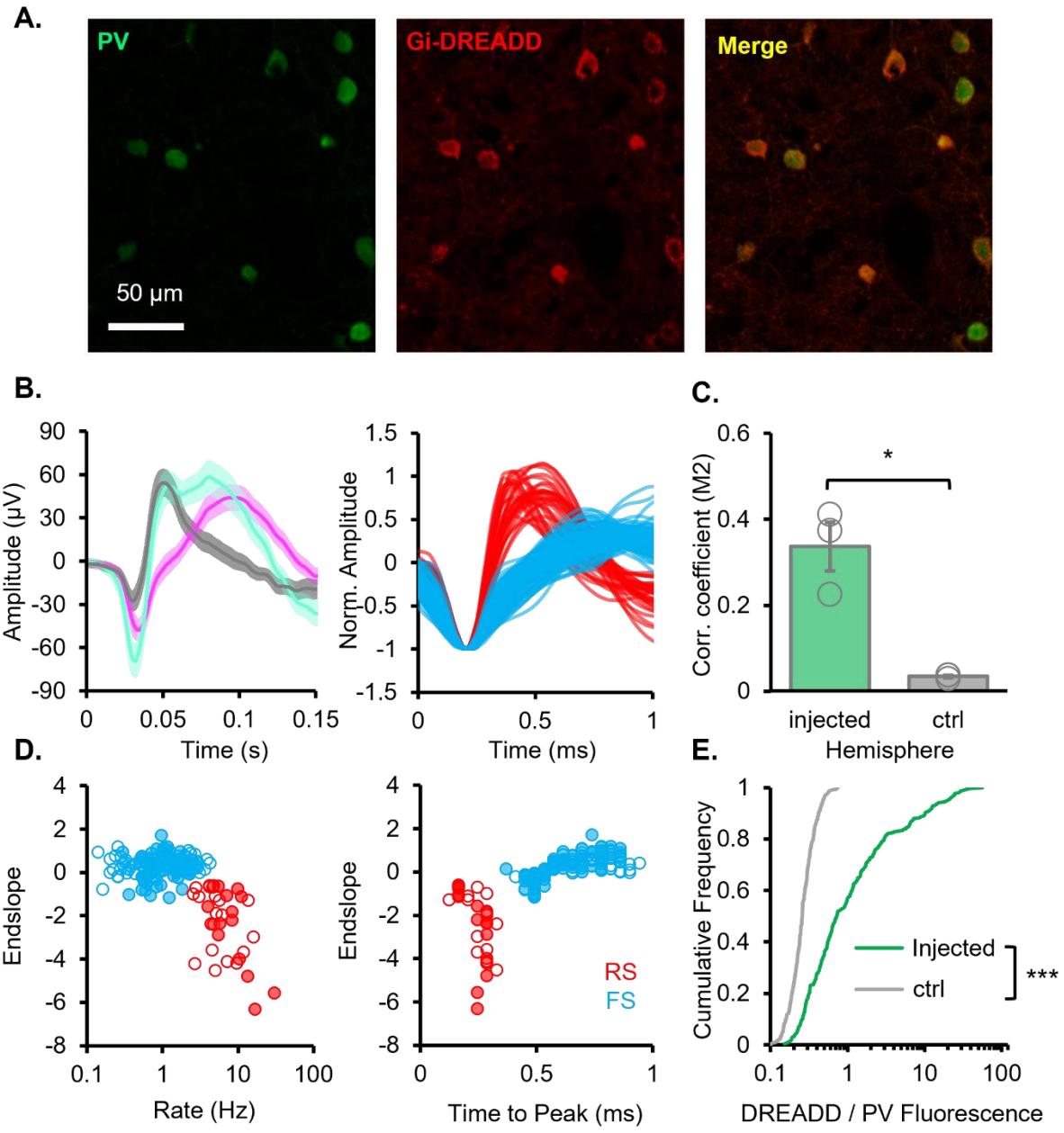

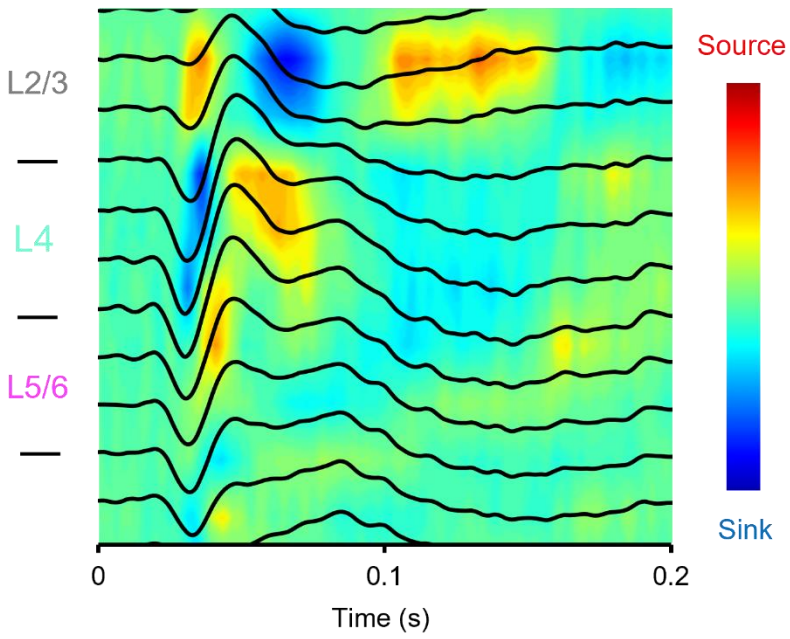

Figure 4: CSD of Trial-averaged VEPs

CSD calculated from trial averaged visually evoked local field potentials (VEPs; black line overlay). Current sources are depicted in red, and current sinks are depicted in blue. The early sharp current sink in layer 4 represents feed-forward input from thalamus. Current sources above and below layer 4 represent feed-forward input to superficial layers 2/3 and deep layers 5/6 (respectively).

"superblocks" by subject and experimental day, ensuring that units reliably sorted into a single sort code across recording blocks. Waveform classification was performed on units recorded in the control condition, and then that classification was applied to units in the subsequent blocks to prevent the chemogenetic response from interfering with unit classification.

3.4.2 Gi-DREADD activation in PV-INs increases VEP amplitude.

To test the hypothesis that activating Gi-DREADD in PV-INs disinhibits PYRs, I examined spontaneous and evoked activity of V1 neurons across the cortical depth. Infected mice were shown visual stimuli consisting of 1 Hz reversing gratings (50 trials ,1 second per trial, 100% contrast, 0.05 cycles per degree, 30° - 180° orientations, “evoked”, or 0% contrast grey screen “spontaneous, as in chapter 2) before and one hour after acute administration of the DREADD ligand, clozapine-N-oxide (CNO, 0.5 mg/kg i.p.). One hour was chosen as the DREADD onset time in alignment with reports that peak LFP responses occurred 45 - 50 minutes after CNO injection(Alexander et al. 2009). I detected a significant increase in VEP amplitude (~150%) across all cortical layers 1 hour following CNO injection in Gi-DREADD infected mice (Fig.5, Fig.6A). No significant change was detected in PV-cre controls (Fig.5, Fig.6B). This aligns with previous reports that Gi-DREADD activation in PV-INs significantly increased VEP amplitude(Kaplan et al. 2016). Increased VEP amplitude was not due to SRP, as SRP expression is reported to required 24 hours and sleep to consolidate(Montgomery et al. 2022). Interestingly, in Kaplan et al., (2016), the activation of Gi-DREADD in PV-INs was shown to transiently occlude the expression of SRP. Following activation of Gi-DREADD, VEP responses to novel and familiar visual stimuli were both significantly enhanced. The relative differences in amplitude were occluded, rendering responses to novel and familiar stimuli indistinguishable from each other(Kaplan et al. 2016). Importantly, further enhancement of VEP was possible beyond that induced by Gi-DREADD, indicating the dynamic range of VEP responses is not saturated by Gi-DREADD activation in PV-INs. VEPs evoked via ipsilateral and contralateral eye

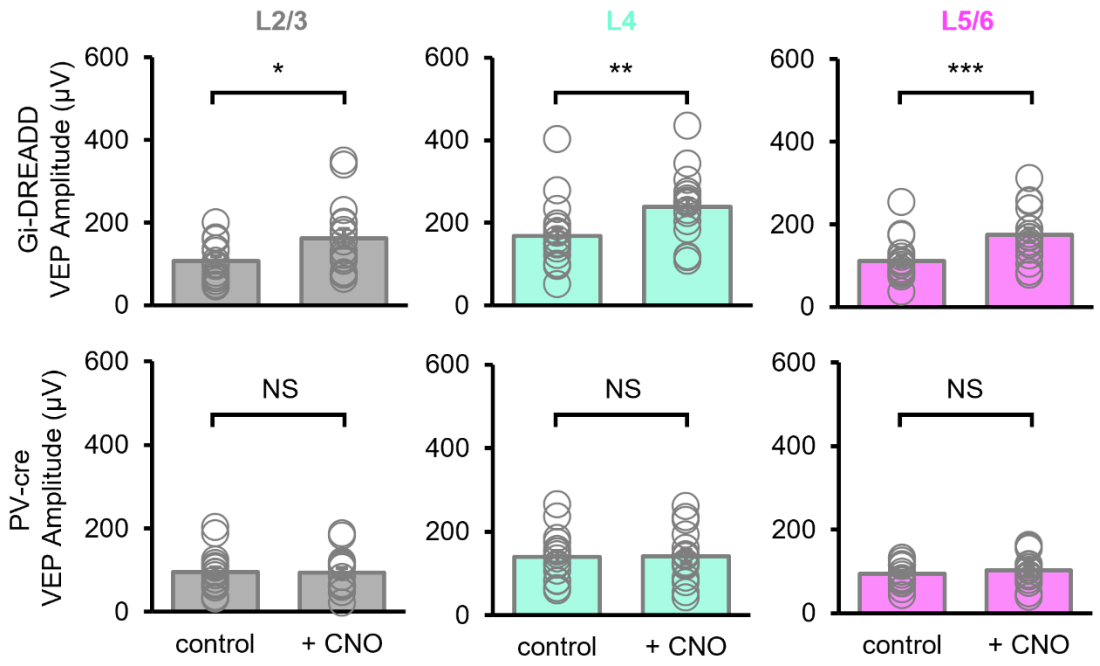

Figure 5: Gi-DREADD activation potentiates VEP amplitudes

Histograms of VEP amplitude (mean +/- SEM) by condition. VEP amplitudes significantly increased following CNO in Gi-DREADD infected mice (top), but not PV-cre control mice (bottom) (Wilcoxon signed rank test; (Gi-DREADD [L2/3]*p < 0.025; n = 16 mice [L4] ** p < 0.0025; n = 17 mice [L5/6] *** p < 0.00025; n = 16 mice; PV-cre ctrl[L2/3] NS; n = 16 mice [L4] NS; n = 16 mice [L5/6] NS, n = 15 mice; Wilcoxon Rank Sum test [Gi-ctrl v. PV-cre ctrl] [L2/3] NS [L4] NS [L5/6] NS; Bonferroni corrected for 2 comparisons)

stimulation were likewise significantly increased by Gi-DREADD activation, but the relative ratio between eye responses was preserved(Kaplan et al. 2016).

Gi-DREADD suppression of PV-INs also resulted in significantly increased visually evoked RS firing rates (Kaplan et al., 2016). Synchronous activation of (RS) excitatory PYRs likely contribute to the enhancement of VEP amplitude following Gi-DREADD activation(Kaplan et al. 2016). The enhancement of VEP amplitude following Gi-DREADD activation is reminiscent of SRP, albeit on an accelerated time course, and it is interesting to speculate that that Gi-DREADD activation in PV-INs enhances VEP responses through similar mechanisms. The recruitment of somatostatin-expressing

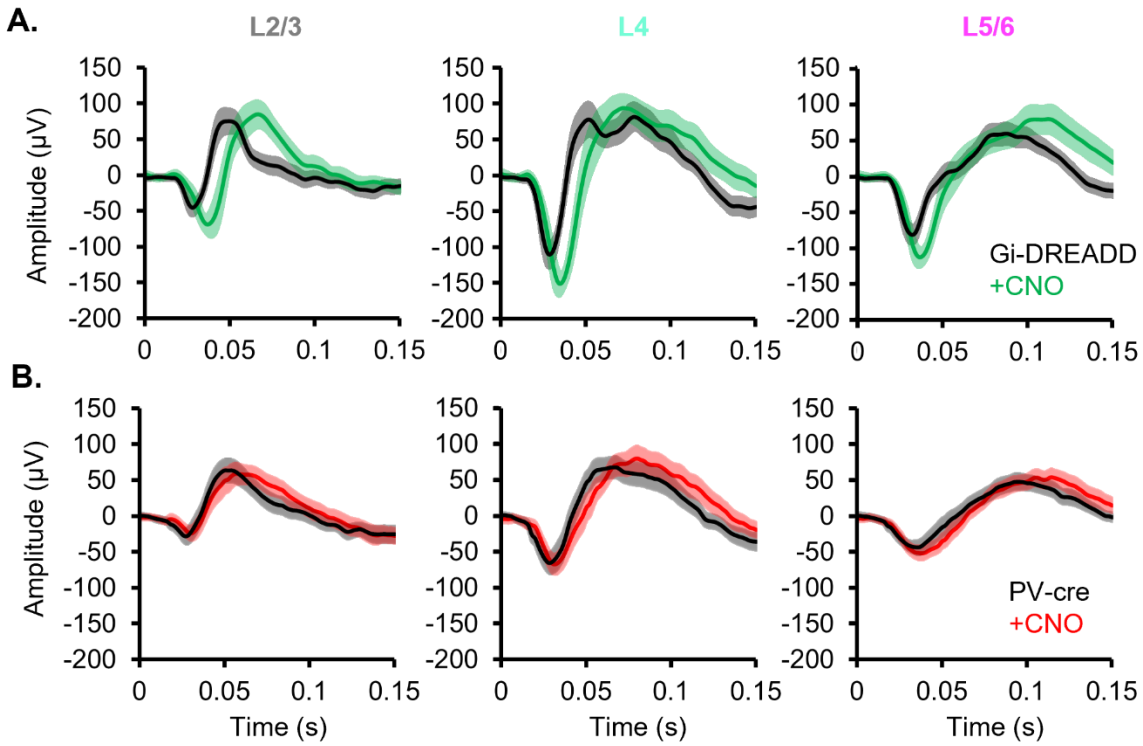

Figure 6: Layer-Averaged VEPS before and After CNO

A. VEPs (mean +/- SEM) averaged by layer for Gi-DREADD infected mice. Note the increase in VEP amplitude from control (black) following CNO injection (green). **B.** As in A, but for PV-cre control mice. VEP amplitudes did not significantly increase from control (black) following CNO injection (red).

interneurons (SST-INs) has been shown to inhibit PV-INs and disinhibit V1 responses during locomotion (Y. Fu et al. 2015). Similarly, activity in SST-INs increases during presentation of familiar stimuli while PV-IN activity decreases, indicating that disinhibition of PV-INs may be an intrinsic mechanism for the enhanced response to familiar stimuli(Hayden et al. 2021).

3.4.3 Gi-DREADD activation in PV-INs increases excitatory / inhibitory balance in V1b.

Activation of Gi-DREADD in PV-INs is known to increase evoked RS firing rates in mouse V1, as well as to decrease evoked calcium responses in infected PV-INs(Kaplan et al. 2016; Kuhlman et al. 2013). As increased spontaneous activity is necessary for DE-induced metaplasticity, I first verified that Gi-DREADD activation in PV-INS increases spontaneous and evoked RS firing rates (Bridi et al. 2018). I detected a significant increase in averaged spontaneous RS firing rates (180 - 260%) across all cortical layers 1 hour following CNO injection in Gi-DREADD infected mice (Fig.7A). A significant shift in the distribution of spontaneous RS firing rates was detected in Gi-DREADD infected mice in L4 and L5/6, but not in L2/3 (Fig.7B). The ~190% - 260% increase in evoked RS firing rates are similar the increases detected in spontaneous RS firing rates, and align with previous reports (Fig.8A – B) (Kaplan et al. 2016). No significant change was detected in either spontaneous RS firing rates in PV-cre control mice (Fig.7A – B; Fig.8A – B). As in chapter 2, it is worth noting that these evoked responses were averaged over an entire one second trial of a reversing grating stimulus, but these evoked responses are most apparent in the first 100 ms immediately following grating reversal (Fig.8 supplement 1). Similar to Chapter 2, z-scores of control evoked single unit firing rates normalized to the within-animal spontaneous firing rate are significantly elevated for both G-DREADD-infected and PV-cre control mice (one-sample Wilcoxon signed rank test), and the distribution of normalized evoked z-scores is significantly different from the distribution of spontaneous firing rate z-scores (Fig.8 Supplement 2).

Figure 7: Gi-DREADD activation increases spontaneous RS firing rates

A. Quantification of spontaneous RS firing rates averaged by layer. Spontaneous RS firing rates significantly increased in all layers following CNO injection in Gi-DREADD infected mice, but not PV-cre control mice (Wilcoxon signed rank test; (Gi-DREADD [L2/3]*p < 0.025; n = 8 mice, 23 units [L4] ** p < 0.0025; n = 10 mice, 31 units [L5/6] ** p < 0.0025; n = 7 mice, 18 units; PV-cre ctrl[L2/3] NS; n = 8 mice [L4] NS; n = 8 mice [L5/6] NS, n = 5 mice; Wilcoxon Rank Sum test [Gi-ctrl v. PV-cre ctrl] [L2/3] NS [L4] NS [L5/6] NS; Bonferroni corrected for 2 comparisons) **B.** Cumulative distribution of all spontaneous RS units. The distribution of spontaneous RS firing rates shifted significantly in L4 and L5/6 following CNO injection in Gi-DREADD infected mice, but not PV-cre control mice (Kolmogorov Smirnov test: Gi-DREADD [L2/3] NS; n = 8 mice, 23 units [L4] **** p < 0.000025; n = 10 mice, 31 units [L5/6] * p < 0.025; n = 7 mice, 18 units; PV-cre ctrl [L2/3] NS; n = 8 mice [L4] NS; n = 8 mice [L5/6] NS, n = 5 mice ; [Gi-ctrl v. PV-cre ctrl] [L2/3] NS [L4] NS [L5/6] NS; Bonferroni corrected for 2 comparisons) **C.** Averaged histograms of PV-cre mice data presented in A and B (n = 9 mice). **D.** Histograms of Gi-DREADD mice data presented in A (n = 10 mice).

Figure 8: Gi-DREADD activation increases evoked RS firing rates

A. Quantification of evoked RS firing rates averaged by layer. Evoked RS firing rates significantly increased in all layers following CNO injection in Gi-DREADD infected mice, but not PV-cre control mice (Wilcoxon signed rank test; (Gi-DREADD [L2/3]*p < 0.025; n = 8 mice, 23 units [L4] ** p < 0.0025; n = 10 mice, 31 units [L5/6] * p < 0.025; n = 7 mice, 18 units; PV-cre ctrl[L2/3] NS; n = 8 mice [L4] NS; n = 8 mice [L5/6] NS, n = 5 mice; Wilcoxon Rank Sum test [Gi-ctrl v. PV-cre ctrl] [L2/3] NS [L4] NS [L5/6] NS; Bonferroni corrected for 2 comparisons) **B.** Cumulative distribution of all evoked RS units. The distribution of evoked RS firing rates shifted significantly in L4 and L5/6 following CNO injection in Gi-DREADD infected mice, but not PV-cre control mice (Kolmogorov Smirnov test: Gi-DREADD [L2/3] NS; n = 8 mice, 23 units [L4] *** p < 0.00025; n = 10 mice, 31 units [L5/6] * p < 0.025; n = 7 mice, 18 units; PV-cre ctrl [L2/3] NS; n = 8 mice [L4] NS; n = 8 mice [L5/6] NS, n = 5 mice ; [Gi-ctrl v. PV-cre ctrl] [L2/3] NS [L4] NS [L5/6] NS; Bonferroni corrected for 2 comparisons) **C.** Averaged histograms of PV-cre mice data presented in A and B (n = 9 mice). **D.** Histograms of Gi-DREADD mice data presented in A (n = 10 mice).

Figure 7: Gi-DREADD activation increases spontaneous RS firing rates

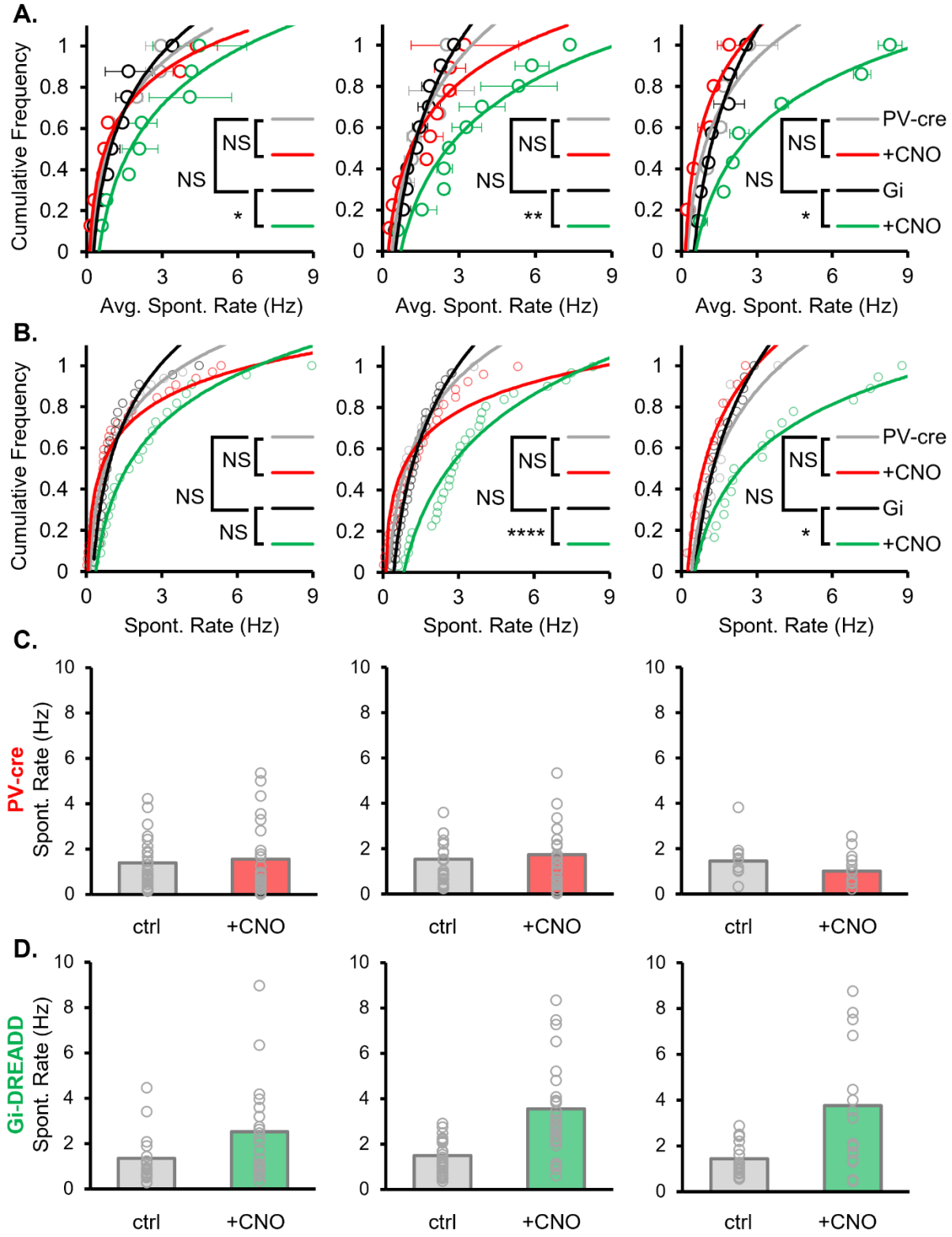

Figure 8: Gi-DREADD activation increases evoked RS firing rates

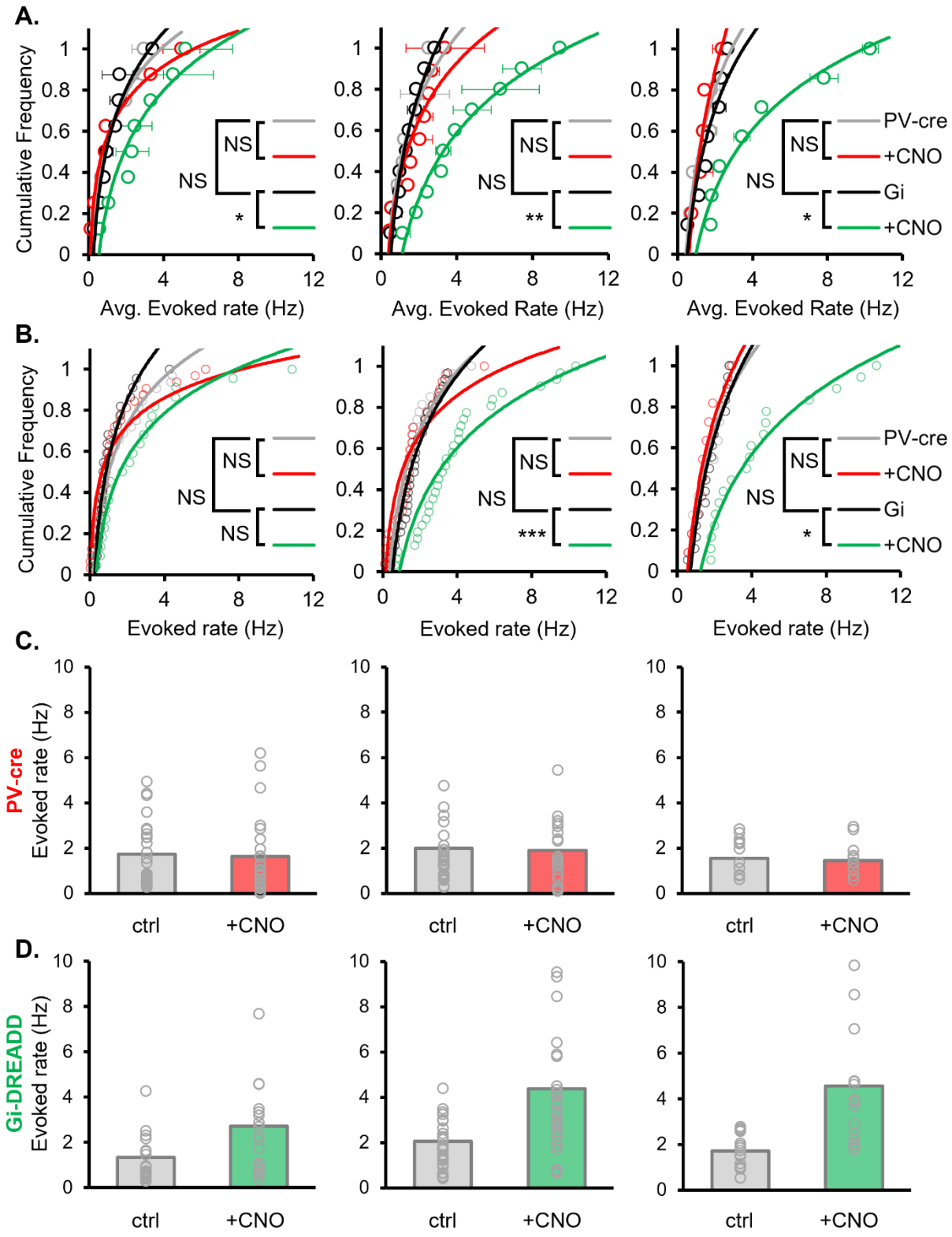

Measurable changes in the function of infected PV-INs following Gi-DREADD activation by CNO include decreased visually-evoked calcium responses and reduced current-evoked firing rates(Kaplan et al. 2016; Kuhlman et al. 2013). However, I detected no significant changes in either spontaneous or evoked FS firing rates following Gi-DREADD activation (Fig.9A; Fig.9B). This discrepancy may be explainable by differences in technique: in acute V1 slices or *in vivo* calcium imaging experiments, Gi-DREADD-expressing PV-INs are readily identifiable by expression of reporter fluorophores (mCitrine in Kaplan et al., 2016, tdTomato in Kuhlman et al., 2013). The extracellular electrodes I use in my experiments are blind to such identifiers, and blind to neurons that are not spiking. The clear and significant increase in RS firing rates in Figs.5 – 8 suggests that RS neurons are disinhibited by chemogenetic suppression of PV-INs(Gomez et al. 2017; Kaplan et al. 2016; Cisneros-Franco and De Villers-Sidani 2019; Kuhlman et al. 2013).

The effect of Gi-DREADD is most often attributed to $G_{\beta\gamma}$-mediated activation of membrane hyperpolarizing GIRKs(Anderson et al. 2021; Roth 2016; Wettschureck and Offermanns 2005). Many studies using Gi-DREADD focus on changes in spiking output from infected cells due to GIRK-mediated membrane hyperpolarization. Concurrent activation of Gi-DREADD and pharmacological blockade of GIRKs with tertiapin-Q (TPNQ) prevented Gi-DREADD-mediated membrane hyperpolarization in striatal neurons(Shan, Fang, and Tian 2022). However, that activation of GPCRs like Gi-DREADD induce a cascade of downstream effects, and attributing the effect of Gi-DREADD to a single metabolic pathway may be an oversimplification (Fig.2). Other effects mediated by Gi-coupled receptors include G_{α}i-mediated inhibition of adenylyl

Figure 9: Gi-DREADD increases spontaneous excitatory / inhibitory balance.

A. (right) Quantification of spontaneous FS firing rates averaged across all layers. Spontaneous FS firing rates did not change after CNO injection in Gi-DREADD infected mice, or PV-cre control mice (Wilcoxon signed rank test; [Gi-DREADD] NS; n = 6 mice, 15 units [PV-cre ctrl] NS; n = 6 mice, 17 units; [Gi-DREADD v. PV-cre ctrl] NS; Bonferroni corrected for 2 comparisons) **(left)** Cumulative distribution of all spontaneous FS units. The distribution of spontaneous FS firing rates was unchanged following CNO injection in Gi-DREADD infected mice and PV-cre control mice (Kolmogorov Smirnov test: ; [Gi-DREADD] NS; n = 6 mice, 15 units [PV-cre ctrl] NS; n = 6 mice, 17 units; [Gi-DREADD v. PV-cre ctrl] NS; Bonferroni corrected for 2 comparisons) **B.** Averaged histograms of data presented in A ([Gi-DREADD] n = 6 mice; [PV-cre] n = 6 mice). **C.** Histograms excitatory / inhibitory balance (mean +/- SEM) averaged by animal across all layers. Spontaneous excitatory inhibitory balance increased following CNO injection in Gi-DREADD-infected mice, but not PV-cre control mice (Wilcoxon signed rank test, [Gi-DREADD] ***p<0.005; n = 10 mice [PV-cre ctrl] NS; n = 9 mice

Figure 10: Gi-DREADD increases evoked excitatory / inhibitory balance.

A. (right) Quantification of evoked FS firing rates averaged across all layers. evoked FS firing rates did not change after CNO injection in Gi-DREADD infected mice, nor in PV-cre control mice (Wilcoxon signed rank test; [Gi-DREADD] NS; n = 6 mice, 15 units [PV-cre ctrl] NS; n = 6 mice, 17 units; [Gi-DREADD v. PV-cre ctrl] NS; Bonferroni corrected for 2 comparisons) **(left)** Cumulative distribution of all evoked FS units. The distribution of evoked FS firing rates was unchanged following CNO injection in Gi-DREADD infected mice and PV-cre control mice (Kolmogorov Smirnov test: ; [Gi-DREADD] NS; n = 6 mice, 15 units [PV-cre ctrl] NS; n = 6 mice, 17 units; [Gi-DREADD v. PV-cre ctrl] NS; Bonferroni corrected for 2 comparisons) **B.** Averaged histograms of data presented in A ([Gi-DREADD] n = 6 mice; [PV-cre] n = 6 mice). **C.** Histograms of excitatory / inhibitory balance (mean +/- SEM) averaged by animal across all layers. evoked excitatory inhibitory balance increased following CNO injection in Gi-DREADD-infected mice, but not PV-cre control mice (Wilcoxon signed rank test, [Gi-DREADD] *p<0.05; n = 10 mice [PV-cre ctrl] NS; n = 9 mice

Figure 9: Gi-DREADD increases spontaneous excitatory / inhibitory balance.

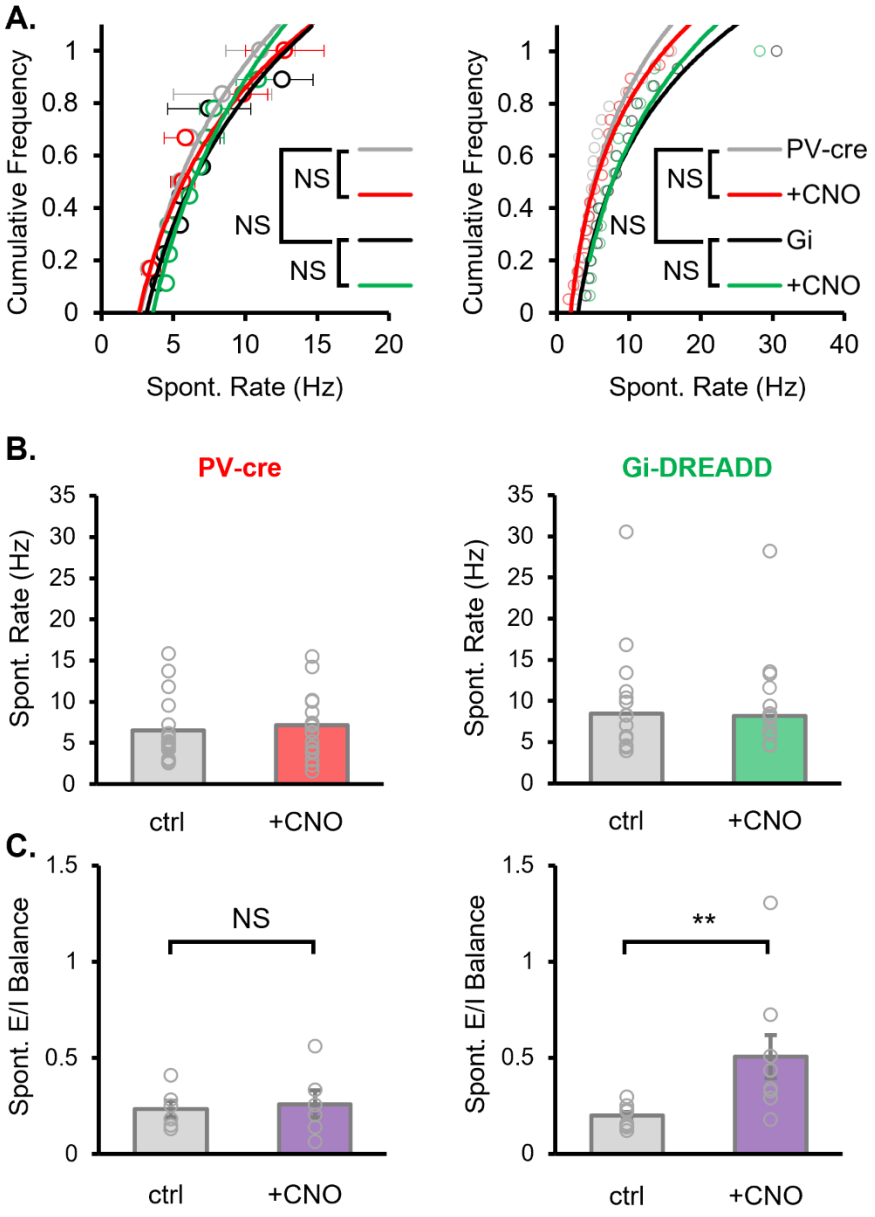

Figure 10: Gi-DREADD increases evoked excitatory / inhibitory balance

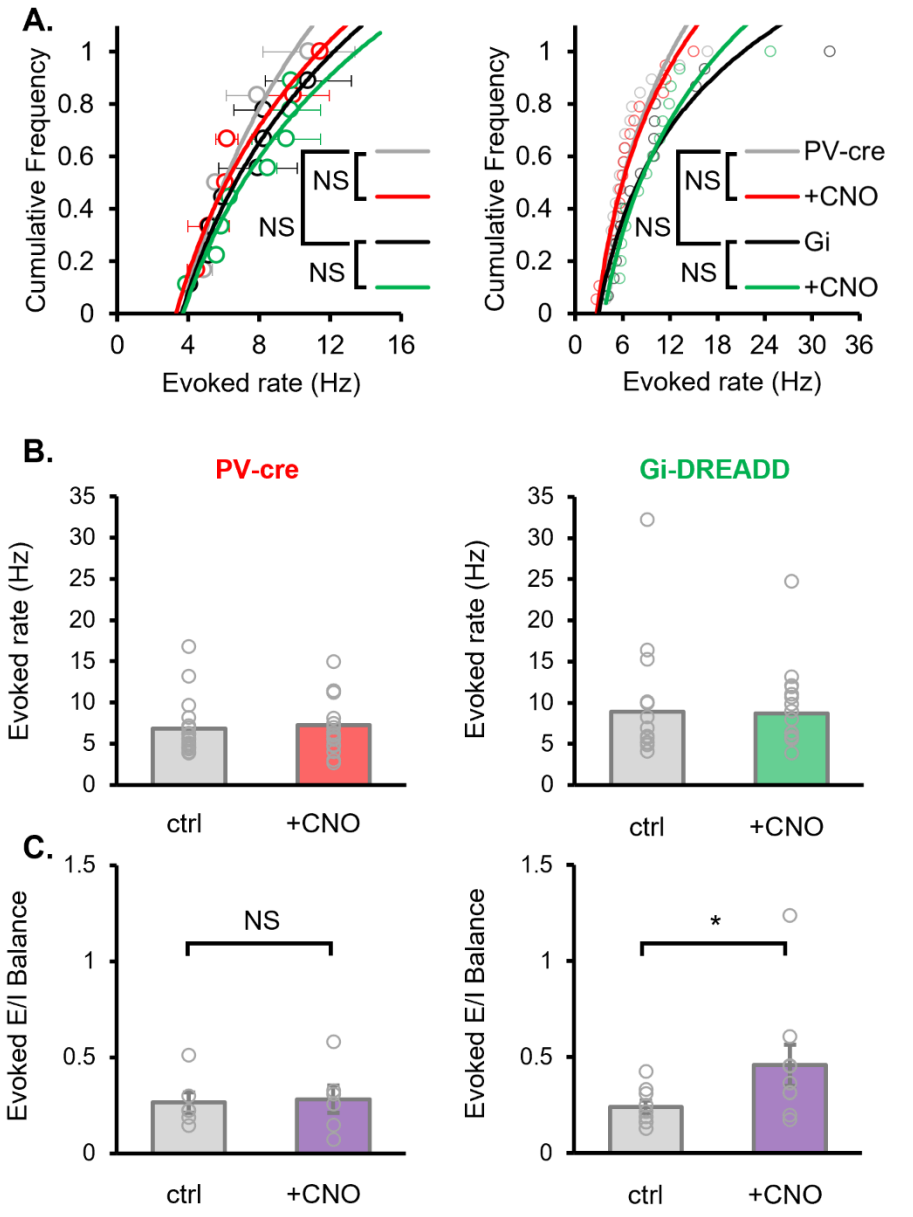

cyclase, $G_{\beta\gamma}$-mediated activation of phospholipase-C-β (PLC-β) and inhibition of N- and P/Q-type voltage gated calcium channels(Wettschureck and Offermanns 2005). Inhibition of voltage gated calcium channels by Gi-DREADD has been shown to simultaneously decrease probability of synaptic vesicle release in infected L2/3 PYRs and induce GIRK-mediated membrane hyperpolarization. Importantly, this dual effect of presynaptic silencing and membrane hyperpolarization happens concurrently indicating that Gi-DREADD receptors are trafficked to the presynaptic membrane without the need for extra intervention(Stachniak, Ghosh, and Sternson 2014). Activation of PLC-β is typically associated with another class of DREADD receptors coupled to Gq. In the PYRs of the forebrain or PV-INs of the basolateral amygdala, activation of Gq-DREADD increases intracellular calcium via downstream activation of PLC-β, causing infected neurons to burst rather than fire tonically(Roth 2016; Alexander et al. 2009; X. Fu et al. 2022). Conversely, activation of PLC-β in V1 neurons (including PV-INS), via adrenergic neuromodulation or Gq-DREADD activation, induces robust NMDA-R-independent spike timing dependent LTD(S. Huang, Huganir, and Kirkwood Alfredo 2013; Hong et al. 2019). Similarly, inhibition of adenylyl cyclase by Gi-DREADD may negatively impact the expression of LTP that is engaged via α-adrenergic neuromodulation in V1(S. Huang, Huganir, and Kirkwood Alfredo 2013). Interestingly, NRG1 and NARP have been shown to strengthen intracortical synapses onto L2/3 PV-INs via an NMDA-R-independent mechanism, indicating that the Gi-DREADD may promote LTD induction at these synapses(Severin et al. 2021; Sun et al. 2016). Gi-DREADD-mediated LTD has not been described before. However it is worth noting that when 24 hours of *in vivo* Gi-DREADD activation in PV-INs precedes acute V1 slice electrophysiology, glutamate

uncaging-induced monosynaptic excitatory drive onto L2/3 PV-INs is reduced, and this effect is reversed by bath treatment with NRG1(Sun et al. 2016).

The regulation of excitatory inputs L2/3 PV-INs exhibit a high degree of specificity with distinct metabolic pathways impacting interlaminar and intralaminar connectivity(Severin et al. 2021). It is possible that different classes of synapse onto PV-INs may be targeted by the activation of Gi-DREADD, biasing the activation of PV-INs to specific connections without decreasing the firing rate. To determine if Gi-DREADD activation decouples PV-IN inhibition from the local V1 network, I calculated changes in E/I balance before and after CNO injection. I detected a significant shift in E/I balance during both spontaneous and evoked stimulus conditions (Fig.9C, Fig.10C). These results are consistent with the hypothesis that Gi-DREADD activation in PV-INS can impede functional GABAergic inhibition in V1 without directly changing the firing rate of infected PV-INs.

3.4.4 Gi-DREADD activation in PV-INs disinhibits V1b increases RS bursting activity.

In chapter 2, I demonstrated that LRx_i causes a significant increase in spontaneous bursting activity in L4. I predicted that Gi-DREADD activation in PV-INs would produce a similar effect. To test this hypothesis, I utilized the MISI spike detection method as in chapter 2(L. Chen et al. 2009). Unlike LRx_i, Gi-DREADD activation significantly increased averaged spontaneous RS burst rates in all cortical layers (Fig.11A). Distributions of spontaneous RS burst rates were significantly shifted across all cortical layers as well (Fig.11B). Gi-DREADD activation also increased evoked bursting rates. Bursting rates were significantly increased in L4 and L5/6, but not in L2/3

Figure 11: Gi-DREADD activation increases spontaneous RS bursting rates

A. Quantification of spontaneous RS bursting rates averaged by layer (mean +/- SEM). Spontaneous RS bursting rates significantly increased in all layers following CNO injection in Gi-DREADD infected mice, but not PV-cre control mice. (Wilcoxon signed rank test; Gi-DREADD [L2/3]**p < 0.0025; n = 8 mice, 23 units [L4] ** p < 0.0025; n = 10 mice, 31 units [L5/6] * p < 0.0025; n = 7 mice, 18 units; PV-cre ctrl[L2/3] NS; n = 8 mice [L4] NS; n = 8 mice [L5/6] NS, n = 5 mice). Gi-DREADD infected mice exhibited significantly different baseline bursting rates versus PV-cre controls. (Wilcoxon Rank Sum test [Gi-ctrl v. PV-cre ctrl] [L2/3] NS [L4] NS [L5/6] ^p < 0.025; Bonferroni corrected for 2 comparisons). **B.** Cumulative distribution of all spontaneous RS units. The distribution of spontaneous RS bursting rates shifted significantly in L4 and L5/6 following CNO injection in Gi-DREADD infected mice, but not PV-cre control mice. (Kolmogorov Smirnov test: Gi-DREADD [L2/3] **p < 0.0025; n = 8 mice, 23 units [L4] ***** p < 0.0000025; n = 10 mice, 31 units [L5/6] *** p < 0.00025; n = 7 mice, 18 units; PV-cre ctrl [L2/3] NS; n = 8 mice [L4] NS; n = 8 mice [L5/6] NS, n = 5 mice) Wilcoxon Rank Sum test [Gi-ctrl v. PV-cre ctrl] [L2/3] NS [L4] NS [L5/6] ***p < 0.00025; Bonferroni corrected for 2 comparisons) **C.** Averaged histograms of PV-cre mice data presented in A and B (n = 9 mice).D. Histograms of Gi-DREADD mice data presented in A (n = 10 mice).

Figure 12: Gi-DREADD activation increases evoked RS bursting rates

A. Quantification of evoked RS bursting rates averaged by layer (mean +/- SEM). evoked RS bursting rates significantly increased in all layers following CNO injection in Gi-DREADD infected mice, but not PV-cre control mice. (Wilcoxon signed rank test; Gi-DREADD [L2/3]**p < 0.0025; n = 8 mice, 23 units [L4] ** p < 0.0025; n = 10 mice, 31 units [L5/6] * p < 0.0025; n = 7 mice, 18 units; PV-cre ctrl[L2/3] NS; n = 8 mice [L4] NS; n = 8 mice [L5/6] NS, n = 5 mice). (Wilcoxon Rank Sum test [Gi-ctrl v. PV-cre ctrl] [L2/3] NS [L4] NS [L5/6] NS; Bonferroni corrected for 2 comparisons). **B.** Cumulative distribution of all evoked RS units. The distribution of evoked RS bursting rates shifted significantly in L4 and L5/6 following CNO injection in Gi-DREADD infected mice, but not PV-cre control mice. (Kolmogorov Smirnov test: Gi-DREADD [L2/3] **p < 0.0025; n = 8 mice, 23 units [L4] ***** p < 0.0000025; n = 10 mice, 31 units [L5/6] **** p < 0.000025; n = 7 mice, 18 units; PV-cre ctrl [L2/3] NS; n = 8 mice [L4] NS; n = 8 mice [L5/6] NS, n = 5 mice) Gi-DREADD infected mice exhibited a significantly different baseline distribution of evoked bursting rates versus PV-cre controls. Wilcoxon Rank Sum test [Gi-ctrl v. PV-cre ctrl] [L2/3] NS [L4] NS [L5/6] ***p < 0.00025; Bonferroni corrected for 2 comparisons) **C.** Averaged histograms of PV-cre mice data presented in A and B (n = 9 mice). D. Histograms of Gi-DREADD mice data presented in A (n = 10 mice).

Figure 11: Gi-DREADD activation increases spontaneous RS bursting rates

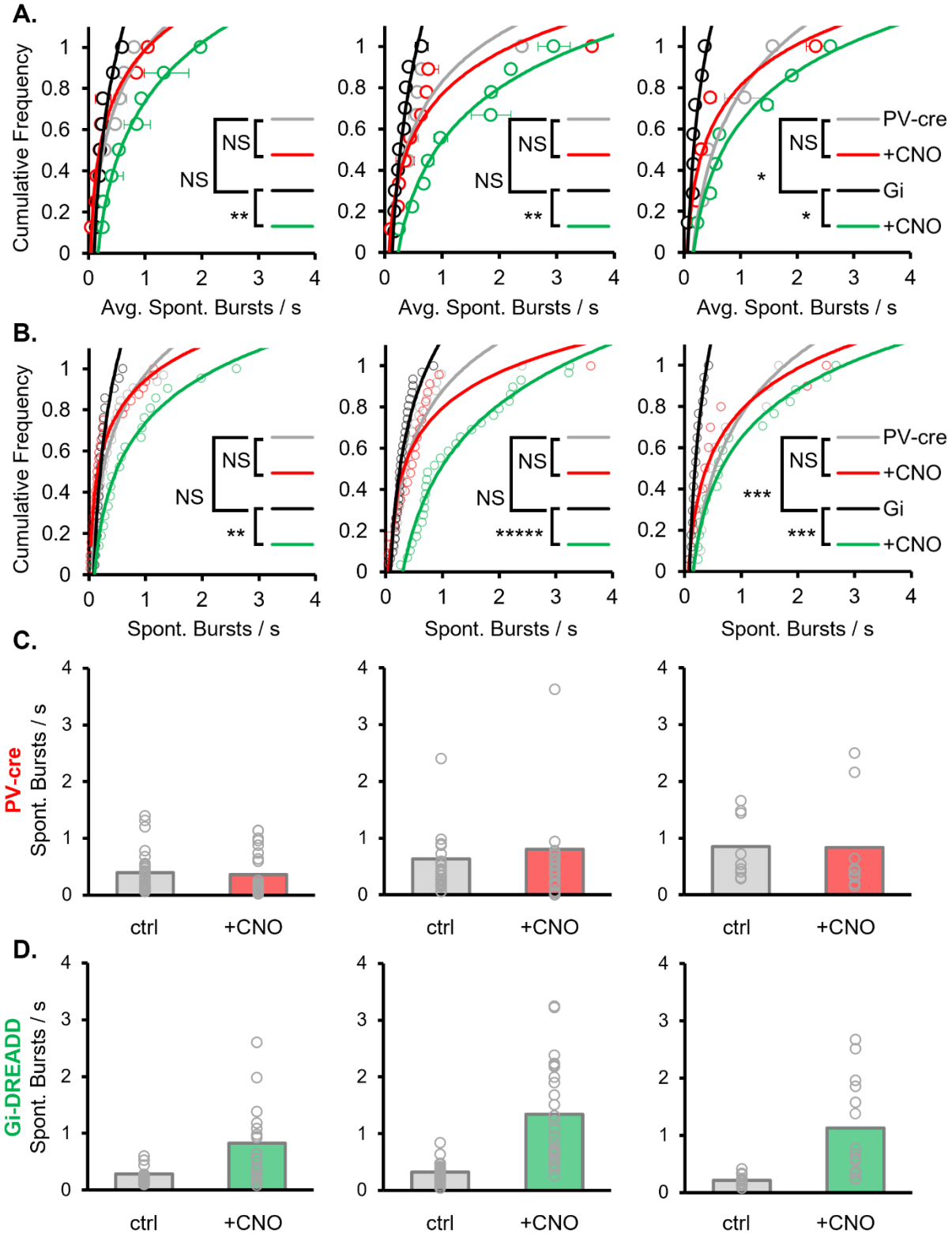

Figure 12: Gi-DREADD activation increases evoked RS bursting rates

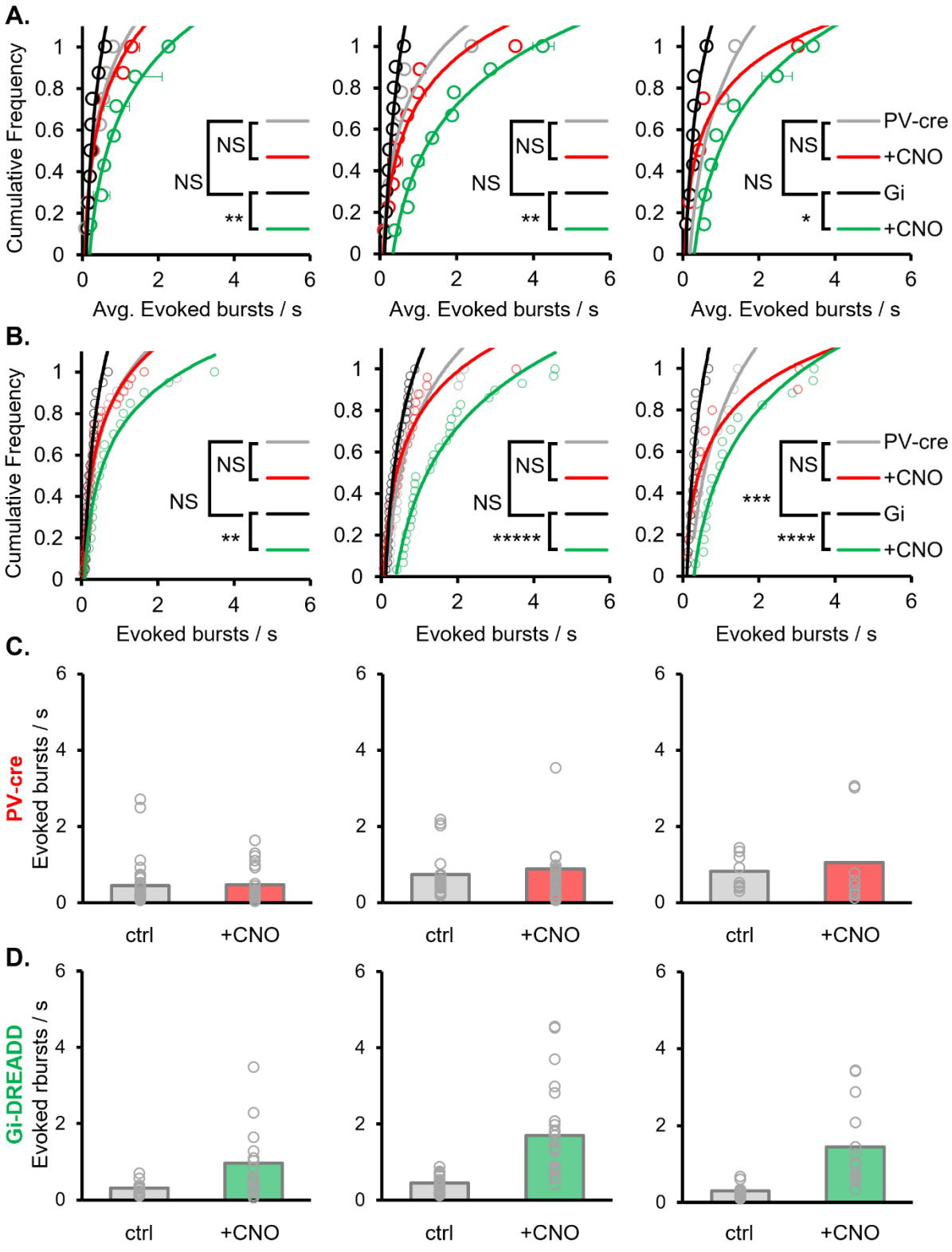

(Fig.12A). Distributions of spontaneous RS burst rates were significantly shifted across all cortical layers as well (Fig.12B). Gi-DREADD activation had no significant effect on averaged spontaneous RS burst duration, but significant shift in the burst duration was detected in Gi-DREAD mice in L2/3 and L4 (Fig.13B). No significant changes were detected in evoked burst duration in either cohort (Fig14). Averaged spontaneous RS burst content was unchanged by Gi-DREADD activation, but there was a significant rightward shift in the distribution of spontaneous RS burst spike content in L4 (Fig. 15A – B). Averaged evoked RS burst spike content increased significantly in L4 and L5/6, whereas the distribution of evoked RS burst spike content shifted significantly only in L4 (Fig.16A – B).

It is possible that stronger TC input during patterned visual stimulation is driving feedforward excitation of Martinotti-type SST-INS in L4. The inhibitory axons of these SST-INs ramify in the upper layers and inhibit the apical dendrites of L2/3 PYRs, and may compensate for the decrease in PV-IN-mediated inhibition in these superficial layers(Ji et al. 2016; Gentet et al. 2012). Optogenetic suppression of SST-INs in barrel cortex increases bursting activity in PYRs, likely by enabling increased integration of dendritic inputs preferentially inhibited by many SST-INs(Gentet et al. 2012). In rat hippocampus, the strength of feedforward somatic inhibition controls the temporal window for input summation; treating hippocampal slices with the $GABA_A$-R antagonist bicuculine increased the window for temporal summation from +/- 5ms to +/- 40 ms(Frederic Pouille and Scanziani 2001). Gi-DREADD activation in PV-INs likely disrupts strong feedforward somatic inhibition, broadening the temporal window for integration of bottom-up inputs to V1 and increasing bursting activity in an analogous

Figure 13: Gi-DREADD activation causes layer-specific shifts in the distribution of spontaneous RS burst duration

A. Quantification of spontaneous RS burst duration averaged by layer (mean +/- SEM). spontaneous RS burst duration was unchanged in Gi-DREADD-infected and PV-cre control mice. (Wilcoxon signed rank test; Gi-DREADD [L2/3] NS; n = 8 mice, 23 units [L4] NS; n = 10 mice, 31 units [L5/6] NS; n = 7 mice, 18 units; PV-cre ctrl[L2/3] NS; n = 8 mice [L4] NS; n = 8 mice [L5/6] NS, n = 5 mice). (Wilcoxon Rank Sum test [Gi-ctrl v. PV-cre ctrl] [L2/3] NS [L4] NS [L5/6] NS; Bonferroni corrected for 2 comparisons). **B.** Cumulative distribution of all spontaneous RS units. The distribution of spontaneous RS burst duration shifted significantly to the left in L2/3 and L4 following CNO injection in Gi-DREADD infected mice, but not PV-cre control mice. (Kolmogorov Smirnov test: Gi-DREADD [L2/3] *$p < 0.025$; n = 8 mice, 23 units [L4] ** $p < 0.0025$; n = 10 mice, 31 units [L5/6] NS; n = 7 mice, 18 units; PV-cre ctrl [L2/3] NS; n = 8 mice [L4] NS; n = 8 mice [L5/6] NS, n = 5 mice) Wilcoxon Rank Sum test [Gi-ctrl v. PV-cre ctrl] [L2/3] NS [L4] NS [L5/6] NS; Bonferroni corrected for 2 comparisons) **C.** Averaged histograms of PV-cre mice data presented in A and B (n = 9 mice). D. Histograms of Gi-DREADD mice data presented in A (n = 10 mice).

Figure 14: Gi-DREADD activation has no effect on evoked RS burst duration

A. Quantification of evoked RS burst duration averaged by layer (mean +/- SEM). evoked RS burst duration was unchanged in Gi-DREADD-infected and PV-cre control mice. (Wilcoxon signed rank test; Gi-DREADD [L2/3] NS; n = 8 mice, 23 units [L4] NS; n = 10 mice, 31 units [L5/6] NS; n = 7 mice, 18 units; PV-cre ctrl[L2/3] NS; n = 8 mice [L4] NS; n = 8 mice [L5/6] NS, n = 5 mice). (Wilcoxon Rank Sum test [Gi-ctrl v. PV-cre ctrl] [L2/3] NS [L4] NS [L5/6] NS; Bonferroni corrected for 2 comparisons). **B.** Cumulative distribution of all evoked RS units. The distribution of evoked RS burst duration was unchanged following CNO injection in Gi-DREADD infected mice and PV-cre control mice. (Kolmogorov Smirnov test: Gi-DREADD [L2/3] NS; n = 8 mice, 23 units [L4] NS; n = 10 mice, 31 units [L5/6] NS; n = 7 mice, 18 units; PV-cre ctrl [L2/3] NS; n = 8 mice [L4] NS; n = 8 mice [L5/6] NS, n = 5 mice) Wilcoxon Rank Sum test [Gi-ctrl v. PV-cre ctrl] [L2/3] NS [L4] NS [L5/6] NS; Bonferroni corrected for 2 comparisons) **C.** Averaged histograms of PV-cre mice data presented in A and B (n = 9 mice). D. Histograms of Gi-DREADD mice data presented in A (n = 10 mice).

Figure 13: Gi-DREADD activation causes layer-specific shifts in the distribution of spontaneous RS burst duration

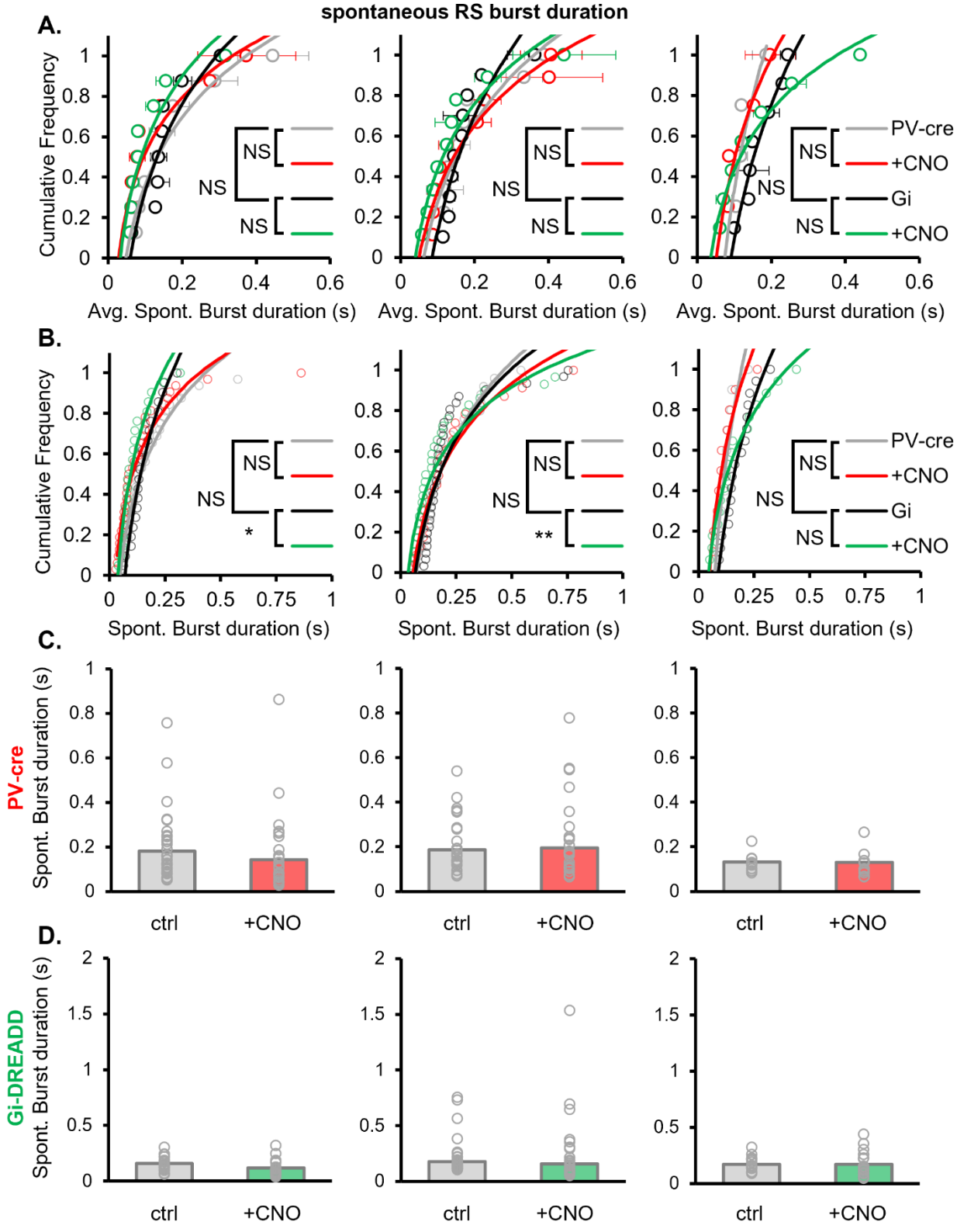

Figure 14: Gi-DREADD activation has no effect on evoked RS burst duration

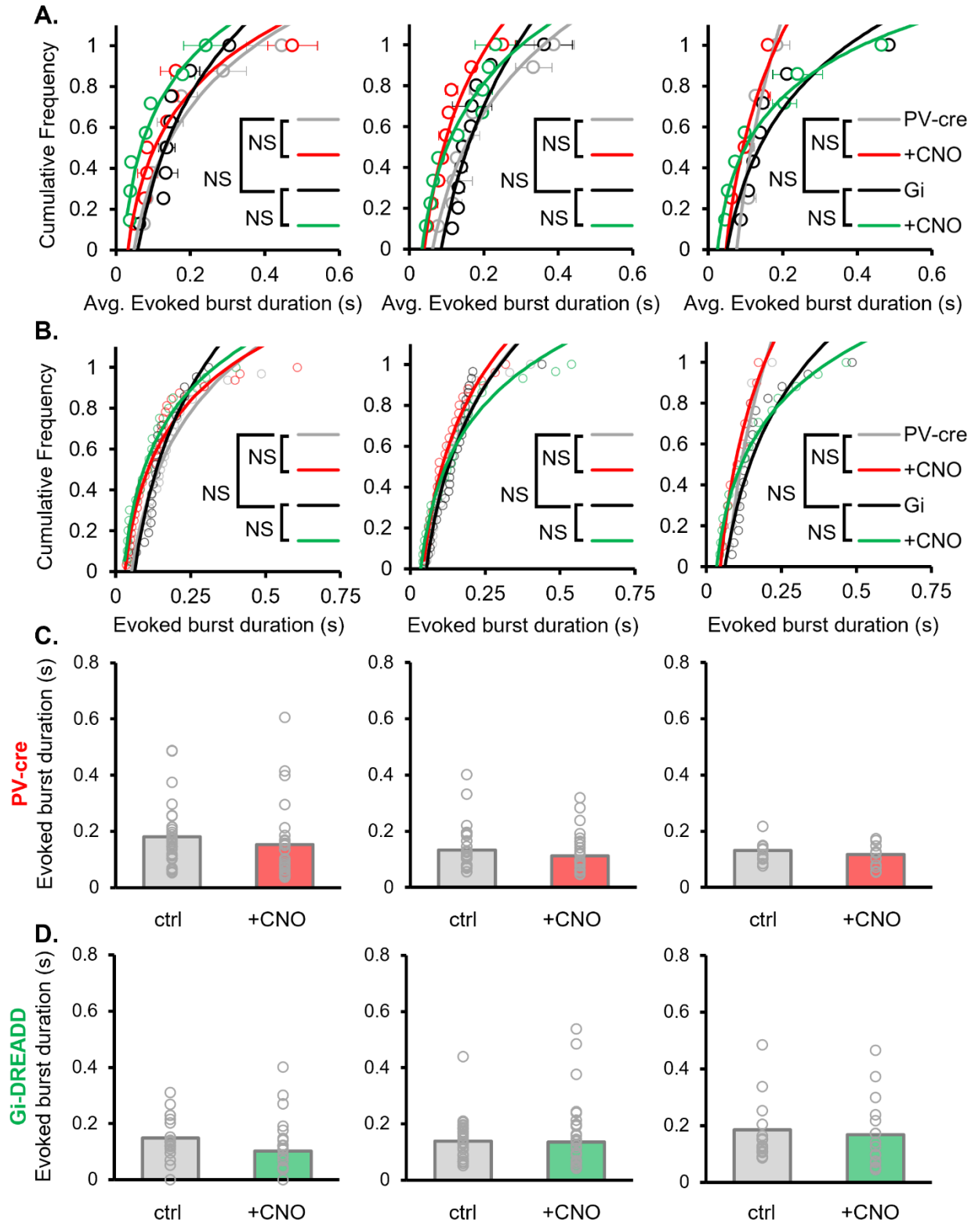

Figure 15: Gi-DREADD activation shifts the distribution of spontaneous RS burst spike content in Layer 4

A. Quantification of spontaneous RS burst spike content averaged by layer (mean +/- SEM). spontaneous RS burst spike content was unchanged in Gi-DREADD-infected and PV-cre control mice. (Wilcoxon signed rank test; Gi-DREADD [L2/3] NS; n = 8 mice, 23 units [L4] NS; n = 10 mice, 31 units [L5/6] NS; n = 7 mice, 18 units; PV-cre ctrl[L2/3] NS; n = 8 mice [L4] NS; n = 8 mice [L5/6] NS, n = 5 mice). (Wilcoxon Rank Sum test [Gi-ctrl v. PV-cre ctrl] [L2/3] NS [L4] NS [L5/6] NS; Bonferroni corrected for 2 comparisons). **B.** Cumulative distribution of all spontaneous RS units. The distribution of spontaneous RS burst spike content was shifted significantly only in L4 following CNO injection in Gi-DREADD infected mice, but not PV-cre control mice. (Kolmogorov Smirnov test: Gi-DREADD [L2/3] NS; n = 8 mice, 23 units [L4] ***p < 0.00025; n = 10 mice, 31 units [L5/6] NS; n = 7 mice, 18 units; PV-cre ctrl [L2/3] NS; n = 8 mice [L4] NS; n = 8 mice [L5/6] NS, n = 5 mice) Wilcoxon Rank Sum test [Gi-ctrl v. PV-cre ctrl] [L2/3] NS [L4] NS [L5/6] NS; Bonferroni corrected for 2 comparisons) **C.** Averaged histograms of PV-cre mice data presented in A and B (n = 9 mice). **D.** Histograms of Gi-DREADD mice data presented in A (n = 10 mice).

Figure 16: Gi-DREADD activation causes layer-specific changes in evoked RS burst spike content

A. Quantification of evoked RS burst spike content averaged by layer (mean +/- SEM). evoked RS burst spike content significantly increased in L4 and L5/6 in Gi-DREADD-infected and PV-cre control mice. (Wilcoxon signed rank test; Gi-DREADD [L2/3] NS; n = 8 mice, 23 units [L4] **p < 0.0025; n = 10 mice, 31 units [L5/6] NS; n = 7 mice, 18 units; PV-cre ctrl[L2/3] NS; n = 8 mice [L4] NS; n = 8 mice [L5/6] NS, n = 5 mice). (Wilcoxon Rank Sum test [Gi-ctrl v. PV-cre ctrl] [L2/3] NS [L4] NS [L5/6] NS; Bonferroni corrected for 2 comparisons). **B.** Cumulative distribution of all evoked RS units. The distribution of evoked RS burst spike content was shifted significantly in L4 following CNO injection in Gi-DREADD infected mice, but not PV-cre control mice. (Kolmogorov Smirnov test: Gi-DREADD [L2/3] NS; n = 8 mice, 23 units [L4] ****p < 0.000025; n = 10 mice, 31 units [L5/6] NS; n = 7 mice, 18 units; PV-cre ctrl [L2/3] NS; n = 8 mice [L4] NS; n = 8 mice [L5/6] NS, n = 5 mice) Wilcoxon Rank Sum test [Gi-ctrl v. PV-cre ctrl] [L2/3] NS [L4] NS [L5/6] NS; Bonferroni corrected for 2 comparisons) **C.** Averaged histograms of PV-cre mice data presented in A and B (n = 9 mice).**D.** Histograms of Gi-DREADD mice data presented in A (n = 10 mice).

Figure 15: Gi-DREADD activation shifts the distribution of spontaneous RS burst spike content in Layer 4

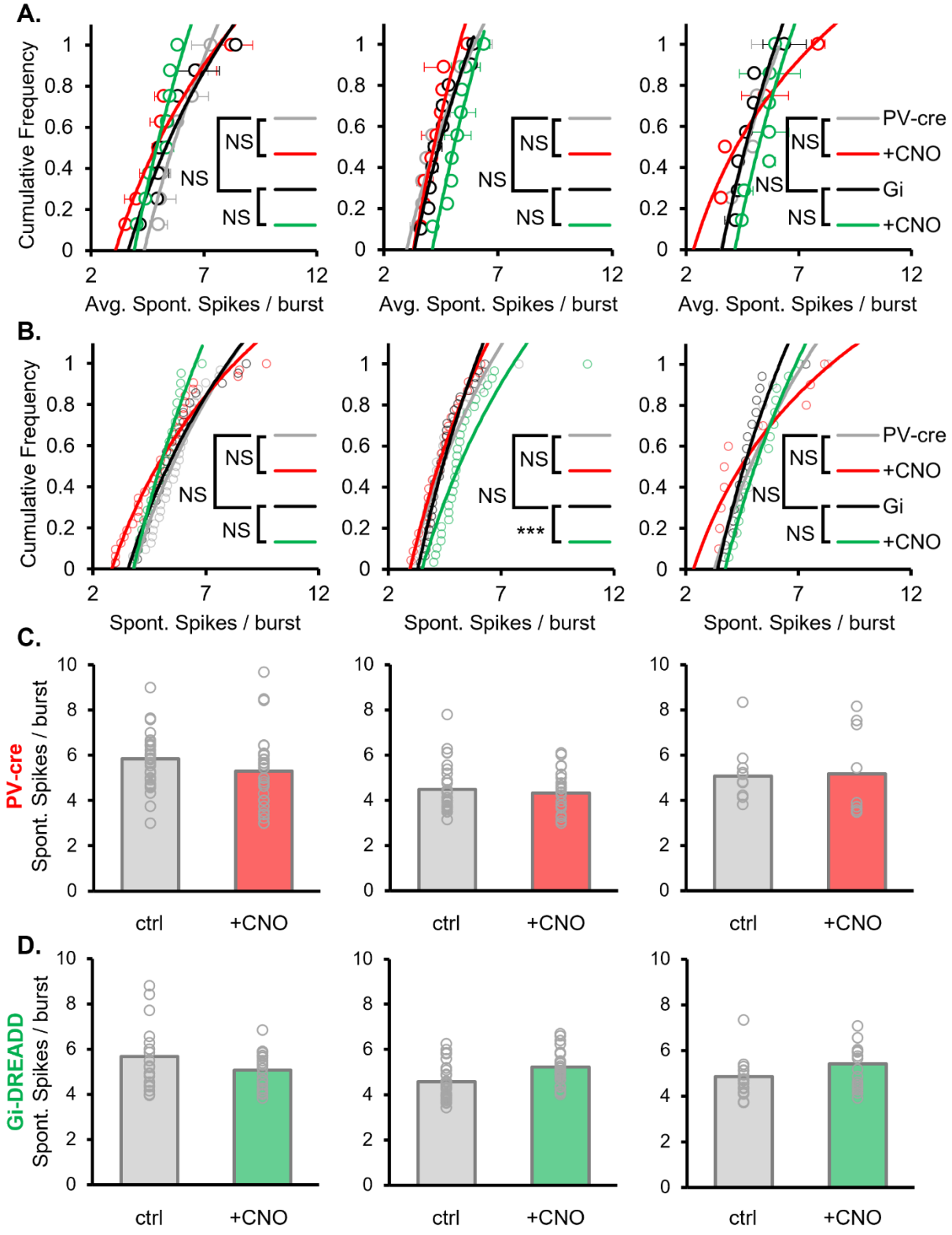

Figure 16: Gi-DREADD activation causes layer-specific changes in evoked RS burst spike content

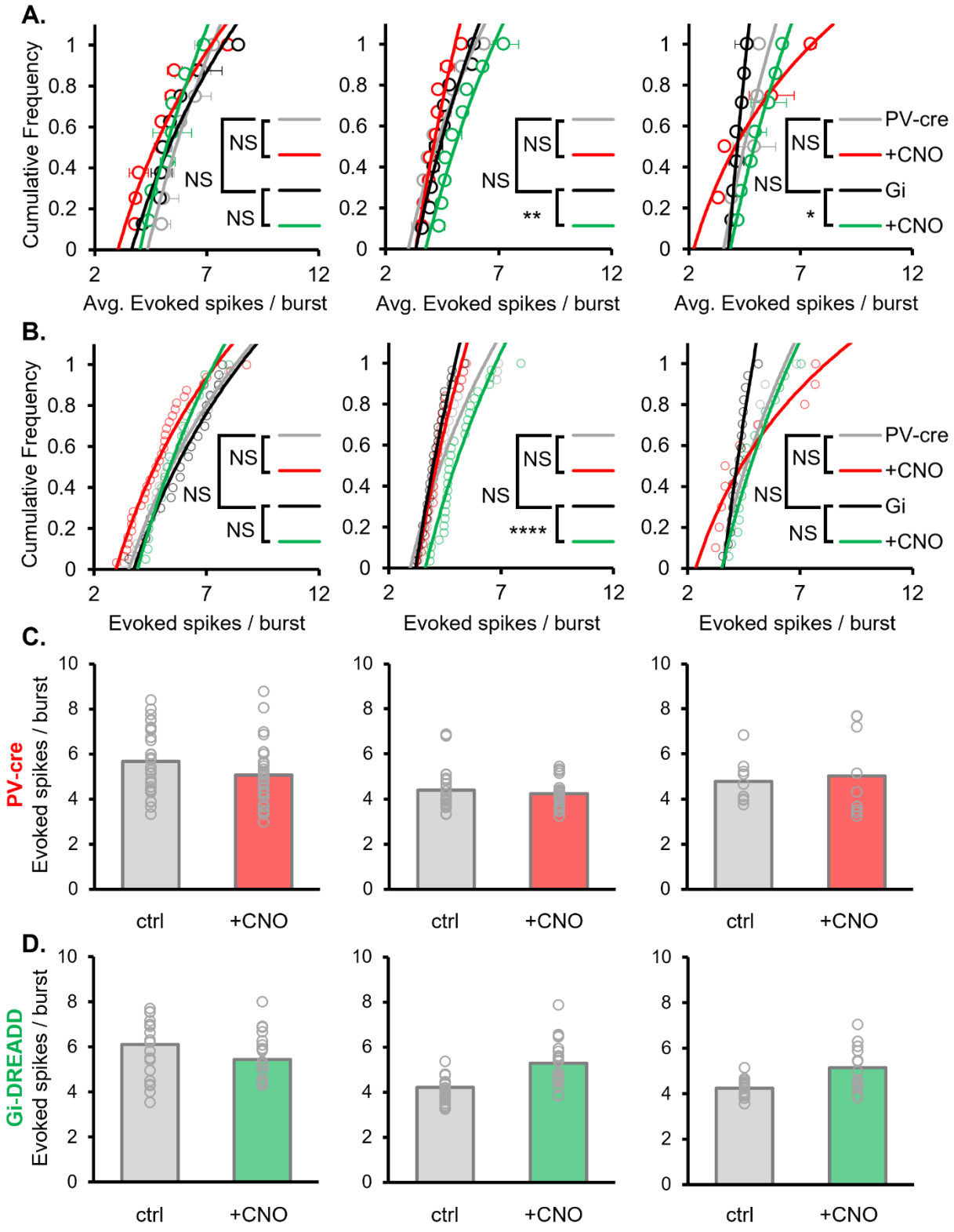

fashion to optogenetic suppression of SST-INs. The discrepancy between changes in burst spike content and burst duration is perhaps more interesting (Fig.15A, Fig.13A). Increased spontaneous bursting rate in RS neurons in the absence of increased burst duration or spikes per burst implies that the mechanisms governing the quantity, but not the properties of bursts are engaged by Gi-DREADD activation in the absence of patterned visual stimuli. Changes in L5/6 bursting during the evoked condition may be due to inhibition of L6 PV-INs, whose inhibitory axons target L4 and L5/6 PYRs and are typically recruited by corticothalamic projection neurons(Bortone, Olsen, and Scanziani 2014). Feedback to the LGN has been proposed as a key mechanism underlying the expression of SRP, and Gi-DREADD activation increases VEP amplitude in a manner reminiscent of SRP(Kaplan et al. 2016; Montgomery et al. 2022). Work in cat LGN has demonstrated an “all-or-nothing” bursting response in thalamic relay neurons: current injection in these neurons results in a single discrete burst, with increasing current steps decreasing the latency to burst onset. At higher levels of current injection, the neuron fires an initial burst before transitioning to tonic firing (Zhan et al. 1999). In this regard, bursts from the thalamus may behave as discreet events that would not vary widely in spike content or duration. Thalamic bursts can be visually induced, and covary with stimulus parameters like contrast(Sanchez et al. 2023). The grey screen stimulus used for spontaneous activity recordings in these experiments is 0% contrast, and therefore should not evoke a strong response from the LGN. However, some L6 PYRs send feedback to the LGN and optogenetic activation of these corticothalamic feedback projections entrains coherent spiking activity between the LGN and L6 PYRs(Durkin et al. 2017). It is therefore possible that disinhibited (RS) PYRs in L6 are recruiting LGN

activity and promoting thalamic bursting. Bursting TC inputs to V1 would then activate L4 PYRs in the absence of strong PV-IN-mediated feedforward inhibition, resulting in bursting activity in L4, which is then transmitted to L2/3 and L5/6. In other words, without patterned activity to modulate the thalamic input, cortical activity may simply reflect the bursting input from the thalamus.

Finally, I looked at the effects of Gi-DREADD activation on (FS) PV-IN bursting characteristics from all cortical layers. Given the earlier descriptions of the impact of Gi-DREADD activation on evoked calcium responses, I predicted that (FS) PV-IN burst rates would decrease following Gi-DREADD activation(Kuhlman et al. 2013; L. Huang et al. 2021). I saw no significant change in averaged spontaneous FS burst rate or duration, but I did detect a significant increase in spontaneous spikes per burst (Fig.17A). A significant rightward shift was also detected in the spontaneous FS burst spike content (Fig.17B). Conversely, no changes were detected in any parameter of averaged evoked FS bursts, while the significant rightward shift in spikes per burst was maintained in the distribution of evoked FS burst content (Fig.18A – B). These unexpected results may be attributable to the same reasons discussed in section 3.4.3.

One caveat to these experiments: a significant difference was detected in L5/6 spontaneous and evoked bursting activity between Gi-DREADD infected and PV-cre control mice across several parameters (Fig.11A – B; Fig.12B; Fig.17A – B). However, the difference precedes the injection of CNO, and were due to differences observed in two subject mice that were slightly younger (~P60 at time of recording, versus ~P80 – P90 for other subjects). These mice were only used for evaluating the effects of CNO on DREADD activation and were not part of the DE and MD cohort in subsequent sections.

Figure 17: Gi-DREADD activation increased spontaneous FS burst spike

A. Quantification of spontaneous FS burst characteristics averaged by animal across al layers (mean +/- SEM). Averaged spontaneous FS burst spike content increased in L5/6 following CNO injection in Gi-DREADD-infected and PV-cre control mice. (Wilcoxon signed rank test; Burst rate: [Gi-DREADD] NS; n = 6 mice, 15 units [PV-cre ctrl] NS; n = 6 mice, 17 units; [Gi-DREADD v. PV-cre ctrl] NS; Bonferroni corrected for 2 comparisons; Burst duration: [Gi-DREADD] NS; n = 6 mice, 15 units [PV-cre ctrl] NS; n = 6 mice, 17 units; [Gi-DREADD v. PV-cre ctrl] NS; Bonferroni corrected for 2 comparisons; Burst spike content: [Gi-DREADD] **p < 0.0025; n = 6 mice, 15 units [PV-cre ctrl] NS; n = 6 mice, 17 units; [Gi-DREADD v. PV-cre ctrl] NS; Bonferroni corrected for 2 comparisons) There was a significant difference in baseline spontaneous FS spike content between Gi-DREADD and PV-cre control mice. (Wilcoxon rank sum test; Burst rate: [PV-cre ctrl vs. Gi-DREADD] NS; n = 12 mice; Bonferroni corrected for 2 comparisons; Burst duration: [PV-cre ctrl vs. Gi-DREADD] NS; n = 12 mice; Bonferroni corrected for 2 comparisons; Burst spike content: [PV-cre ctrl vs. Gi-DREADD]**p < 0.0025; n = 12 mice; Bonferroni corrected for 2 comparisons) **B.** Cumulative distribution of all spontaneous FS units. The distribution of spontaneous FS burst spike content shifted significantly following CNO injection in Gi-DREADD infected mice but not PV-cre control mice (Kolmogorov Smirnov test ; Burst rate: [Gi-DREADD] NS; n = 6 mice, 15 [PV-cre ctrl] NS; n = 6 mice; [Gi-DREADD v. PV-cre ctrl] NS; Bonferroni corrected for 2 comparisons; Burst duration: [Gi-DREADD] NS; n = 6 mice, 15 [PV-cre ctrl] NS; n = 6 mice; [Gi-DREADD v. PV-cre ctrl] NS; Bonferroni corrected for 2 comparisons; Burst spike content: [Gi-DREADD] ****p < 0.000025; n = 6 mice, 15 [PV-cre ctrl] NS; n = 6 mice; [Gi-DREADD v. PV-cre ctrl] NS; Bonferroni corrected for 2 comparisons) There was a significant difference in baseline spontaneous FS burst duration and spike content between Gi-DREADD and PV-cre control mice. (Wilcoxon rank sum test; Burst rate: [PV-cre ctrl vs. Gi-DREADD] NS; n = 12 mice; Bonferroni corrected for 2 comparisons; Burst duration: [PV-cre ctrl vs. Gi-DREADD] *p < 0.025; n = 12 mice; Bonferroni corrected for 2 comparisons; Burst spike content: [PV-cre ctrl vs. Gi-DREADD] ***p < 0.00025; n = 12 mice; Bonferroni corrected for 2 comparisons) **C.** Averaged histograms of PV-cre mice data presented in A and B (n = 9 mice). **D.** Histograms of Gi-DREADD mice data presented in A (n = 10 mice).

Figure 17: Gi-DREADD activation increased spontaneous FS burst spike

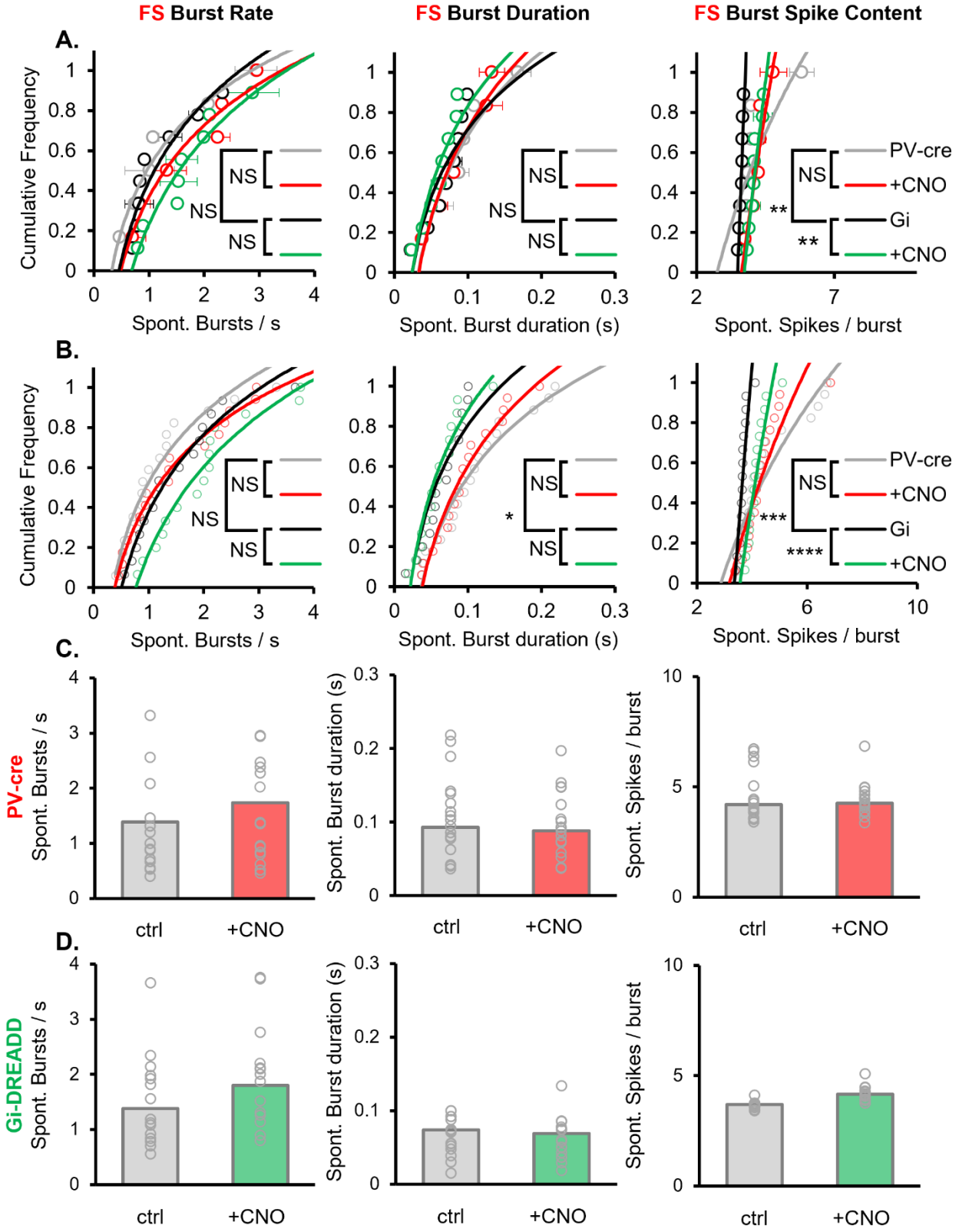

Figure 18: Gi-DREADD activation shifts the distribution of evoked FS burst spike content

A. Quantification of evoked FS burst characteristics averaged by animal across al layers (mean +/- SEM). Averaged evoked FS burst spike content increased in L5/6 following CNO injection in Gi-DREADD-infected and PV-cre control mice. (Wilcoxon signed rank test; Burst rate: [Gi-DREADD] NS; n = 6 mice, 15 units [PV-cre ctrl] NS; n = 6 mice, 17 units; [Gi-DREADD v. PV-cre ctrl] NS; Bonferroni corrected for 2 comparisons; Burst duration: [Gi-DREADD] NS; n = 6 mice, 15 units [PV-cre ctrl] NS; n = 6 mice, 17 units; [Gi-DREADD v. PV-cre ctrl] NS; Bonferroni corrected for 2 comparisons; Burst spike content: [Gi-DREADD] NS; n = 6 mice, 15 units [PV-cre ctrl] NS; n = 6 mice, 17 units; [Gi-DREADD v. PV-cre ctrl] NS; Bonferroni corrected for 2 comparisons) (Wilcoxon rank sum test; Burst rate: [PV-cre ctrl vs. Gi-DREADD] NS; n = 12 mice; Bonferroni corrected for 2 comparisons; Burst duration: [PV-cre ctrl vs. Gi-DREADD] NS; n = 12 mice; Bonferroni corrected for 2 comparisons; Burst spike content: [PV-cre ctrl vs. Gi-DREADD NS; n = 12 mice; Bonferroni corrected for 2 comparisons) **B.** Cumulative distribution of all evoked FS units. The distribution of evoked FS burst spike content shifted significantly following CNO injection in Gi-DREADD infected mice but not PV-cre control mice (Kolmogorov Smirnov test; Burst rate: [Gi-DREADD] NS; n = 6 mice, 15 [PV-cre ctrl] NS; n = 6 mice; [Gi-DREADD v. PV-cre ctrl] NS; Bonferroni corrected for 2 comparisons; Burst duration: [Gi-DREADD] NS; n = 6 mice, 15 [PV-cre ctrl] NS; n = 6 mice; [Gi-DREADD v. PV-cre ctrl] NS; Bonferroni corrected for 2 comparisons; Burst spike content: [Gi-DREADD] **p < 0.0025; n = 6 mice, 15 [PV-cre ctrl] NS; n = 6 mice; [Gi-DREADD v. PV-cre ctrl] NS; Bonferroni corrected for 2 comparisons) (Wilcoxon rank sum test; Burst rate: [PV-cre ctrl vs. Gi-DREADD] NS; n = 12 mice; Bonferroni corrected for 2 comparisons; Burst duration: [PV-cre ctrl vs. Gi-DREADD] NS; n = 12 mice; Bonferroni corrected for 2 comparisons; Burst spike content: [PV-cre ctrl vs. Gi-DREADD] NS; n = 12 mice; Bonferroni corrected for 2 comparisons) **C.** Averaged histograms of PV-cre mice data presented in A and B (n = 9 mice).**D.** Histograms of Gi-DREADD mice data presented in A (n = 10 mice).

Figure 18: Gi-DREADD activation shifts the distribution of evoked FS burst spike content

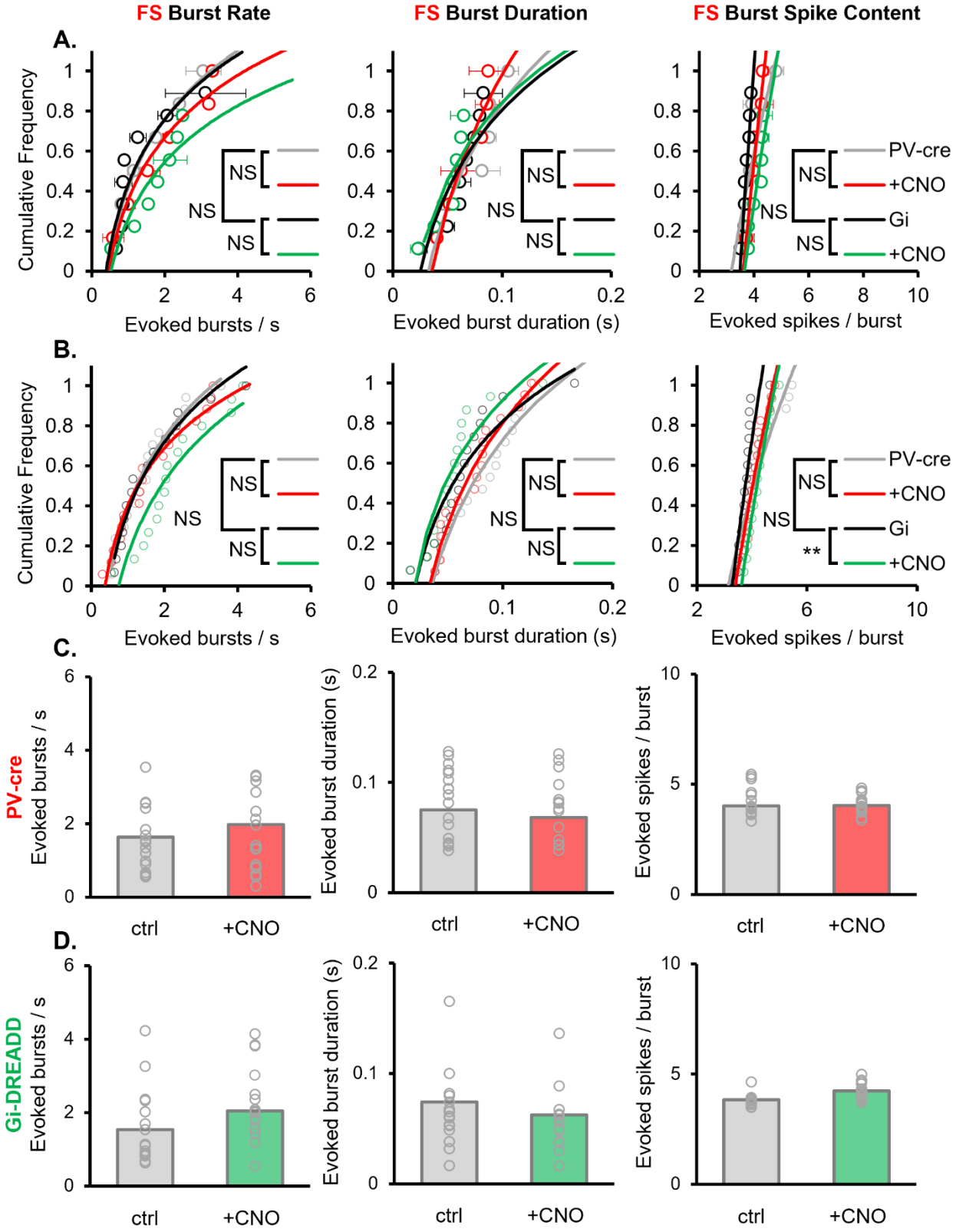

3.4.5 Disinhibition of V1b prevents MD-induced ocular dominance shifts during LRx, but not loss of acuity.

I was originally motivated to test the impact of Gi-DREADD suppression of PV IN output on DE/LRx after it was shown to enable an ocular dominance shift in post-CP aged mice. PV IN-specific activation of Gi-DREADD *in vivo* decreased visually evoked GCaMP6 calcium responses in infected PV-INs, indicating that PV-IN activity was being suppressed(Kuhlman et al. 2013; L. Huang et al. 2021). Gi-DREADD-expressing PV-cre mice then underwent MD at P35 and received two injections of CNO (5mg/kg animal weight), 12 hours apart, suppressing PV-IN activity for ~ 24 hours. The MD eye was opened on the third day, and calcium imaging responses to contralateral (deprived) eye stimulation were compared to ipsilateral (non-deprived) eye stimulus responses. One day of PV-IN suppression caused a decrease in calcium responses to deprived-eye visual stimulation, indicative of an ocular dominance shift. Interestingly, because PV-IN responses were suppressed for just one day, only the initial response to monocular deprivation would be impacted. Deprived eye depression characteristically precedes open eye potentiation by two to four days(Frenkel and Bear 2004; Kuhlman et al. 2013). This previously reported Gi-DREADD experiment was meant to replicate the impact the circuit-level effects of monocular deprivation in CP-aged V1, wherein reduced PV-IN-mediated inhibition resulting from decreased input from the deprived eye enabled excitatory PYR activity in deprived V1 to become increased versus control, enabling subsequent OD shifts (Kuhlman et al. 2013). In Kuhlman et al., (2013), the interpretation was that increased excitatory activity enabled ODP based on competition between the eyes. In our current model of ODP induction, the transient reduction in PV-IN firing rates

by MD behaves in much the same way as DE: disinhibition of excitatory cortical responses leads to an upregulation of GluN2B-containing NMDA-Rs within the local L2/3 circuit, enabling spike-timing dependent LTD of deprived-eye responses(Bridi et al. 2018; Severin et al. 2021).

In Chapter 2, I demonstrated that spontaneous and evoked (RS) PYR firing rates are significantly increased following ten days of DE during LRx_i, and that average activity returns to baseline levels on the subsequent day, LRx_s. An intriguing possibility is that DE rejuvenates V1 to a pre-CP, hyper-excitable state, and that subsequent visual experience during LRx is necessary to recruit PV-INs and reduce excitability to a level that enables the expression of ODP. Manipulations that decrease recruitment of PV-INs exhibit opposing effects depending on state of maturation of cortical inhibition. Over expression of a dominant negative NARP mutant in adult mice enables a juvenile-like OD shifts following brief MD, likely via disruption of patterns of local intralaminar excitatory drive onto PV-INs in L2/3(Severin et al. 2021). Conversely, constitutive knockdown of NARP prior to the CP prevents the expression of ODP, as does overexpression of NARP during the CP(Severin et al. 2021; Yu Gu et al. 2013). If the hyper-excitability of dark exposed V1 mimics the pre-CP juvenile brain, decreasing recruitment of PV-INs during LRx may function like constitutive knockdown of NARP prior to the CP and block the expression of ODP.

I therefore tested the hypothesis that prolonged disinhibition of V1 activity during LRx would occlude the reactivation of ODP. PV-cre mice were implanted in adulthood, and approximately half received intracortical injection of AAV-hsyn-FLEX-hM4D-(Gi)-mCherry to the left hemisphere of the binocular visual cortex (P53 – P80; males [Gi-

DREADD, PV-cre ctrl] n = 5,5; females [Gi-DREADD, PV-cre ctrl] n = 6, 5). Experiments were performed in mice >P90 to avoid the potential confounds of ODP that may be initiated late into adulthood in mice (Sawtell et al. 2003). After evaluating the effect of Gi-DREADD and confirming the lack of off-target CNO effects, subjects were shown monocular visual stimuli to calculate ocular dominance indices (ODI). Monocular visual spatial acuity was estimated physiologically via VEP amplitude, which covaries with the spatial frequency of the visual stimulus(Montey, Eaton, and Quinlan 2013; He et al. 2007). ODI reflects the normal contralateral bias in visual response amplitude in mice. Implanted mice were transferred to a light-tight dark room at age P90 – P97 for ten days. Prior to LRx_i, mice were injected with CNO (0.5 mg/kg) in the dark using IR illumination night vision goggles. Subsequently, they were removed from the dark room and underwent monocular deprivation surgery contralateral to the injected hemisphere (i.e., the right eye). Both Gi-DREADD-injected and PV-cre control mice received twice daily injections of CNO for two and a half days, allowing for CNO washout before eye-opening and a subsequent round of post-LRx visual stimulations.

Disinhibition of V1b via Gi-DREADD activation during LRx occludes the reactivation of ODP. No shifts in ODI were detected in Gi-DREADD infected mice. As expected, DE/LRx reactivated sensitivity of MD in PV-cre controls (Fig.19, left). Importantly, the changes in ODI were due to both deprived eye depression and open eye potentiation, the former is the hallmark of juvenile ODP(Fig.19, red waveforms)(Frenkel and Bear 2004). This result is in accordance with our model of experience dependent homeostatic plasticity engaged by DE/LRx. In normal adulthood, spontaneous activity is low relative to evoked, DE increases spontaneous activity

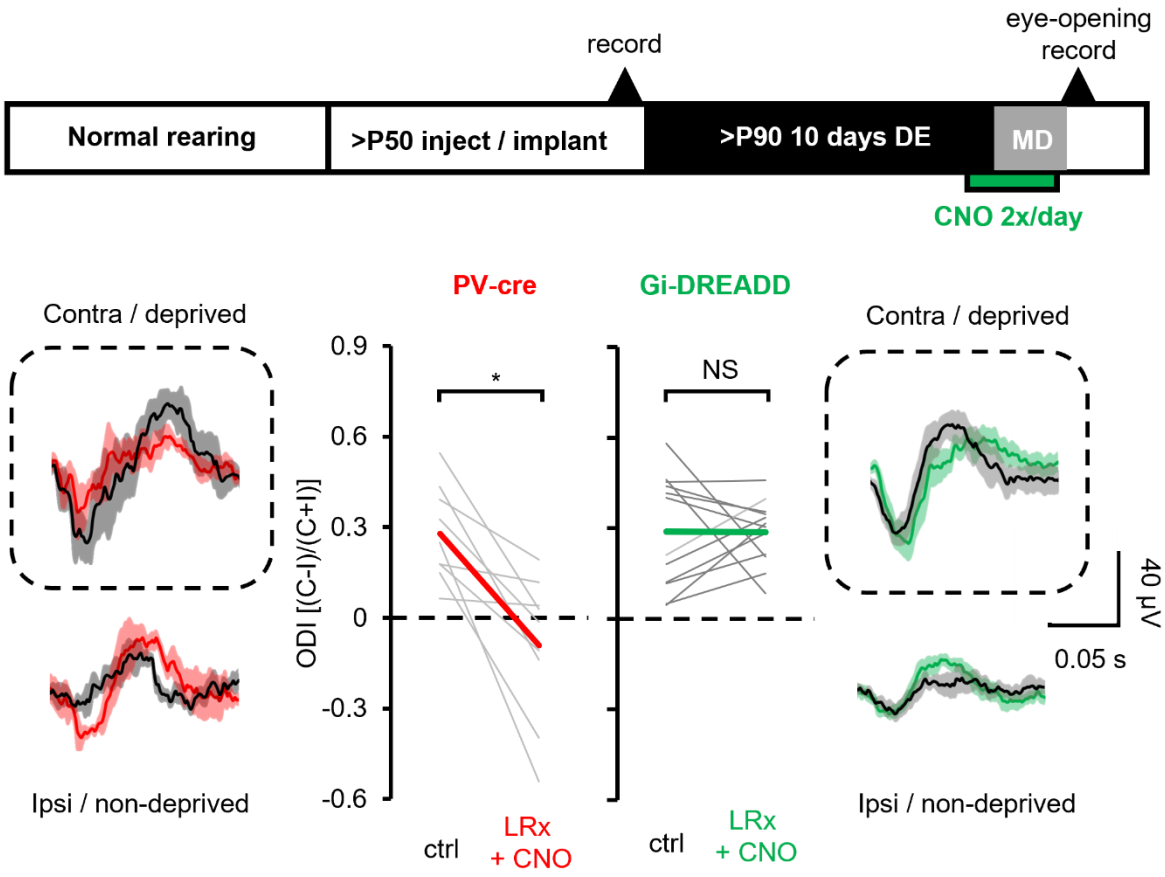

Figure 19: Gi-DREADD activation during LRx blocks the reactivation of ODP

(Top) Experimental timeline. **(bottom)** Quantification of ODI following DE + LRx + MD averaged by animal. Gi-DREADD activation prevented negative shifts in ODI in Gi-DREAD-infected mice (green line), but not in PV-cre control mice (red line). ODI shifts were prevented in all layers (Wilcoxon signed rank test; (Gi-DREADD [L2/3] NS; n = 9 mice [L4] NS; n = 10 mice [L5/6] NS, n = 10 mice; PV-cre ctrl [L2/3] *p < 0.025; n = 9 mice [L4] *p < 0.025; n = 9 mice [L5/6] *p < 0.025; n = 9 mice; Wilcoxon Rank Sum test [Gi-ctrl v. PV-cre ctrl] [L2/3] NS [L4] NS [L5/6] NS; Bonferroni corrected for 2 comparisons) **B.** Average L4 VEPs recorded before and after DE + LRx + CNO. **(left)** Note that in PV-cre control mice, the deprived eye VEP depresses, and the open eye VEP potentiates.

driving the upregulation of GluN2b-containing NMDA-Rs and lowering the threshold for LTP. While this sets the stage for LTP during LRx, activity levels are too elevated to allow meaningful STDP between visual inputs. In chapter 2, I showed that activity decreases to baseline levels following one day of LRx. I propose that this decrease in spontaneous activity allows evoked activity to drive STDP LTP. Plasticity following LRx

is further enabled by MMP-9 activation at TC synapses. However, Gi-DREADD activation elevated spontaneous activity levels, and the noise floor of activity is too high to allow meaningful competition between the eyes, thereby blocking a change in ODI.

Supporting this notion, we previously showed that two days of bilateral lid suture coupled with concurrent Gi-DREADD activation in PV-INs was sufficient to cause an upregulation of GluN2B-containing NMDA-Rs, whereas Gi-DREADD activation alone was not(Bridi et al. 2018). This result demonstrates that un-patterned stimulation through the eyelids does not increase spontaneous V1 activity sufficiently to lower the threshold for LTP, nor does Gi-DREADD activation alone. Combining approaches can shift spontaneous activity to the level required to enable metaplasticity. Similarly, Gi-DREADD combined with LRx maintains V1 in a state of plasticity-occluding hyperexcitability. Conversely, as discussed above, mismatched visual input coupled with Gi-DREADD activation in PV-INs with normal visual experience enables spontaneous activity in the deprived hemisphere to reach a the permissive for enabling ODP(Kuhlman et al. 2013). Taken together, these results demonstrate the additive effect of prior visual experience and PV-IN inhibition to the benefit or detriment of ODP. Interestingly, Gi-DREADD activation did not block the reactivation of plasticity of acuity (Fig.20). This is consistent with previous reports demonstrating that the plasticity of acuity resides in the LGN. Mice lacking systemic expression of NgR1, a receptor for the axon outgrowth inhibiting molecular Nogo, express ODP throughout life and spontaneously recover acuity following MD. Targeted deletion of NgR1 in cortical PV-INs enabled spontaneous recovery of ODI from monocular deprivation, but did not

permit spontaneous recovery of visual acuity from monocular deprivation(Stephany et al. 2014).

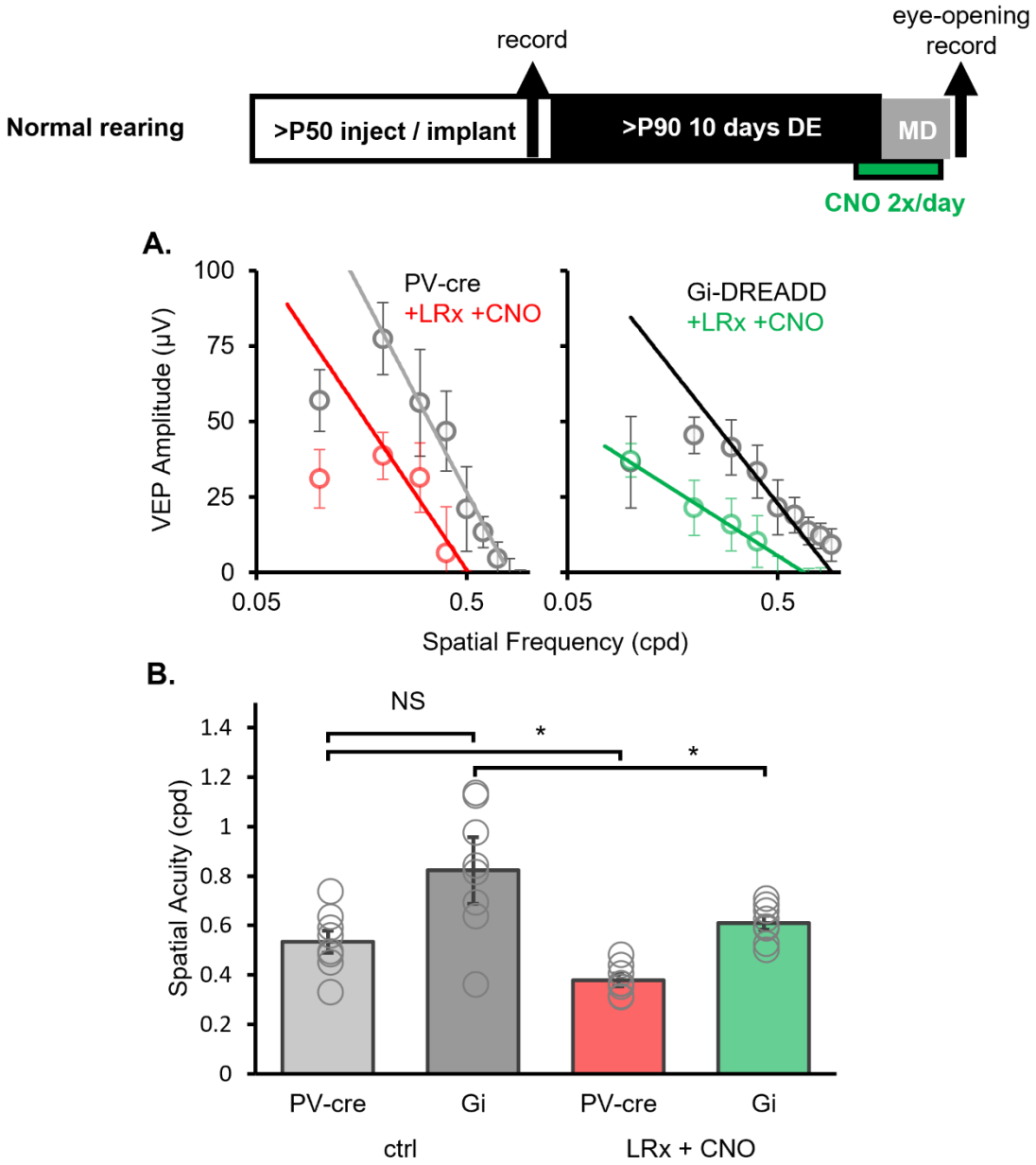

Figure 20: Reactivation of Acuity plasticity unaffected by Gi-DREADD activation

(top) experimental timeline. **A.** Linear regression of L4 VEP amplitude in response to reversing grating of increasing spatial frequency (cycles per degree, cpd). **B** Histograms quantifying the x-intercept of trendlines derived from within animal estimates of VEP acuity (mean +/- SEM). VEP-estimate of acuity was not significantly different between Gi-DREADD and PV-cre control mice (Wilcoxon rank sum test, NS). VEP-derived acuity significantly decreased in both Gi-DREADD and PV-cre control mice (Wilcoxon signed rank test, *p < 0.025, Bonferroni corrected for two comparisons).

Chapter 4: Implications and future directions

Previously I discussed how Gi-DREADD activation in normally-reared post-CP aged mice reactivates plasticity(Kuhlman et al. 2013). In chapter 3, I demonstrated that this reactivation of ODP is dependent on prior visual history: ten days of sensory deprivation via DE coupled with Gi-DREADD activation in PV-INs during LRx occluded the reactivation of ODP. Given this result, it is possible that the outcome of some proposed pharmacological interventions for amblyopia may also be dependent upon prior visual experience. For instance, the antidepressant drug fluoxetine has been shown to promote adult ODP via stabilization of TrkB receptors, increasing BDNF/TRKB signaling and enhancing ODP in post-CP adult rodents(Casarotto et al. 2021; Cannarozzo et al. 2023). TrkB is the endogenous receptor for BDNF, an important signaling molecule implicated in the maturation of inhibitory circuitry, the timing of the CP (Z. J. Huang et al. 1999). In the hippocampus, BDNF/TrkB signaling upregulates the expression of NARP and increases neural excitability by increasing cell surface expression of GluA1-containing AMPA-Rs (Mariga et al. 2015; Casarotto et al. 2021).In the visual cortex, BDNF is expressed primarily in cortical pyramidal neurons, particularly in L2/3 and L5, and is not expressed by PV-INs, whereas TrkB expression is highly enriched in PV-INs and pyramidal neurons(Gorba 1999; Bracken and Tyrrigiano 2009) Blocking TrkB signaling in rodent V1 decreases the excitability of pyramidal neurons and decreases visual acuity in rodents(Heimel et al. 2010). *In vivo* exogenous application of BDNF in CP-aged rats increases spontaneous visual cortical neural activity but did not prevent OD shifts from occurring following MD in L2/3(Lodovichi et al. 2000). It is therefore possible that increased BDNF/TrkB signaling by fluoxetine during

LRx could function similarly to Gi-DREADD activation of PV-INs, artificially maintaining spontaneous hyper-excitability and occluding the reactivation of ODP. Alternatively, enhancing BDNF/TrkB signaling during LRx may aid in recovery of deprived eye responses: blocking TrkB signaling has no effect on deprived eye depression during the CP, but is necessary for recovery of deprived eye responses by binocular vision during the CP(Kaneko et al. 2008).

Pharmacological interventions aimed at treating amblyopia may also impact the time course of DE required to reactivate ODP. Of particular interest is ketamine, and its metabolite (2R, 6R)-hydroxynorketamine (HNK). Ketamine has long been used for its potent hypnotic and analgesic effects(Sleigh et al. 2014). Traditionally the effects of ketamine were primarily attributed to its action as a non-competitive, use-dependent antagonist of NMDA-Rs, acting via a “fast trapping block” mechanism by competing with magnesium in the channel pore(Hansen et al. 2021). This blockade of NMDA-Rs has been shown to occlude the expression of LTP and LTD (Desmond et al. 1991; D. X. Zhang and Levy 1992). Interestingly, the metabolic half-life of ketamine is only 3 hours, yet its effects long outlast its metabolism, arguing against a purely ionotropic mechanism of action(Sleigh et al. 2014).

It is now understood that the rapid, long-lasting impacts of ketamine treatment can be attributed to two metabolic pathways. In particular, ketamine interacts with the NRG1/ErbB4 and BDNF/TrkB signaling, both of which are implicated in the maturation and maintenance of inhibitory circuitry and the expression of ODP(Cannarozzo et al. 2023; Casarotto et al. 2021; S.F Grieco et al. 2016; Z. J. Huang et al. 1999; Y. Gu et al. 2016). Ketamine binds directly to and stabilize dimerized TrkB receptors, decoupling

them from the phosphatase PTPσ, which normally dephosphorylates and deactivates TrkB(Casarotto et al. 2021). By decreasing TrkB dephosphorylation, ketamine increases endogenous BDNF signaling, promoting the reactivation of ODP and recovery of acuity in adult rodent amblyopes (Cannarozzo et al. 2023; S.F Grieco et al. 2016). Importantly, the effect of ketamine treatment is faster at reactivating ODP than fluoxetine (daily fluoxetine treatment for 28 days, versus ketamine treatment every other day for 8 days)(Cannarozzo et al. 2023) More importantly, a major metabolite of ketamine, HNK, not only produces stronger OD shifts than either fluoxetine and ketamine, but is also a significantly weaker inhibitor NMDA-R activity, does not produce the psychomimetic effects often associated with NMDA-R blockade, and has significantly less abuse potential in humans versus ketamine(Cannarozzo et al. 2023; Sleigh et al. 2014).

The reactivation of ODP by ketamine/HNK seems counter-intuitive at first given that increased BDNF signaling is associated with increased maturation of PV-INs and causes an early closure of the critical period(Z. J. Huang et al. 1999). Indeed, HNK has been shown to upregulate NARP in hippocampus, and overexpression of NARP in the cortex CP-aged mice occludes ODP(Ju et al. 2022; Severin et al. 2021). The direct relationship between neural activity, BDNF, and NARP is well established in the hippocampus, and while plausible, a definitive link has not been described between BDNF and NARP in the cortex(Mariga et al. 2015). However, it is known that TrkB receptors are also expressed by excitatory neurons, and that TrkB activation concurrently increases excitatory drive onto cortical pyramidal neurons and enables the functional “unmasking” of silent NMDA-R only synapses via insertion of AMPA-Rs(Gorba 1999; Sommeijer et al. 2017; Bracken and Tyrrigiano 2009; Itami et al. 2003).

BDNF has also been shown to increase tyrosine phosphorylation of NR2B-contianing NMDA-Rs in the hippocampus and potentiates their function(Lin et al. 1998). Importantly, HNK (and ketamine) also downregulate NRG1 signaling and decreases excitatory drive onto layer 2/3 PV-INs via the NRG1/ErbB4 pathway(S.F Grieco et al. 2016). NRG1 increases translaminar excitatory drive onto L2/3 PV-INs from L4 PYRs, while NARP increases short-range intra-L2/3 excitatory drive onto PV-INs from local L2/3 PYRs (Severin et al. 2021). The ability ketamine and HNK to reactivate ODP in post CP adults therefore implies that plasticity-promoting effects of ketamine/HNK are able to overcome any plasticity occluding effects that may be engaged by BDNF signaling in L2/3 (S.F Grieco et al. 2016).

How would HNK interact with DE plus LRx? Exogenous application of BDNF in pre-CP aged rat (P5 – 6) visual cortical slices blocks TTX-induced synaptic scaling, making it possible that pre-treatment with drugs interacting with the BDNF/TrkB pathway could similarly occlude DE-induced homeostatic increases in spontaneous RS PYR activity in L2/3 (Desai, Rutherford, and Turrigiano 1999). Importantly, 22 hours of dark exposure in adulthood has been shown to decrease the expression of BDNF in adult rodent V1 across all cortical layers(Capsoni et al. 1999). Decreased endogenous expression BDNF during DE may then counteract the possible metaplasticity-occluding effects of TrkB activation such as NARP upregulation, although the same would be true for BDNF-mediated enhancement of plasticity. Importantly, a single dose of HNK in adult mice has also been shown to decrease expression of NRG1, reducing excitatory drive onto PV-INs and neural inhibition in L2/3 by 50% for at least 24 hours(S.F Grieco et al. 2016). Thus, pre-treatment with HNK before DE may avoid the potential upregulation of

NARP on PV-INs by HNK while simultaneously allowing for the HNK-mediated disruption of the NRG1/erbb4 pathway. It is important to note that while the mechanism underlying ketamine/HNK's effect on BDNF signaling has been shown to be stabilization and decreases dephosphorylation of dimerized TrkB receptors, the direct upstream effect of ketamine/HNK on NRG1/ErbB4 signaling is not yet known(Casarotto et al. 2021). If ketamine/HNK-mediated changes in NRG1 signaling is downstream of BDNF signaling, decreased endogenous BDNF signaling during DE may also occlude the downregulation of NRG1. Arguing against this likelihood, it has previously been shown that NRG1 signaling is actually upstream of BDNF signaling, at least in developing neurons when GABA-mediated chloride currents can be depolarizing: NRG1 treatment increases expression of BDNF via excitatory $GABA_A$-R activation in developing neurons; BDNF upregulation was blocked by inhibiting ErbB4 with the inhibitor ag1478, and by inhibiting $GABA_A$-Rs with the antagonist picrotoxin(Pandya and Pillai 2014; Ben-Ari 2014). Interestingly, GABA-mediated depolarization has been demonstrated in L2/3 and L5/6 of developing mouse neocortex (P2 – P10), but GABA-mediated depolarization only caused spiking in L5/6(Rheims et al. 2008). Lastly, while ketamine/HNK alone can drive recovery from amblyopia in rodents, slight deficits to acuity in amblyopic mice persisted in these experimental animals; additionally, daily HNK treatment was shown to impair explicit and implicit memory formation in mice(S.F Grieco et al. 2016; Riggs et al. 2021). Previously, we have shown that MD following three days of DE produces significantly weaker OD shifts versus MD following ten days of DE; but ten days of sensory deprivation may be too cumbersome to effectively employ in human populations(He et al. 2007). One intriguing possibility is that, rather

than relying on a purely pharmacological or behavioral approach, pre-treatment with a pharmacological agent such as HNK before DE could “kick-start” the physiological changes induced by sensory deprivation. If true, the rapid increase in spontaneous activity could shorten the duration of DE required to reactivate ODP from over a week, to a much more manageable three-day weekend, significantly enhancing the translational potential of DE plus LRx as a treatment for amblyopia in humans.

Appendix A: Chapter 2 tables

Table 1: Spont. (RS) PYR / Animal averages							
Experiment		**L2/3**		**L4**		**L5/6**	
		***p < 0.05**	**z**	***p < 0.05**	**z**	***p < 0.05**	**z**
Spike rate	**ctrl v. LRx_i**	0.125	-1.753	0.016*	-2.366	0.219	-1.352
	ctrl v. LRx_s	1.000	0.447	1.000	-0.135	0.625	-0.674
Bursts / s	**ctrl v. LRx_i**	0.313	-1.214	0.047*	-2.028	0.688	0.507
Burst duration	**ctrl v. LRx_i**	1.000	0.135	0.688	0.507	1.000	0.000
Spikes per burst	**ctrl v. LRx_i**	0.625	-0.674	0.469	0.845	0.578	-0.676

Table 2: Evoked (RS) PYR / Animal averages							
Experiment		**L2/3**		**L4**		**L5/6**	
		***p < 0.05**	**z**	***p < 0.05**	**z**	***p < 0.05**	**z**
Spike rate	**ctrl v. LRx_i**	0.188	-1.483	0.031*	-2.197	0.938	-0.169
	ctrl v. LRx_s	0.500	1.342	0.438	0.944	0.313	1.214
Bursts / s	**ctrl v. LRx_i**	0.313	-1.214	0.031*	-2.197	0.938	0.169
Burst duration	**ctrl v. LRx_i**	1.000	0.135	0.688	0.507	0.297	-1.183
Spikes per burst	**ctrl v. LRx_i**	0.625	-0.674	0.219	1.352	0.578	-0.676

Table 3: (RS) PYR / All unit distributions					
Experiment	**Stimulus**	**exp.**	**L2/3**	**L4**	**L5/6**
			***p < 0.05**		
Spike rate	**Spont.**	**ctrl v. LRx_i**	0.024*	1.00e-3*	0.028*
		ctrl v. LRx_s	0.824	0.830	0.906
	Evoked	**ctrl v. LRx_i**	0.092	0.01253*	0.679
		ctrl v. LRx_s	0.045*	0.066	0.011*
Bursts / s	**Spont.**	**ctrl v. LRx_i**	0.519	7.05e-3*	0.147
	evoked	**ctrl v. LRx_s**	0.188	0.136	0.731
Burst duration	**Spont.**	**ctrl v. LRx_i**	0.519	0.066	0.365
	evoked	**ctrl v. LRx_s**	0.970	0.589	0.293
Spikes per burst	**Spont.**	**ctrl v. LRx_i**	0.049*	0.912	0.187
	evoked	**ctrl v. LRx_s**	0.519	0.890	0.045*

Table 4: (FS) PV-IN / Animal averages				
Measure	**Stimulus**	**exp.**	**All Layers**	
			***p < 0.05**	**z**
Spike rate	**Spont.**	**ctrl v. LRx_i**	1.000	0.000
		ctrl v. LRx_s	0.313	1.214
	Evoked	**ctrl v. LRx_i**	0.531	0.627
		ctrl v. LRx_s	0.438	0.944
Bursts / s	**Spont.**	**ctrl v. LRx_i**	0.531	-0.627
	evoked	**ctrl v. LRx_i**	1.000	0.000
Burst duration	**Spont.**	**ctrl v. LRx_i**	0.531	0.627
	evoked	**ctrl v. LRx_i**	0.835	-0.209
Spikes per burst	**Spont.**	**ctrl v. LRx_i**	0.296	1.044
	evoked	**ctrl v. LRx_i**	0.403	-0.836

Table 5: E/I Balance				
Measurement	**Stimulus**	**experiment**	**All Layers**	
			***p < 0.05**	**z**
Spike rate	**Spont.**	**ctrl v. LRx_i**	0.375	-1.095
		ctrl v. LRx_s	0.063	-2.023
	Evoked	**ctrl v. LRx_i**	3.67e-3*	-2.089
		ctrl v. LRx_s	0.313	1.214

Table 6: (FS) PV-IN / all unit distributions			
Measure	**Stimulus**	**exp.**	**All layers**
			***p < 0.05**
Spike rate	**Spont.**	**ctrl v. LRx_i**	0.879
		ctrl v. LRx_s	0.434
	Evoked	**ctrl v. LRx_i**	0.931
		ctrl v. LRx_s	0.714
Bursts / s	**Spont.**	**ctrl v. LRx_i**	0.471
	evoked	**ctrl v. LRx_i**	0.489
Burst duration	**Spont.**	**ctrl v. LRx_i**	0.135
	evoked	**ctrl v. LRx_i**	0.642
Spikes per burst	**Spont.**	**ctrl v. LRx_i**	0.824
	evoked	**ctrl v. LRx_i**	0.144

Appendix B: Chapter 3 Tables

Table 1: Spont. (RS) PYR / Animal averages							
Experiment		L2/3		L4		L5/6	
		*p < 0.025	z	*p < 0.025	z	*p < 0.025	z
Spike rate	cre v CNO	1.000	0.000	0.652	-0.533	0.188	1.483
	Gi v CNO	0.016*	-2.380	1.95e-3*	-2.803	0.031	-2.197
	cre v Gi	0.884	-0.133	0.968	0.041	1.000	0.000
Bursts / s	cre v CNO	0.641	0.560	0.496	-0.770	0.875	0.365
	Gi v CNO	7.81e-3*	-2.521	3.91e-3*	-2.666	0.016*	-2.366
	cre v Gi	0.458	0.736	0.151	1.429	0.012*	2.362
Burst duration	cre v CNO	0.023*	2.240	0.652	-0.533	1.000	0.000
	Gi v CNO	0.078	1.820	0.359	1.007	0.938	0.169
	cre v Gi	0.884	-0.133	0.780	-0.286	0.230	-1.228
Spikes per burst	cre v CNO	0.383	0.980	0.652	0.533	0.875	0.365
	Gi v CNO	0.195	1.400	0.074	-1.836	0.156	-1.521
	cre v Gi	0.442	0.788	0.661	-0.449	0.788	0.283

Table 2: Evoked (RS) PYR / Animal averages							
Experiment		L2/3		L4		L5/6	
		*p < 0.025	z	*p < 0.025	z	*p < 0.025	z
Spike rate	cre v CNO	0.742	0.420	1.000	-0.059	1.000	0.135
	Gi v CNO	0.016*	-2.380	2.95e-3*	-2.803	0.016*	-2.366
	cre v Gi	0.574	0.578	0.842	-0.204	0.876	-0.162
Bursts / s	cre v CNO	0.383	-0.980	0.426	-0.889	1.000	0.000
	Gi v CNO	0.047	-2.028	3.91e-3*	-2.666	0.016*	-2.366
	cre v Gi	0.779	0.289	0.222	1.236	0.024*	2.173
Burst duration	cre v CNO	0.039	2.100	0.039	2.073	0.375	1.095
	Gi v CNO	0.109	1.690	0.734	0.415	0.297	1.183
	cre v Gi	0.574	0.578	0.605	-0.530	0.788	-0.283
Spikes per burst	cre v CNO	0.461	0.840	0.652	-0.533	0.875	-0.365
	Gi v CNO	0.219	1.352	7.81e-3*	-2.547	0.016*	-2.366
	cre v Gi	0.536	-0.637	1.000	0.000	0.164	1.417

Table 3: (FS) PV-IN / Animal averages				
Measurement	**Stimulus**	**exp.**	**All Layers**	
			***p < 0.025**	**z**
Spike rate	**Spont.**	**cre v. CNO**	0.563	-0.734
		Gi v. CNO	0.820	0.296
		cre v. Gi	0.689	-0.412
	evoked	**cre v. CNO**	1.000	0.105
		Gi v. CNO	0.820	0.296
		cre v. Gi	0.689	-0.412
Bursts / s	**Spont.**	**cre v. CNO**	0.219	-1.363
		Gi v. CNO	0.039	-2.073
		cre v. Gi	1.000	0.000
	evoked	**cre v. CNO**	0.313	-1.153
		Gi v. CNO	0.164	-1.481
		cre v. Gi	0.955	-0.059
Burst duration	**Spont.**	**cre v. CNO**	0.563	0.734
		Gi v. CNO	0.301	1.125
		cre v. Gi	0.456	0.766
	evoked	**cre v. CNO**	0.438	0.943
		Gi v. CNO	0.020*	2.310
		cre v. Gi	0.529	0.648
Spikes per burst	**Spont.**	**cre v. CNO**	0.563	-0.734
		Gi v. CNO	7.81e-3*	-2.547
		cre v. Gi	7.59e-3*	2.534
	evoked	**cre v. CNO**	1.000	-0.105
		Gi v. CNO	0.027	-2.192
		cre v. Gi	0.113	1.591

Table 4: E/I balance				
Measurement	Stimulus	experiment	All Layers	
			*p < 0.05	z
E/I balance	Spont.	cre v. CNO	0.688	-0.524
		Gi v. CNO	3.91e-3*	-2.666
	evoked	cre v. CNO	0.438	-0.943
		Gi v. CNO	0.027*	-2.192

Table 5: (RS) PYR / All unit distributions					
Measurement	Stimulus	experiment	L2/3	L4	L5/6
			*p < 0.025		
Spikes per burst	Spont.	cre v. CNO	0.069	0.892	0.111
		Gi v. CNO	0.304	5.68e-3*	0.081
		cre v. Gi	0.561	0.696	0.356
	evoked	cre v. CNO	0.132	0.877	0.111
		Gi v. CNO	0.497	2.90e-06*	0.081
		cre v. Gi	0.658	0.270	0.072

Table 6: (FS) PV-IN / all unit distributions			
Measurement	**Stimulus**	**exp.**	**All layers**
			***p < 0.025**
Bursts / s	Spont.	cre v. CNO	0.387
		Gi v. CNO	0.308
		cre v. Gi	0.442
	evoked	cre v. CNO	0.930
		Gi v. CNO	0.051
		cre v. Gi	0.934
Burst duration	Spont.	cre v. CNO	0.930
		Gi v. CNO	0.589
		cre v. Gi	0.015*
	evoked	cre v. CNO	0.387
		Gi v. CNO	0.589
		cre v. Gi	0.050
Spikes per burst	Spont.	cre v. CNO	0.673
		Gi v. CNO	4.26e-5*
		cre v. Gi	3.45e-4*
	evoked	cre v. CNO	0.930
		Gi v. CNO	1.14e-3*
		cre v. Gi	0.110

Table 7: Ocular dominance index				
Measurement		L2/3	L4	L5/6
		*p < 0.025		
ODI	Gi v. CNO	0.426	0.027	0.769
	cre v. CNO	3.90e-3*	3.90e-3*	7.80e-3*
	cre v. CNO	0.3865	0.9097	0.3075

Table 8: Acuity		
Measurement		L4
		*p < 0.025
Acuity	Cre: MD + LRx + CNO	7.80e-3*
	Gi: MD + LRx + CNO	0.016*
	cre v. Gi	0.279

Bibliography

Afef, Ouelhazi, Lussiez Rudy, and Molotchnikoff Stéphane. 2022. “Ketamine Promotes Adaption-Induced Orientation Plasticity and Vigorous Network Changes.” *Brain Research* 1797 (June). https://doi.org/10.1016/j.brainres.2022.148111.

Alexander, Georgia M., Sarah C. Rogan, Atheir I. Abbas, Blaine N. Armbruster, Ying Pei, John A. Allen, Randal J. Nonneman, et al. 2009. “Remote Control of Neuronal Activity in Transgenic Mice Expressing Evolved G Protein-Coupled Receptors.” *Neuron* 63 (1): 27–39. https://doi.org/10.1016/j.neuron.2009.06.014.

Anderson, Eden M., Skyler Demis, Hunter D’Acquisto, Annabel Engelhardt, and Matthew Hearing. 2021. “The Role of Parvalbumin Interneuron GIRK Signaling in the Regulation of Affect and Cognition in Male and Female Mice.” *Frontiers in Behavioral Neuroscience* 15 (March): 1–16. https://doi.org/10.3389/fnbeh.2021.621751.

Anggono, Victor, and Richard L. Huganir. 2012. “Regulation of AMPA Receptor Trafficking and Synaptic Plasticity.” *Current Opinion in Neurobiology* 22 (3): 461–69. https://doi.org/10.1016/j.conb.2011.12.006.

Anomal, Renata, Etienne de Villers-Sidani, Michael M. Merzenich, and Rogerio Panizzutti. 2013. “Manipulation of BDNF Signaling Modifies the Experience-Dependent Plasticity Induced by Pure Tone Exposure during the Critical Period in the Primary Auditory Cortex.” *PLoS ONE* 8 (5): 2–7. https://doi.org/10.1371/journal.pone.0064208.

Armbruster, Blaine N., Xiang Li, Mark H. Pausch, Stefan Herlitze, and Bryan L. Roth. 2007. “Evolving the Lock to Fit the Key to Create a Family of G Protein-Coupled Receptors Potently Activated by an Inert Ligand.” *Proceedings of the National Academy of Sciences of the United States of America* 104 (12): 5163–68. https://doi.org/10.1073/pnas.0700293104.

Attebo, K, P Mitchell, R Cumming, W Smith, N Jolly, and R Sparkes. 1998. “Prevalence and Causes of Amblyopia in an Adult Population.” *Ophthalmology* 105: 154–59. https://doi.org/10.1016/S0161-6420(98)91862-0.

Barkat, Tania Rinaldi, Daniel B. Polley, and Takao K. Hensch. 2011. “A Critical Period for Auditory Thalamocortical Connectivity.” *Nature Neuroscience* 14 (9): 1189–1996. https://doi.org/10.1038/nn.2882.

Ben-Ari, Y. 2014. “The GABA Excitatory/Inhibitory Developmental Sequence: A Personal Journey.” *Neuroscience* 279: 187–219. https://doi.org/10.1016/j.neuroscience.2014.08.001.

Bender, D., M. Holschbach, and G. Stöcklin. 1994. “Synthesis of n.c.a. Carbon-11 Labelled Clozapine and Its Major Metabolite Clozapine-N-Oxide and Comparison of Their Biodistribution in Mice.” *Nuclear Medicine and Biology* 21 (7): 921–25. https://doi.org/10.1016/0969-8051(94)90080-9.

Berardi, Nicoletta, Tommaso Pizzorusso, and Lamberto Maffei. 2000. “Critical Periods during Sensory Development.” *Current Opinion in Neurobiology* 10 (1): 138–45. https://doi.org/10.1016/S0959-4388(99)00047-1.

Bi, Guo Qiang, and Mu Ming Poo. 1998. “Synaptic Modifications in Cultured

Hippocampal Neurons: Dependence on Spike Timing, Synaptic Strength, and Postsynaptic Cell Type." *Journal of Neuroscience* 18 (24): 10464–72. https://doi.org/10.1523/jneurosci.18-24-10464.1998.

Bortone, Dante S., Shawn R. Olsen, and Massimo Scanziani. 2014. "Translaminar Inhibitory Cells Recruited by Layer 6 Corticothalamic Neurons Suppress Visual Cortex." *Neuron* 82 (2): 474–85. https://doi.org/10.1016/j.neuron.2014.02.021.

Bracken, Bethany K., and Gina G. Tyrrigiano. 2009. "Experience-Dependent Regulation of TrkB Isoforms in Rodent Visual Cortex." *Developmental Neurobiology* 69 (5): 267–78. https://doi.org/10.1002/dneu.20701.

Bridi, Michelle C. D., Roberto de Pasquale, Crystal L. Lantz, Yu Gu, Andrew Borrell, Se-Young Choi, Kaiwen He, et al. 2018. "Two Distinct Mechanisms for Experience-Dependent Homeostasis." *Nature Neuroscience* 21 (6): 843–50. https://doi.org/10.1038/s41593-018-0150-0.

Bröcher, Susanne, Alain Artola, and Wolf Singer. 1992. "Intracellular Injection of Ca2+ Chelators Blocks Induction of Long-Term Depression in Rat Visual Cortex." *Proceedings of the National Academy of Sciences of the United States of America* 89 (1): 123–27. https://doi.org/10.1073/pnas.89.1.123.

Cannarozzo, Cecilia, Anna Rubiolo, Plinio Casarotto, and Eero Castrén. 2023. "Ketamine and Its Metabolite 2R,6R-Hydroxynorketamine Promote Ocular Dominance Plasticity and Release Tropomyosin-Related Kinase B from Inhibitory Control without Reducing Perineuronal Nets Enwrapping Parvalbumin Interneurons." *European Journal of Neuroscience* 57 (6): 940–50.

https://doi.org/10.1111/ejn.15929.

Capsoni, S., E. Tongiorgi, A. Cattaneo, and L. Domenici. 1999. “Differential Regulation of Brain-Derived Neurotrophic Factor Messenger RNA Cellular Expression in the Adult Rat Visual Cortex.” *Neuroscience* 93 (3): 1033–40. https://doi.org/10.1016/S0306-4522(99)00240-7.

Casarotto, Plinio C., Mykhailo Girych, Senem M. Fred, Vera Kovaleva, Rafael Moliner, Giray Enkavi, Caroline Biojone, et al. 2021. “Antidepressant Drugs Act by Directly Binding to TRKB Neurotrophin Receptors.” *Cell* 184 (5): 1299-1313.e19. https://doi.org/10.1016/j.cell.2021.01.034.

Chen, JY, Peter Lonjers, and Christopher Lee. 2013. “Heterosynaptic Plasticity Prevents Runaway Synaptic Dynamics.” *The Journal of …* 33 (40): 15915–29. https://doi.org/10.1523/JNEUROSCI.5088-12.2013.

Chen, Lin, Yong Deng, Weihua Luo, Zhen Wang, and Shaoqun Zeng. 2009. “Detection of Bursts in Neuronal Spike Trains by the Mean Inter-Spike Interval Method.” *Progress in Natural Science* 19 (2): 229–35. https://doi.org/10.1016/j.pnsc.2008.05.027.

Chen, Wendy S., and Mark F. Bear. 2007. “Activity-Dependent Regulation of NR2B Translation Contributes to Metaplasticity in Mouse Visual Cortex.” *Neuropharmacology* 52 (1): 200–214. https://doi.org/10.1016/j.neuropharm.2006.07.003.

Chokshi, Varun, Ming Gao, Bryce D. Grier, Ashley Owens, Hui Wang, Paul F. Worley, and Hey Kyoung Lee. 2019. “Input-Specific Metaplasticity in the Visual Cortex

Requires Homer1a-Mediated MGluR5 Signaling." *Neuron* 104 (4): 736-748.e6. https://doi.org/10.1016/j.neuron.2019.08.017.

Chung, Seungsoo, Ji Hyun Jeong, Sukjin Ko, Xin Yu, Young Hwan Kim, John T.R. Isaac, and Alan P. Koretsky. 2017. "Peripheral Sensory Deprivation Restores Critical-Period-like Plasticity to Adult Somatosensory Thalamocortical Inputs." *Cell Reports* 19 (13): 2707–17. https://doi.org/10.1016/j.celrep.2017.06.018.

Cisneros-Franco, J. Miguel, and Étienne De Villers-Sidani. 2019. "Reactivation of Critical Period Plasticity in Adult Auditory Cortex through Chemogenetic Silencing of Parvalbumin-Positive Interneurons." *Proceedings of the National Academy of Sciences of the United States of America* 116 (52): 26329–31. https://doi.org/10.1073/pnas.1913227117.

Coleman, J. E., K. Law, and Mark F. Bear. 2009. "Anatomical Origins of Ocular Dominance in Mouse Primary Visual Cortex." *Neuroscience* 161 (2): 561–71. https://doi.org/10.1016/j.neuroscience.2009.03.045.

Cummings, Jennifer A., Rosel M. Mulkey, Roger A. Nicoll, and Robert C. Malenka. 1996. "Ca2+ Signaling Requirements for Long-Term Depression in the Hippocampus." *Neuron* 16 (4): 825–33. https://doi.org/10.1016/S0896-6273(00)80102-6.

Cynader, M., and D.E. Mitchel. 1983. "Prolonged Sensitivity to Monocular Deprivation in Dark-Reared Cats: Effects of Age and Visual Exposure." *Developmental Brain Research* 8 (2–3): 155–64. https://doi.org/10.1016/0165-3806(83)90002-0.

Desai, Niraj S., Robert H. Cudmore, Sacha B. Nelson, and Gina G. Turrigiano. 2002.

"Critical Periods for Experience-Dependent Synaptic Scaling in Visual Cortex." *Nature Neuroscience* 5 (8): 783–89. https://doi.org/10.1038/nn878.

Desai, Niraj S., Lana C. Rutherford, and Gina G. Turrigiano. 1999. "BDNF Regulates the Intrinsic Excitability of Cortical Neurons." *Learning and Memory* 6 (3): 284–91. https://doi.org/10.1101/lm.6.3.284.

Desmond, Nancy L., Costa M. Colbert, De Xing Zhang, and William B. Levy. 1991. "NMDA Receptor Antagonists Block the Induction of Long-Term Depression in the Hippocampal Dentate Gyrus of the Anesthetized Rat." *Brain Research* 552 (1): 93–98. https://doi.org/10.1016/0006-8993(91)90664-H.

Ding, Chen-Yun, Yan-Ting Ding, Haifeng Ji, Yao-Yi Wang, Xinwen Zhang, and Dong-Min Yin. 2023. "Genetic Labeling Reveals Spatial and Cellular Expression Pattern of Neuregulin 1 in Mouse Brain." *Cell & Bioscience* 13 (1): 79. https://doi.org/10.1186/s13578-023-01032-4.

Dixon, Christine, Pankaj Sah, Joseph W. Lynch, and Angelo Keramidas. 2014. "GABAa Receptor α and γ Subunits Shape Synaptic Currents via Different Mechanisms." *Journal of Biological Chemistry* 289 (9): 5399–5411. https://doi.org/10.1074/jbc.M113.514695.

Dudek, Serena M., and Michael J. Friedlander. 1996. "Developmental Down-Regulation of LTD in Cortical Layer IV and Its Independence of Modulation by Inhibition." *Neuron* 16 (6): 1097–1106. https://doi.org/10.1016/S0896-6273(00)80136-1.

Duffy, Kevin R., Alexander J. Lingley, Kaitlyn D. Holman, and Donald E. Mitchell. 2016. "Susceptibility to Monocular Deprivation Following Immersion in Darkness Either

Late into or beyond the Critical Period." *Journal of Comparative Neurology* 524 (13): 2643–53. https://doi.org/10.1002/cne.23985.

Durand, Guylaine M., Yury Kovalchuk, and Arthur Konnerth. 1996. "Long-Term Potentiation and Functional Synapse Induction in Developing Hippocampus." *Nature* 381 (6577): 71–75. https://doi.org/10.1038/381071a0.

Durkin, Jaclyn, Aneesha K. Suresh, Julie Colbath, Christopher Broussard, Jiaxing Wu, Michal Zochowski, and Sara J. Aton. 2017. "Cortically Coordinated NREM Thalamocortical Oscillations Play an Essential, Instructive Role in Visual System Plasticity." *Proceedings of the National Academy of Sciences of the United States of America* 114 (39): 10485–90. https://doi.org/10.1073/pnas.1710613114.

Erzurumlu, Reha S., and Patricia Gaspar. 2012. "Development and Critical Period Plasticity of the Barrel Cortex." *European Journal of Neuroscience* 35 (10): 1540–53. https://doi.org/10.1111/j.1460-9568.2012.08075.x.

Fagiolini, M, and Takao K. Hensch. 2000. "Inhibitory Threshold for Critical-Period Activation in Primary Visual Cortex." *Nature* 404 (6774): 183–86. https://doi.org/10.1038/35004582.

Fagiolini, Michela, Hiroyuki Katagiri, Hiroyuki Miyamoto, Hisashi Mori, Seth G.N. Grant, Masayoshi Mishina, and Takao K. Hensch. 2003. "Separable Features of Visual Cortical Plasticity Revealed by N-Methyl-D-Aspartate Receptor 2A Signaling." *Proceedings of the National Academy of Sciences of the United States of America* 100 (5): 2854–59. https://doi.org/10.1073/pnas.0536089100.

Feller, Marla B., and Massimo Scanziani. 2005. "A Precritical Period for Plasticity in

Visual Cortex.” *Current Opinion in Neurobiology* 15 (1): 94–100. https://doi.org/10.1016/j.conb.2005.01.012.

Fong, Ming Fai, Peter S.B. Finnie, Taekeun Kim, Aurore Thomazeau, Eitan S. Kaplan, Samuel F. Cooke, and Mark F. Bear. 2020. “Distinct Laminar Requirements for Nmda Receptors in Experience-Dependent Visual Cortical Plasticity.” *Cerebral Cortex* 30 (4): 2555–72. https://doi.org/10.1093/CERCOR/BHZ260.

Franks, Kevin M., and Jeffry S. Isaacson. 2005. “Synapse-Specific Downregulation of NMDA Receptors by Early Experience: A Critical Period for Plasticity of Sensory Input to Olfactory Cortex.” *Neuron* 47 (1): 101–14. https://doi.org/10.1016/j.neuron.2005.05.024.

Frenkel, Mikhail Y., and Mark F. Bear. 2004. “How Monocular Deprivation Shifts Ocular Dominance in Visual Cortex of Young Mice.” *Neuron* 44 (6): 917–23. https://doi.org/10.1016/j.neuron.2004.12.003.

Frenkel, Mikhail Y., Nathaniel B. Sawtell, Antonia Cinira M Diogo, Bongjune Yoon, Rachael L. Neve, and Mark F. Bear. 2006. “Instructive Effect of Visual Experience in Mouse Visual Cortex.” *Neuron* 51 (3): 339–49. https://doi.org/10.1016/j.neuron.2006.06.026.

Fu, Xin, Eric Teboul, Grant L. Weiss, Pantelis Antonoudiou, Chandrashekhar D. Borkar, Jonathan P. Fadok, Jamie Maguire, and Jeffrey G. Tasker. 2022. “Gq Neuromodulation of BLA Parvalbumin Interneurons Induces Burst Firing and Mediates Fear-Associated Network and Behavioral State Transition in Mice.” *Nature Communications* 13 (1): 1–16. https://doi.org/10.1038/s41467-022-28928-y.

Fu, Yu, Megumi Kaneko, Yunshuo Tang, Arturo Alvarez-buylla, and Michael P. Strkyer. 2015. “A Cortical Disinhibitory Circuit for Enhancing Adult Plasticity.” *ELife* 4: 1–12. https://doi.org/10.7554/eLife.05558.

Fuchs, Jannon L., and Eduardo Salazar. 1998. “Effects of Whisker Trimming on GABA(A) Receptor Binding in the Barrel Cortex of Developing and Adult Rats.” *Journal of Comparative Neurology* 395 (2): 209–16. https://doi.org/10.1002/(SICI)1096-9861(19980601)395:2<209::AID-CNE5>3.0.CO;2-6.

Fukumoto, Kenichi, Manoela V. Fogaca, Rong Jian Liu, Catharine Duman, Taro Kato, Xiao Yuan Li, and Ronald S. Duman. 2019. “Activity-Dependent Brain-Derived Neurotrophic Factor Signaling Is Required for the Antidepressant Actions of (2R,6R)-Hydroxynorketamine.” *Proceedings of the National Academy of Sciences of the United States of America* 116 (1): 297–302. https://doi.org/10.1073/pnas.1814709116.

Garcia, Rolando A.G., Kuzhalini Vasudevan, and Andres Buonanno. 2000. “The Neuregulin Receptor ErbB-4 Interacts with PDZ-Containing Proteins at Neuronal Synapses.” *Proceedings of the National Academy of Sciences of the United States of America* 97 (7): 3596–3601. https://doi.org/10.1073/pnas.97.7.3596.

Gentet, L J, Y Kremer, H Taniguchi, Z. Josh Huang, J F Staiger, and C C Petersen. 2012. “Unique Functional Properties of Somatostatin-Expressing GABAergic Neurons in Mouse Barrel Cortex.” *Nat Neurosci* 15 (4): 607–12. https://doi.org/10.1038/nn.3051.

Ghit, Amr, Dina Assal, Ahmed S. Al-Shami, and Diaa Eldin E Hussein. 2021. “GABAA Receptors: Structure, Function, Pharmacology, and Related Disorders.” *Journal of Genetic Engineering and Biotechnology* 19 (1): 123. https://doi.org/10.1186/s43141-021-00224-0.

Goel, Anubhuthi, Bin Jiang, Linda W Xu, Lihua Song, A. Kirkwood Alfredo, and Hey-Kyoung Lee. 2006. “Cross-Modal Regulation of Synaptic AMPA Receptors in Primary Sensory Cortices by Visual Experience.” *Nature Neuroscience* 9 (8): 1001–3. https://doi.org/10.1038/nn1725.

Goel, Anubhuthi, and Hey-kyoung Lee. 2007. “Persistence of Experience-Induced Homeostatic Synaptic Plasticity through Adulthood in Superficial Layers of Mouse Visual Cortex” 27 (25): 6692–6700. https://doi.org/10.1523/JNEUROSCI.5038-06.2007.

Goldberg, Ethan M., Shigeo Watanabe, Su Ying Chang, Rolf H. Joho, Z. Josh Huang, Christopher S. Leonard, and Bernardo Rudy. 2005. “Specific Functions of Synaptically Localized Potassium Channels in Synaptic Transmission at the Neocortical GABAergic Fast-Spiking Cell Synapse.” *Journal of Neuroscience* 25 (21): 5230–35. https://doi.org/10.1523/JNEUROSCI.0722-05.2005.

Gomez, Juan L., Jordi Bonaventura, Wojciech Lesniak, William B. Mathews, Polina Sysa-Shah, Lionel A. Rodriguez, Randall J. Ellis, et al. 2017. “Chemogenetics Revealed: DREADD Occupancy and Activation via Converted Clozapine.” *Science* 357 (6350): 503–7. https://doi.org/10.1126/science.aan2475.

Gorba, Thorsten. 1999. “Expression of TrkB and TrkC but Not BDNF MRNA in

Neurochemically Identified Interneurons in Rat Visual Cortex in Vivo and in Organotypic Cultures." *European Journal of Neuroscience* 11 (4): 1179–90. https://doi.org/10.1046/j.1460-9568.1999.00551.x.

Gordon, Joshua a, and M P Stryker. 1996. "Experience-Dependent Plasticity of Binocular Responses in the Primary Visual Cortex of the Mouse." *The Journal of Neuroscience : The Official Journal of the Society for Neuroscience* 16 (10): 3274–86. https://doi.org/10.1523/JNEUROSCI.16-10-03274.1996.

Grabert, J., and P. Wahle. 2009. "Visual Experience Regulates Kv3.1b and Kv3.2 Expression in Developing Rat Visual Cortex." *Neuroscience* 158 (2): 654–64. https://doi.org/10.1016/j.neuroscience.2008.07.035.

Grieco, S.F, X Qiao, X. Zheng, Y. Liu, L. Chen, H. Zhang, Z. Yu, et al. 2016. "Subanesthetic Ketamine Reactivates Adult Cortical Plasticity to Restore Vision from Amblyopia." *Current Biology* 176 (1): 139–48. https://doi.org/10.1016/j.cub.2020.07.008.Subanesthetic.

Grieco, Steven F., Xin Qiao, Kevin G. Johnston, Lujia Chen, Renetta R. Nelson, Cary Lai, Todd C. Holmes, and Xiangmin Xu. 2021. "Neuregulin Signaling Mediates the Acute and Sustained Antidepressant Effects of Subanesthetic Ketamine." *Translational Psychiatry* 11 (1). https://doi.org/10.1038/s41398-021-01255-4.

Gu, Y., T. Tran, S. Murase, A. Borrell, A. Kirkwood Alfredo, and Elizabeth M. Quinlan. 2016. "Neuregulin-Dependent Regulation of Fast-Spiking Interneuron Excitability Controls the Timing of the Critical Period." *Journal of Neuroscience* 36 (40): 10285–95. https://doi.org/10.1523/JNEUROSCI.4242-15.2016.

Gu, Yu, Shiyong Huang, MichaelC Chang, Paul Worley, A. Kirkwood Alfredo, and Elizabeth M. Quinlan. 2013. “Obligatory Role for the Immediate Early Gene NARP in Critical Period Plasticity.” *Neuron* 79 (2): 335–46. https://doi.org/10.1016/j.neuron.2013.05.016.

Gunton, Kammi B. 2013. “Advances in Amblyopia: What Have We Learned from PEDIG Trials?” *Pediatrics* 131 (3): 540–47. https://doi.org/10.1542/peds.2012-1622.

Guo, Yatu, Shiyong Huang, Roberto de Pasquale, Kevin McGehrin, Hey Kyoung Lee, Kanxing Zhao, and A. Kirkwood Alfredo. 2012. “Dark Exposure Extends the Integration Window for Spike-Timing-Dependent Plasticity.” *Journal of Neuroscience* 32 (43): 15027–35. https://doi.org/10.1523/JNEUROSCI.2545-12.2012.

Hager, A. M., P. J. Gagolewicz, S. Rodier, M. C. Kuo, T. C. Dumont, and H. C. Dringenberg. 2015. “Metaplastic Up-Regulation of LTP in the Rat Visual Cortex by Monocular Visual Training: Requirement of Task Mastery, Hemispheric Specificity, and NMDA-GluN2B Involvement.” *Neuroscience* 293: 171–86. https://doi.org/10.1016/j.neuroscience.2015.02.027.

Hansen, Kasper B., Lonnie P. Wollmuth, Derek Bowie, Hiro Furukawa, Frank S. Menniti, Alexander I. Sobolevsky, Geoffrey T. Swanson, et al. 2021. “Structure, Function, and Pharmacology of Glutamate Receptor Ion Channels.” Edited by Eric Barker. *Pharmacological Reviews* 73 (4): 1469–1658. https://doi.org/10.1124/pharmrev.120.000131.

Harris, Kenneth D., and Gordon M.G. Shepherd. 2015. “The Neocortical Circuit:

Themes and Variations." *Nature Neuroscience* 18 (2): 170–81. https://doi.org/10.1038/nn.3917.

Hayashi, Y, S H Shi, J a Esteban, a Piccini, J C Poncer, and R Malinow. 2000. "Driving AMPA Receptors into Synapses by LTP and CaMKII: Requirement for GluR1 and PDZ Domain Interaction." *Science (New York, N.Y.)* 287 (5461): 2262–67. https://doi.org/10.1126/science.287.5461.2262.

Hayden, Dustin J., Daniel P. Montgomery, Samuel F. Cooke, and Mark F. Bear. 2021. "Visual Recognition Is Heralded by Shifts in Local Field Potential Oscillations and Inhibitory Networks in Primary Visual Cortex." *Journal of Neuroscience* 41 (29): 6257–72. https://doi.org/10.1523/JNEUROSCI.0391-21.2021.

He, Hai-Yan, William Hodos, and Elizabeth M. Quinlan. 2006. "Visual Deprivation Reactivates Rapid Ocular Dominance Plasticity in Adult Visual Cortex." *The Journal of Neuroscience : The Official Journal of the Society for Neuroscience* 26 (11): 2951–55. https://doi.org/10.1523/JNEUROSCI.5554-05.2006.

He, Hai-Yan, Baisali Ray, Katie Dennis, and Elizabeth M. Quinlan. 2007. "Experience-Dependent Recovery of Vision Following Chronic Deprivation Amblyopia." *Nature Neuroscience* 10 (9): 1134–36. https://doi.org/10.1038/nn1965.

Heimel, J. Alexander, M. Hadi Saiepour, Sridhara Chakravarthy, Josephine M. Hermans, and Christiaan N. Levelt. 2010. "Contrast Gain Control and Cortical TrkB Signaling Shape Visual Acuity." *Nature Neuroscience* 13 (5): 642–48. https://doi.org/10.1038/nn.2534.

Hensch, Takao K. 2005. "Critical Period Plasticity in Local Cortical Circuits." *Nature*

Reviews Neuroscience 6 (11): 877–88. https://doi.org/10.1038/nrn1787.

Hensch, Takao K., Michela Fagiolini, Nobuko Mataga, Michael P. Stryker, Steinunn Baekkeskov, and Shera F. Kash. 1998. “Local GABA Circuit Control of Experience-Dependent Plasticity in Developing Visual Cortex.” *Science* 282 (5393): 1504–8. https://doi.org/10.1126/science.282.5393.1504.

Hensch, Takao K., and Elizabeth M. Quinlan. 2018. “Critical Periods in Amblyopia.” *Visual Neuroscience* 35: E014. https://doi.org/10.1017/S0952523817000219.

Heynen, Arnold J., and Mark F. Bear. 2001. “Long-Term Potentiation of Thalamocortical Transmission in the Adult Visual Cortex in Vivo.” *Journal of Neuroscience* 21 (24): 9801–13. https://doi.org/10.1523/jneurosci.21-24-09801.2001.

Holmes, Jonathan M., and Michael P Clarke. 2006. “Amblyopia.” *The Lancet* 367: 1343–51. https://doi.org/10.1016/S0140-6736(06)68581-4.

Holmes, Jonathan M., Elizabeth L Lazar, B Michele Melia, William F Astle, Linda R Dagi, Sean P Donahue, Marcela G Frazier, et al. 2011. “Effect of Age on Response to Amblyopia Treatment in Children.” *Archives of Ophthalmology (Chicago, Ill. : 1960)* 129 (11): 1451–57. https://doi.org/10.1001/archophthalmol.2011.179.

Hong, S. Z., Shiyong Huang, Daniel Severin, and A. Kirkwood Alfredo. 2019. “Pull-Push Neuromodulation of Cortical Plasticity Enables Rapid Bi-Directional Shifts in Ocular Dominance.” *BioRxiv*, 1–20. https://doi.org/10.1101/2019.12.13.875849.

Hooks, Bryan M., and Chinfei Chen. 2020. “Circuitry Underlying Experience-Dependent Plasticity in the Mouse Visual System.” *Neuron* 106 (1): 21–36.

https://doi.org/10.1016/j.neuron.2020.01.031.

Hou, Chuan, Mark W. Pettet, and Anthony M. Norcia. 2014. “Acuity-Independent Effects of Visual Deprivation on Human Visual Cortex.” *Proceedings of the National Academy of Sciences of the United States of America* 111 (30). https://doi.org/10.1073/pnas.1404361111.

Hu, Budan, Zongshun Liu, Jiao Zhao, Li Zeng, Gengsheng Hao, Dan Shui, and Ke Mao. 2022. “The Global Prevalence of Amblyopia in Children: A Systematic Review and Meta-Analysis.” *Frontiers in Pediatrics* 10 (May): 1–10. https://doi.org/10.3389/fped.2022.819998.

Huang, Lawrence, Peter Ledochowitsch, Ulf Knoblich, Jérôme Lecoq, Gabe J. Murphy, R. Clay Reid, Saskia E.J. de Vries, et al. 2021. “Relationship between Simultaneously Recorded Spiking Activity and Fluorescence Signal in Gcamp6 Transgenic Mice.” *ELife* 10: 1–19. https://doi.org/10.7554/eLife.51675.

Huang, Shiyong, Yu Gu, Elizabeth M. Quinlan, and A. Kirkwood Alfredo. 2010. “A Refractory Period for Rejuvenating GABAergic Synaptic Transmission and Ocular Dominance Plasticity with Dark Exposure.” *The Journal of Neuroscience* 30: 16636–42. https://doi.org/10.1523/JNEUROSCI.4384-10.2010.

Huang, Shiyong, Kristen Hokenson, Sabita Bandyopadhyay, Shelley J Russek, and A. Kirkwood Alfredo. 2015. “Brief Dark Exposure Reduces Tonic Inhibition in Visual Cortex.” *The Journal of Neuroscience : The Official Journal of the Society for Neuroscience* 35 (48): 15916–20. https://doi.org/10.1523/JNEUROSCI.1813-15.2015.

Huang, Shiyong, RL Huganir, and A. Kirkwood Alfredo. 2013. “Adrenergic Gating of Hebbian Spike-Timing-Dependent Plasticity in Cortical Interneurons.” *The Journal of Neuroscience* 33 (32): 13171–78. https://doi.org/10.1523/JNEUROSCI.5741-12.2013.

Huang, Z. Josh, A. Kirkwood Alfredo, Tommaso Pizzorusso, Vittorio Porciatti, Bernardo Morales, Mark F. Bear, Lamberto Maffei, and Susumu Tonegawa. 1999. “BDNF Regulates the Maturation of Inhibition and the Critical Period of Plasticity in Mouse Visual Cortex.” *Cell* 98 (6): 739–55. https://doi.org/10.1016/S0092-8674(00)81509-3.

Hubel, David H., and Torsten N. Wiesel. 1964. “Effects of Monocular Deprivation in Kittens.” *Naunyn-Schmiedebergs Archiv Für Experimentelle Pathologie Und Pharmakologie* 248 (6): 492–97. https://doi.org/10.1007/BF00348878.

Hubel, DH, and TN Wiesel. 1959. “Receptive Fields of Single Neurons in the Cat’s Striate Cortex.” *Journal of Physiology* 148: 574–91.

Iacaruso, M. Florencia, Ioana T. Gasler, and Sonja B. Hofer. 2017. “Synaptic Organization of Visual Space in Primary Visual Cortex.” *Nature* 547 (7664): 449–52. https://doi.org/10.1038/nature23019.

Itami, Chiaki, Fumitaka Kimura, Tomoko Kohno, Masato Matsuoka, Masumi Ichikawa, Tadaharu Tsumoto, and Shun Nakamura. 2003. “Brain-Derived Neurotrophic Factor-Dependent Unmasking of ‘Silent’ Synapses in the Developing Mouse Barrel Cortex.” *Proceedings of the National Academy of Sciences* 100 (22): 13069–74. https://doi.org/10.1073/pnas.2131948100.

Itami, Chiaki, Fumitaka Kimura, and Shun Nakamura. 2007. “Brain-Derived Neurotrophic Factor Regulates the Maturation of Layer 4 Fast-Spiking Cells after the Second Postnatal Week in the Developing Barrel Cortex.” *Journal of Neuroscience* 27 (9): 2241–52. https://doi.org/10.1523/JNEUROSCI.3345-06.2007.

Iwai, Youichi, Michela Fagiolini, Kunihiko Obata, and Takao K. Hensch. 2003. “Rapid Critical Period Induction by Tonic Inhibition in Visual Cortex.” *Journal of Neuroscience* 23 (17): 6695–6702. https://doi.org/10.1523/jneurosci.23-17-06695.2003.

Jenks, Kyle R., and Jason D. Shepherd. 2020. “Experience-Dependent Development and Maintenance of Binocular Neurons in the Mouse Visual Cortex.” *Cell Reports* 30 (6): 1982-1994.e4. https://doi.org/10.1016/j.celrep.2020.01.031.

Ji, Xu Ying, Brian Zingg, Lukas Mesik, Zhongju Xiao, Li I. Zhang, and Huizhong W. Tao. 2016. “Thalamocortical Innervation Pattern in Mouse Auditory and Visual Cortex: Laminar and Cell-Type Specificity.” *Cerebral Cortex* 26 (6): 2612–25. https://doi.org/10.1093/cercor/bhv099.

Jiang, Bin, Shiyong Huang, Roberto de Pasquale, Daniel Millman, Lihua Song, Hey Kyoung Lee, T. Tsumoto Tadaharu, and A. Kirkwood Alfredo. 2010. “The Maturation of GABAergic Transmission in Visual Cortex Requires Endocannabinoid-Mediated LTD of Inhibitory Inputs during a Critical Period.” *Neuron* 66 (2): 248–59. https://doi.org/10.1016/j.neuron.2010.03.021.

Jiang, Bin, Mario Treviño, and A. Kirkwood Alfredo. 2007. “Sequential Development of Long-Term Potentiation and Depression in Different Layers of the Mouse Visual

Cortex.” *The Journal of Neuroscience : The Official Journal of the Society for Neuroscience* 27 (36): 9648–52. https://doi.org/10.1523/JNEUROSCI.2655-07.2007.

Jiao, Chong, Ming Li, and Dewen Hu. 2022. “The Neurons in Mouse V1 Show Different Degrees of Spatial Clustering.” *Brain Research Bulletin* 190 (April): 62–68. https://doi.org/10.1016/j.brainresbull.2022.09.011.

Jones, Seth V., Lisa Stanek-Rattiner, Michael Davis, and Kerry J. Ressler. 2007. “Differential Regional Expression of Brain-Derived Neurotrophic Factor Following Olfactory Fear Learning.” *Learning and Memory* 14 (12): 816–20. https://doi.org/10.1101/lm.781507.

Ju, Lingsha, Jiaojiao Yang, Tingting Zhu, Panmiao Liu, and Jianjun Yang. 2022. “BDNF-TrkB Signaling-Mediated Upregulation of Narp Is Involved in the Antidepressant-like Effects of (2R,6R)-Hydroxynorketamine in a Chronic Restraint Stress Mouse Model.” *BMC Psychiatry* 22 (1): 1–10. https://doi.org/10.1186/s12888-022-03838-x.

Kaneko, Megumi, Jessica L. Hanover, Pamela M. England, and Michael P. Stryker. 2008. “TrkB Kinase Is Required for Recovery, but Not Loss, of Cortical Responses Following Monocular Deprivation.” *Nature Neuroscience* 11 (4): 497–504. https://doi.org/10.1038/nn2068.

Kaneko, Megumi, and Michael P. Stryker. 2014. “Sensory Experience during Locomotion Promotes Recovery of Function in Adult Visual Cortex.” *ELife* 2014: 1–16. https://doi.org/10.7554/eLife.02798.001.

Kaplan, Eitan S, Sam F Cooke, Robert W Komorowski, Alexander A Chubykin, Aurore

Thomazeau, Lena A Khibnik, Jeffrey P Gavornik, and Mark F. Bear. 2016. "Contrasting Roles for Parvalbumin-Expressing Inhibitory Neurons in Two Forms of Adult Visual Cortical Plasticity." *ELife* 5: 1–27. https://doi.org/10.7554/eLife.11450.

Katagiri, Hiroyuki, Michela Fagiolini, and Takao K. Hensch. 2007. "Optimization of Somatic Inhibition at Critical Period Onset in Mouse Visual Cortex." *Neuron* 53: 805–12. https://doi.org/10.1016/j.neuron.2007.02.026.

Kayser, Christoph, Rodrigo F Salazar, and Peter Konig. 2003. "Responses to Natural Scenes in Cat V1." *Journal of Neurophysiology* 90 (3): 1910–20. https://doi.org/10.1152/jn.00195.2003.

Kimura, Rie, and Yumiko Yoshimura. 2021. "The Contribution of Low Contrast–Preferring Neurons to Information Representation in the Primary Visual Cortex after Learning." *Science Advances* 7 (48). https://doi.org/10.1126/sciadv.abj9976.

Kloc, Michelle, and Arianna Maffei. 2014. "Target-Specific Properties of Thalamocortical Synapses onto Layer 4 of Mouse Primary Visual Cortex." *Journal of Neuroscience* 34 (46): 15455–65. https://doi.org/10.1523/JNEUROSCI.2595-14.2014.

Knott, Graham W., Charles Quairiaux, Christel Genoud, and Egbert Welker. 2002. "Formation of Dendritic Spines with GABAergic Synapses Induced by Whisker Stimulation in Adult Mice." *Neuron* 34 (2): 265–73. https://doi.org/10.1016/S0896-6273(02)00663-3.

Kondo, Satoru, Takashi Yoshida, and Kenichi Ohki. 2016. "Mixed Functional Microarchitectures for Orientation Selectivity in the Mouse Primary Visual Cortex." *Nature Communications* 7: 1–16. https://doi.org/10.1038/ncomms13210.

Kötter, Rolf, Dirk Schubert, Jonas Dyhrfjeld-Johnsen, Heiko J Luhmann, and Jochen F Staiger. 2005. “Optical Release of Caged Glutamate for Stimulation of Neurons in the in Vitro Slice Preparation.” *Journal of Biomedical Optics* 10 (1): 11003. https://doi.org/10.1117/1.1852555.

Krahe, Rüdiger, and Fabrizio Gabbiani. 2004. “Burst Firing in Sensory Systems.” *Nature Reviews. Neuroscience* 5 (1): 13–23. https://doi.org/10.1038/nrn1296.

Kuhlman, Sandra J., Nicholas D ND Olivas, Elaine Tring, Taruna Ikrar, Xiangmin Xu, and Joshua T Trachtenberg. 2013. “A Disinhibitory Microcircuit Initiates Critical-Period Plasticity in the Visual Cortex.” *Nature* 501 (7468): 543–46. https://doi.org/10.1038/nature12485.

Kuhlman, Sandra J., Elaine Tring, and Joshua T Trachtenberg. 2011. “Fast-Spiking Interneurons Have an Initial Orientation Bias That Is Lost with Vision.” *Nature Neuroscience* 14 (9): 1121–23. https://doi.org/10.1038/nn.2890.

Lantz, Crystal L., and Elizabeth M. Quinlan. 2021. “High-Frequency Visual Stimulation Primes Gamma Oscillations for Visually Evoked Phase Reset and Enhances Spatial Acuity.” *Cerebral Cortex Communications* 2 (2): 1–14. https://doi.org/10.1093/texcom/tgab016.

Lau, Chunyue Geoffrey, Huiqi Zhang, and Venkatesh N. Murthy. 2022. “Deletion of TrkB in Parvalbumin Interneurons Alters Cortical Neural Dynamics.” *Journal of Cellular Physiology* 237 (1): 949–64. https://doi.org/10.1002/jcp.30571.

Lee, Christopher M., Carl Stoelzel, Marina Chistiakova, and Maxim Volgushev. 2012. “Heterosynaptic Plasticity Induced by Intracellular Tetanization in Layer 2/3

Pyramidal Neurons in Rat Auditory Cortex." *Journal of Physiology* 590 (10): 2253–71. https://doi.org/10.1113/jphysiol.2012.228247.

Lee, Sung-Jin, Mengping Wei, Chen Zhang, Stephan Maxeiner, ChangHui Pak, Salome Calado Botelho, Justin Trotter, Fredrik H. Sterky, and Thomas C. Südhof. 2017. "Presynaptic Neuronal Pentraxin Receptor Organizes Excitatory and Inhibitory Synapses." *The Journal of Neuroscience* 37 (5): 1062–80. https://doi.org/10.1523/JNEUROSCI.2768-16.2016.

Lewis, Eastman M., Hayli E. Spence, Neha Akella, and Andres Buonanno. 2022. "Pathway-Specific Contribution of Parvalbumin Interneuron NMDARs to Synaptic Currents and Thalamocortical Feedforward Inhibition." *Molecular Psychiatry*, no. May (September): 1–11. https://doi.org/10.1038/s41380-022-01747-9.

Li, Ye, David Fitzpatrick, and Leonard E. White. 2006. "The Development of Direction Selectivity in Ferret Visual Cortex Requires Early Visual Experience." *Nature Neuroscience* 9 (5): 676–81. https://doi.org/10.1038/nn1684.

Lin, Siang Yo, Kuo Wu, Eric S. Levine, Howard T.J. Mount, Piin Chau Suen, and Ira B. Black. 1998. "BDNF Acutely Increases Tyrosine Phosphorylation of the NMDA Receptor Subunit 2B in Cortical and Hippocampal Postsynaptic Densities." *Molecular Brain Research* 55 (1): 20–27. https://doi.org/10.1016/S0169-328X(97)00349-5.

Lodovichi, Claudia, Nicoletta Berardi, Tommaso Pizzorusso, and Lamberto Maffei. 2000. "Effects of Neurotrophins on Cortical Plasticity: Same or Different?" *Journal of Neuroscience* 20 (6): 2155–65. https://doi.org/10.1523/jneurosci.20-06-

02155.2000.

Lu, Hui-Chen, Ernesto Gonzalez, and Michael C. Crair. 2001. “Barrel Cortex Critical Period Plasticity Is Independent of Changes in NMDA Receptor Subunit Composition.” *Neuron* 32 (4): 619–34. https://doi.org/10.1016/S0896-6273(01)00501-3.

Lu, Jiangteng, Jason Tucciarone, Ying Lin, and Z. Josh Huang. 2014. “Input-Specific Maturation of Synaptic Dynamics of Parvalbumin Interneurons in Primary Visual Cortex.” *Proceedings of the National Academy of Sciences of the United States of America* 111 (47): 1–6. https://doi.org/10.1073/pnas.1400694111.

MacDermott, Amy B., Mark L. Mayer, Gary L. Westbrook, Stephen J. Smith, and Jeffery L. Barker. 1986. “NMDA-Receptor Activation Increases Cytoplasmic Calcium Concentration in Cultured Spinal Cord Neurones.” *Nature* 321 (6069): 519–22. https://doi.org/10.1038/321519a0.

MacLaren, Duncan AA, Richard W Browne, Jessica K Shaw, Sandhya Krishnan Radhakrishnan, Prachi Khare, Rodrigo A España, and Stewart D Clark. 2016. “Clozapine-n-Oxide Administration Produces Behavioral Effects in Long-Evans Rats - Implications for Designing DREADD Experiments CNO Converts into Bioactive Compounds in Rats.” *ENeuro* 10 (October): 219–16. https://doi.org/10.1523/ENEURO.0219-16.2016.

Maffei, Arianna, Sacha B. Nelson, and Gina G. Turrigiano. 2004. “Selective Reconfiguration of Layer 4 Visual Cortical Circuitry by Visual Deprivation.” *Nature Neuroscience* 7 (12): 1353–59. https://doi.org/10.1038/nn1351.

Magee, Jeffrey C., and Christine Grienberger. 2020. “Synaptic Plasticity Forms and Functions.” *Annual Review of Neuroscience* 43: 95–117. https://doi.org/10.1146/annurev-neuro-090919-022842.

Mahler, Stephen V., and Gary Aston-Jones. 2018. “CNO Evil? Considerations for the Use of DREADDs in Behavioral Neuroscience.” *Neuropsychopharmacology* 43 (5): 934–36. https://doi.org/10.1038/npp.2017.299.

Manvich, Daniel F., Kevin A. Webster, Stephanie L. Foster, Martilias S. Farrell, James C. Ritchie, Joseph H. Porter, and David Weinshenker. 2018. “The DREADD Agonist Clozapine N-Oxide (CNO) Is Reverse-Metabolized to Clozapine and Produces Clozapine-like Interoceptive Stimulus Effects in Rats and Mice.” *Scientific Reports* 8 (1): 1–10. https://doi.org/10.1038/s41598-018-22116-z.

Mariga, Abigail, Juliane Glaser, Leo Mathias, Desheng Xu, Meifang Xiao, Paul Worley, Ipe Ninan, and Moses V. Chao. 2015. “Definition of a Bidirectional Activity-Dependent Pathway Involving BDNF and Narp.” *Cell Reports* 13 (9): 1747–56. https://doi.org/10.1016/j.celrep.2015.10.064.

Markram, Henry, Joachim Lübke, Michael Frotscher, and Bert Sakmann. 1997. “Regulation of Synaptic Efficacy by Coincidence of Postsynaptic APs and EPSPs.” *Science* 275 (5297): 213–15. https://doi.org/10.1126/science.275.5297.213.

Markram, Henry, Maria Toledo-Rodriguez, Yun Wang, Anirudh Gupta, Gilad Silberberg, and Caizhi Wu. 2004. “Interneurons of the Neocortical Inhibitory System.” *Nature Reviews. Neuroscience* 5 (10): 793–807. https://doi.org/10.1038/nrn1519.

Matsuda, Yoshi Taka, Hiroyuki Miyamoto, Rolf H. Joho, and Takao K. Hensch. 2021.

"Kv3.1 Channels Regulate the Rate of Critical Period Plasticity." *Neuroscience Research* 167: 3–10. https://doi.org/10.1016/j.neures.2021.04.003.

McCurry, Cortina L., Jason D. Shepherd, Daniela Tropea, Kuan H. Wang, Mark F. Bear, and Mriganka Sur. 2010. "Loss of Arc Renders the Visual Cortex Impervious to the Effects of Sensory Experience or Deprivation." *Nature Neuroscience* 13 (4): 450–57. https://doi.org/10.1038/nn.2508.

Mitchell, Simon J., and R. Angus Silver. 2003. "Shunting Inhibition Modulates Neuronal Gain during Synaptic Excitation." *Neuron* 38 (3): 433–45. https://doi.org/10.1016/S0896-6273(03)00200-9.

Montey, Karen L, Nicolette C Eaton, and Elizabeth M. Quinlan. 2013. "Repetitive Visual Stimulation Enhances Recovery from Severe Amblyopia." *Learning & Memory (Cold Spring Harbor, N.Y.)* 20: 311–17. https://doi.org/10.1101/lm.030361.113.

Montey, Karen L, and Elizabeth M. Quinlan. 2011. "Recovery from Chronic Monocular Deprivation Following Reactivation of Thalamocortical Plasticity by Dark Exposure." *Nature Communications* 2 (May): 317. https://doi.org/10.1038/ncomms1312.

Montgomery, Daniel P., Dustin J. Hayden, Francesca A. Chaloner, Samuel F. Cooke, and Mark F. Bear. 2022. "Stimulus-Selective Response Plasticity in Primary Visual Cortex: Progress and Puzzles." *Frontiers in Neural Circuits* 15 (January): 1–18. https://doi.org/10.3389/fncir.2021.815554.

Monyer, Hannah, Nail Burnashev, David J. Laurie, Bert Sakmann, and Peter H. Seeburg. 1994. "Developmental and Regional Expression in the Rat Brain and Functional Properties of Four NMDA Receptors." *Neuron* 12 (3): 529–40.

https://doi.org/10.1016/0896-6273(94)90210-0.

Morishita, Hirofumi, Julie M. Miwa, Nathaniel Heintz, and Takao K. Hensch. 2010. "Lynx1, a Cholinergic Brake, Limits Plasticity in Adult Visual Cortex." *Science* 330 (6008): 1238–40. https://doi.org/10.1126/science.1195320.

Murase, S., Daniel E. Winkowski, Ji Liu, Patrick O. Kanold, and Elizabeth M. Quinlan. 2019. "Homeostatic Regulation of Perisynaptic Matrix Metalloproteinase 9 (MMP9) Activity in the Amblyopic Visual Cortex." *ELife* 8: 1–18. https://doi.org/10.7554/eLife.52503.

Murase, Sachiko, Crystal L. Lantz, and Elizabeth M. Quinlan. 2017. "Light Reintroduction after Dark Exposure Reactivates Plasticity in Adults via Perisynaptic Activation of MMP-9." *ELife* 6 (September): 1–23. https://doi.org/10.7554/eLife.27345.

Murase, Sachiko, Daniel E. Winkowski, Ji Liu, Patrick O. Kanold, and Elizabeth M. Quinlan. 2019. "Homeostatic Regulation of Perisynaptic Matrix Metalloproteinase 9 (MMP9) Activity in the Amblyopic Visual Cortex." *ELife* 8: 1–18. https://doi.org/10.7554/eLife.52503.

Nabavi, Sadegh, Helmut W. Kessels, Stephanie Alfonso, Jonathan Aow, Rocky Fox, and Roberto Malinow. 2013. "Metabotropic NMDA Receptor Function Is Required for NMDA Receptor-Dependent Long-Term Depression." *Proceedings of the National Academy of Sciences of the United States of America* 110 (10): 4027–32. https://doi.org/10.1073/pnas.1219454110.

Nakamura, Mari, Patricia Valerio, Stitipragyan Bhumika, and Tania Rinaldi Barkat. 2020.

"Sequential Organization of Critical Periods in the Mouse Auditory System." *Cell Reports* 32 (8): 108070. https://doi.org/10.1016/j.celrep.2020.108070.

Niell, Cristopher M., and Michael P. Stryker. 2008. "Highly Selective Receptive Fields in Mouse Visual Cortex." *The Journal of Neuroscience* 28 (30): 7520–36. https://doi.org/10.1523/JNEUROSCI.0623-08.2008.

Noorden, G K von. 1973. "Histological Studies of the Visual System in Monkeys with Experimental Amblyopia." *Investigative Ophthalmology* 12 (10): 727–38. http://www.ncbi.nlm.nih.gov/pubmed/4206140.

O'Brien, Richard J., Xu Desheng, Ronald S. Petralia, Oswald Steward, Richard L. Huganir, and Paul Worley. 1999. "Synaptic Clustering of AMPA Receptors by the Extracellular Immediate- Early Gene Product Narp." *Neuron* 23 (2): 309–23. https://doi.org/10.1016/S0896-6273(00)80782-5.

Packer, A. M., and R. Yuste. 2011. "Dense, Unspecific Connectivity of Neocortical Parvalbumin-Positive Interneurons: A Canonical Microcircuit for Inhibition?" *Journal of Neuroscience* 31 (37): 13260–71. https://doi.org/10.1523/JNEUROSCI.3131-11.2011.

Packwood, E a, O a Cruz, P J Rychwalski, and R V Keech. 1999. "The Psychosocial Effects of Amblyopia Study." *Journal of AAPOS : The Official Publication of the American Association for Pediatric Ophthalmology and Strabismus / American Association for Pediatric Ophthalmology and Strabismus* 3: 15–17. https://doi.org/10.1016/S1091-8531(99)70089-3.

Pandey, Anurag, Neil Hardingham, and Kevin Fox. 2022. "Differentiation of Hebbian

and Homeostatic Plasticity Mechanisms within Layer 5 Visual Cortex Neurons." *Cell Reports* 39 (9): 110892. https://doi.org/10.1016/j.celrep.2022.110892.

Pandya, Chirayu D., and Anilkumar Pillai. 2014. "TrkB Interacts with ErbB4 and Regulates NRG1-Induced NR2B Phosphorylation in Cortical Neurons before Synaptogenesis." *Cell Communication and Signaling* 12 (1): 1–11. https://doi.org/10.1186/s12964-014-0047-9.

Park, Pojeong, Heather Kang, Thomas M. Sanderson, Zuner A. Bortolotto, John Georgiou, Min Zhuo, Bong Kiun Kaang, and Graham L. Collingridge. 2018. "The Role of Calcium-Permeable AMPARs in Long-Term Potentiation at Principal Neurons in the Rodent Hippocampus." *Frontiers in Synaptic Neuroscience* 10 (November): 1–11. https://doi.org/10.3389/fnsyn.2018.00042.

Peirson, Stuart N., Laurence A. Brown, Carina A. Pothecary, Lindsay A. Benson, and Angus S. Fisk. 2018. "Light and the Laboratory Mouse." *Journal of Neuroscience Methods* 300: 26–36. https://doi.org/10.1016/j.jneumeth.2017.04.007.

Petrus, E., G. Rodriguez, R. Patterson, B. Connor, P. O. Kanold, and H.-K. Lee. 2015. "Vision Loss Shifts the Balance of Feedforward and Intracortical Circuits in Opposite Directions in Mouse Primary Auditory and Visual Cortices." *Journal of Neuroscience* 35 (23): 8790–8801. https://doi.org/10.1523/JNEUROSCI.4975-14.2015.

Petrus, Emily, Terence T. Anguh, Huy Pho, Angela Lee, Nicholas Gammon, and Hey-Kyoung Lee. 2011. "Developmental Switch in the Polarity of Experience-Dependent Synaptic Changes in Layer 6 of Mouse Visual Cortex." *Journal of Neurophysiology*

106 (5): 2499–2505. https://doi.org/10.1152/jn.00111.2011.

Petrus, Emily, Amal Isaiah, Adam P. Jones, David Li, Hui Wang, Hey Kyoung Lee, and Patrick O. Kanold. 2014. “Crossmodal Induction of Thalamocortical Potentiation Leads to Enhanced Information Processing in the Auditory Cortex.” *Neuron* 81 (3): 664–73. https://doi.org/10.1016/j.neuron.2013.11.023.

Petrus, Emily, G. Rodriguez, R. Patterson, B. Connor, P. O. Kanold, and H.-K. Lee. 2015. “Vision Loss Shifts the Balance of Feedforward and Intracortical Circuits in Opposite Directions in Mouse Primary Auditory and Visual Cortices.” *Journal of Neuroscience* 35 (23): 8790–8801. https://doi.org/10.1523/JNEUROSCI.4975-14.2015.

Philpot, Benjamin D, Aarti K Sekhar, Harel Z Shouval, and Mark F. Bear. 2001. “Visual Experience and Deprivation Bidirectionally Modify the Composition and Function of NMDA Receptors in Visual Cortex.” *Neuron* 29: 157–69. http://www.neuron.org/cgi/.

Poo, Cindy, and Jeffry S. Isaacson. 2007. “An Early Critical Period for Long-Term Plasticity and Structural Modification of Sensory Synapses in Olfactory Cortex.” *Journal of Neuroscience* 27 (28): 7553–58. https://doi.org/10.1523/JNEUROSCI.1786-07.2007.

Pouille, F, and M Scanziani. 2001. “Enforcement of Temporal Fidelity in Pyramidal Cells by Somatic Feed-Forward Inhibition.” *Science (New York, N.Y.)* 293 (August): 1159–63. https://doi.org/10.1126/science.1060342.

Pouille, Frederic, and Massimo Scanziani. 2001. “Enforcement of Temporal Fidelity in Pyramidal Cells by Somatic Feed-Forward Inhibition.” *Science* 293 (August): 1159–

64.

Priebe, Nicholas J., and David Ferster. 2008. “Inhibition, Spike Threshold, and Stimulus Selectivity in Primary Visual Cortex.” *Neuron* 57 (4): 482–97. https://doi.org/10.1016/j.neuron.2008.02.005.

Prinz, Astrid A., Dirk Bucher, and Eve Marder. 2004. “Similar Network Activity from Disparate Circuit Parameters.” *Nature Neuroscience* 7 (12): 1345–52. https://doi.org/10.1038/nn1352.

Prusky, Glen T., and Robert M. Douglas. 2003. “Developmental Plasticity of Mouse Visual Acuity.” *European Journal of Neuroscience* 17 (August 2002): 167–73. https://doi.org/10.1046/j.1460-9568.2003.02420.x.

Quast, Kathleen B., Rebecca K. Reh, Maddalena D. Caiati, Nancy Kopell, Michelle M. McCarthy, and Takao K. Hensch. 2023. “Rapid Synaptic and Gamma Rhythm Signature of Mouse Critical Period Plasticity.” *Proceedings of the National Academy of Sciences* 120 (2): 2017. https://doi.org/10.1073/pnas.2123182120.

Quirk, Michael C., Dara L. Sosulski, Claudia E. Feierstein, Naoshige Uchida, and Zachary F. Mainen. 2009. “A Defined Network of Fast-Spiking Interneurons in Orbitofrontal Cortex: Responses to Behavioral Contingencies and Ketamine Administration.” *Frontiers in Systems Neuroscience* 3 (NOV): 1–13. https://doi.org/10.3389/neuro.06.013.2009.

Rahi, Jugnoo S, Stuart Logan, Christine Timms, Isabelle Russell-Eggitt, and David Taylor. 2002. “Risk, Causes, and Outcomes of Visual Impairment after Loss of Vision in the Non-Amblyopic Eye: A Population-Based Study.” *The Lancet* 360

(9333): 597–602. https://doi.org/10.1016/S0140-6736(02)09782-9.

Ravi, Anagh Sinha, Menglong Zeng, Xudong Chen, Gerardo Sandoval, Javier Diaz-Alonso, Mingjie Zhang, and Roger A. Nicoll. 2022. “Long-Term Potentiation Reconstituted with an Artificial TARP/PSD-95 Complex.” *Cell Reports* 41 (2): 111483. https://doi.org/10.1016/j.celrep.2022.111483.

Rheims, Sylvain, Marat Minlebaev, Anton Ivanov, Alfonso Represa, Rustem Khazipov, Gregory L. Holmes, Yehezkel Ben-Ari, and Yuri Zilberter. 2008. “Excitatory GABA in Rodent Developing Neocortex in Vitro.” *Journal of Neurophysiology* 100 (2): 609–19. https://doi.org/10.1152/jn.90402.2008.

Ridder, W. H., and S. Nusinowitz. 2006. “The Visual Evoked Potential in the Mouse - Origins and Response Characteristics.” *Vision Research* 46 (6–7): 902–13. https://doi.org/10.1016/j.visres.2005.09.006.

Riggs, Lace M., Xiaoxian An, Edna F.R. Pereira, and Todd D. Gould. 2021. “(R,S)-Ketamine and (2R,6 R)-Hydroxynorketamine Differentially Affect Memory as a Function of Dosing Frequency.” *Translational Psychiatry* 11 (1). https://doi.org/10.1038/s41398-021-01685-0.

Rimehaug, Atle E, Alexander J Stasik, Espen Hagen, Yazan N Billeh, and H Joshua. 2022. “Uncovering Circuit Mechanisms of Current Sinks and Sources with Biophysical Simulations of Primary Visual Cortex,” 1–44. https://doi.org/https://doi.org/10.1101/2022.02.22.481540.

Rodríguez, Gabriela, Darpan Chakraborty, Katrina M. Schrode, Rinki Saha, Isabel Uribe, Amanda M. Lauer, and Hey Kyoung Lee. 2018. “Cross-Modal Reinstatement

of Thalamocortical Plasticity Accelerates Ocular Dominance Plasticity in Adult Mice.” *Cell Reports* 24 (13): 3433-3440.e4. https://doi.org/10.1016/j.celrep.2018.08.072.

Roth, Bryan L. 2016. “DREADDs for Neuroscientists.” *Neuron* 89 (4): 683–94. https://doi.org/10.1016/j.neuron.2016.01.040.

Rudy, Bernardo, Gordon Fishell, Soohyun Lee, and Jens Hjerling-Leffler. 2011. “Three Groups of Interneurons Account for Nearly 100% of Neocortical GABAergic Neurons.” *Developmental Neurobiology* 71 (1): 45–61. https://doi.org/10.1002/dneu.20853.

Rudy, Bernardo, and Chris J. McBain. 2001. “Kv3 Channels: Voltage-Gated K+ Channels Designed for High-Frequency Repetitive Firing.” *Trends in Neurosciences* 24 (9): 517–26. https://doi.org/10.1016/S0166-2236(00)01892-0.

Rumpel, Simon, Hanns Hatt, and Kurt Gottmann. 1998. “Silent Synapses in the Developing Rat Visual Cortex: Evidence for Postsynaptic Expression of Synaptic Plasticity.” *Journal of Neuroscience* 18 (21): 8863–74. https://doi.org/10.1523/jneurosci.18-21-08863.1998.

Sanchez, Alyssa N, Henry J Alitto, Daniel L Rathbun, Tucker G Fisher, and W Martin Usrey. 2023. “Stimulus Contrast Modulates Burst Activity in the Lateral Geniculate Nucleus.” *Current Research in Neurobiology* 4 (December 2022): 100096. https://doi.org/10.1016/j.crneur.2023.100096.

Sawtell, N B, Mikhail Y. Frenkel, B D Philpot, K Nakazawa, S Tonegawa, and Mark F. Bear. 2003. “NMDA Receptor-Dependent Ocular Dominance Plasticity in Adult

Visual Cortex.” *Neuron* 38 (Md): 977–85. https://doi.org/S0896627303003234 [pii].

Senzai, Yuta, Antonio Fernandez-Ruiz, and György Buzsáki. 2019. “Layer-Specific Physiological Features and Interlaminar Interactions in the Primary Visual Cortex of the Mouse.” *Neuron* 101 (3): 500-513.e5. https://doi.org/10.1016/j.neuron.2018.12.009.

Severin, Daniel, Su Z. Hong, Seung-Eon Roh, Shiyong Huang, Jiechao Zhou, Michelle C. D. Bridi, Ingie Hong, et al. 2021. “All-or-None Disconnection of Pyramidal Inputs onto Parvalbumin-Positive Interneurons Gates Ocular Dominance Plasticity.” *Proceedings of the National Academy of Sciences* 118 (37). https://doi.org/10.1073/pnas.2105388118.

Shan, Qiang, Qimeng Fang, and Yao Tian. 2022. “Evidence That GIRK Channels Mediate the DREADD-HM4Di Receptor Activation-Induced Reduction in Membrane Excitability of Striatal Medium Spiny Neurons.” *ACS Chemical Neuroscience* 13 (14): 2084–91. https://doi.org/10.1021/acschemneuro.2c00304.

Shepherd, Gordon M G, Thomas A Pologruto, and Karel Svoboda. 2003. “Circuit Analysis of Experience-Dependent Plasticity in the Developing Rat Barrel Cortex” 38 (i): 277–89.

Shepherd, Jason D, and Richard L Huganir. 2007. “The Cell Biology of Synaptic Plasticity: AMPA Receptor Trafficking.” *Annual Review of Cell and Developmental Biology* 23 (1): 613–43. https://doi.org/10.1146/annurev.cellbio.23.090506.123516.

Sia, Gek Ming, Jean Claude Béïque, Gavin Rumbaugh, Richard Cho, Paul F. Worley, and Richard L. Huganir. 2007. “Interaction of the N-Terminal Domain of the AMPA

Receptor GluR4 Subunit with the Neuronal Pentraxin NP1 Mediates GluR4 Synaptic Recruitment." *Neuron* 55 (1): 87–102. https://doi.org/10.1016/j.neuron.2007.06.020.

Sleigh, Jamie, Martyn Harvey, Logan Voss, and Bill Denny. 2014. "Ketamine - More Mechanisms of Action than Just NMDA Blockade." *Trends in Anaesthesia and Critical Care* 4 (2–3): 76–81. https://doi.org/10.1016/j.tacc.2014.03.002.

Sommeijer, Jean-Pierre, Mehran Ahmadlou, M. Hadi Saiepour, Koen Seignette, Rogier Min, J. Alexander Heimel, and Christiaan N. Levelt. 2017. "Thalamic Inhibition Regulates Critical-Period Plasticity in Visual Cortex and Thalamus." *Nature Neuroscience* 20 (12): 1. https://doi.org/10.1038/s41593-017-0002-3.

Southwell, Derek G., Robert C. Froemke, Arturo Alvarez-Buylla, Michael P. Stryker, and Sunil P. Gandhi. 2010. "Cortical Plasticity Induced by Inhibitory Neuron Transplantation." *Science* 327 (5969): 1145–48. https://doi.org/10.1126/science.1183962.

Stachniak, Tevye J., Anirvan Ghosh, and Scott M. Sternson. 2014. "Chemogenetic Synaptic Silencing of Neural Circuits Localizes a Hypothalamus→Midbrain Pathway for Feeding Behavior." *Neuron* 82 (4): 797–808. https://doi.org/10.1016/j.neuron.2014.04.008.

Stephany, C.-E., L. L. H. Chan, S. N. Parivash, H. M. Dorton, M. Piechowicz, S. Qiu, and A. W. McGee. 2014. "Plasticity of Binocularity and Visual Acuity Are Differentially Limited by Nogo Receptor." *Journal of Neuroscience* 34 (35): 11631–40. https://doi.org/10.1523/JNEUROSCI.0545-14.2014.

Stern, Edward A., Miguel Maravall, and Karel Svoboda. 2001. “Rapid Development and Plasticity of Layer 2/3 Maps in Rat Barrel Cortex in Vivo.” *Neuron* 31 (2): 305–15. https://doi.org/10.1016/S0896-6273(01)00360-9.

Stratford, K. J., K. Tarczy-Hornoch, K. A.C. Martin, N. J. Bannister, and J. J.B. Jack. 1996. “Excitatory Synaptic Inputs to Spiny Stellate Cells in Cat Visual Cortex.” *Nature* 382 (6588): 258–61. https://doi.org/10.1038/382258a0.

Sun, Yanjun, Taruna Ikrar, Melissa F Davis, Todd C Holmes, Sunil P Gandhi, Xiangmin Xu, Todd C Holmes, Sunil P Gandhi, and Xiangmin Xu. 2016. “Neuregulin-1/ErbB4 Signaling Regulates Visual Cortical Plasticity.” *Neuron* 92: 1–14. https://doi.org/http://dx.doi.org/10.1016/j.neuron.2016.08.033.

Tamamaki, Nobuaki, Yuchio Yanagawa, Ryohei Tomioka, Jun Ichi Miyazaki, Kunihiko Obata, and Takeshi Kaneko. 2003. “Green Fluorescent Protein Expression and Colocalization with Calretinin, Parvalbumin, and Somatostatin in the GAD67-GFP Knock-In Mouse.” *Journal of Comparative Neurology* 467 (1): 60–79. https://doi.org/10.1002/cne.10905.

Tamás, G, E H Buhl, a Lörincz, and P Somogyi. 2000. “Proximally Targeted GABAergic Synapses and Gap Junctions Synchronize Cortical Interneurons.” *Nature Neuroscience* 3 (4): 366–71. https://doi.org/10.1038/73936.

Taniguchi, Hiroki. 2014. “Genetic Dissection of GABAergic Neural Circuits in Mouse Neocortex.” *Frontiers in Cellular Neuroscience* 8 (January): 8. https://doi.org/10.3389/fncel.2014.00008.

Vetencourt, José Fernando Maya, Alessandro Sale, Alessandro Viegi, Laura Baroncelli,

Roberto De Pasquale, Olivia F. O'Leary, Eero Castrén, and Lamberto Maffei. 2008. "The Antidepressant Fluoxetine Restores Plasticity in the Adult Visual Cortex." *Science* 320 (5874): 385–88. https://doi.org/10.1126/science.1150516.

Walz, Wolfgang. 2013. *Stimulation and Inhibition of Neurons*. Edited by Paul M. Pilowsky, Melissa M.J. Farnham, and Angelina Y. Fong. Vol. 78. Neuromethods. Totowa, NJ: Humana Press. https://doi.org/10.1007/978-1-62703-233-9.

Wang, Bor-Shuen, Rashmi Sarnaik, and Jianhua Cang. 2010. "Critical Period Plasticity Matches Binocular Orientation Preference in the Visual Cortex." *Neuron* 65 (2): 246–56. https://doi.org/10.1016/j.neuron.2010.01.002.

Wang, Lang, Michelle Kloc, Yan Gu, Shaoyu Ge, and Arianna Maffei. 2013. "Layer-Specific Experience-Dependent Rewiring of Thalamocortical Circuits." *Journal of Neuroscience* 33 (9): 4181–91. https://doi.org/10.1523/JNEUROSCI.4423-12.2013.

Wang, Lang, and Arianna Maffei. 2014. "Inhibitory Plasticity Dictates the Sign of Plasticity at Excitatory Synapses." *Journal of Neuroscience* 34 (4): 1083–93. https://doi.org/10.1523/JNEUROSCI.4711-13.2014.

Wettschureck, Nina, and Stefan Offermanns. 2005. "Mammalian G Proteins and Their Cell Type Specific Functions." *Physiological Reviews* 85 (4): 1159–1204. https://doi.org/10.1152/physrev.00003.2005.

Williams, Graham V., Srinivas G. Rao, and Patricia S. Goldman-Rakic. 2002. "The Physiological Role of 5-HT2A Receptors in Working Memory." *Journal of Neuroscience* 22 (7): 2843–54. https://doi.org/10.1523/jneurosci.22-07-02843.2002.

Williams, Joanna M., Diane Guévremont, Sara E. Mason-Parker, Carthika Luxmanan, Warren P. Tate, and Wickliffe C. Abraham. 2007. “Differential Trafficking of AMPA and NMDA Receptors during Long-Term Potentiation in Awake Adult Animals.” *Journal of Neuroscience* 27 (51): 14171–78. https://doi.org/10.1523/JNEUROSCI.2348-07.2007.

Wilson, Daniel E, David E Whitney, Benjamin Scholl, and David Fitzpatrick. 2016. “Orientation Selectivity and the Functional Clustering of Synaptic Inputs in Primary Visual Cortex.” *Nature Neuroscience*, no. June: 1–10. https://doi.org/10.1038/nn.4323.

Wu, Connie, and Dandan Sun. 2015. “GABA Receptors in Brain Development, Function, and Injury.” *Metabolic Brain Disease* 30 (2): 367–79. https://doi.org/10.1007/s11011-014-9560-1.

Xu, Yan, Meng Lin Wang, Hui Tao, Chi Geng, Feng Guo, Bin Hu, Ran Wang, and Xiao Yu Hou. 2022. “ErbB4 in Parvalbumin-Positive Interneurons Mediates Proactive Interference in Olfactory Associative Reversal Learning.” *Neuropsychopharmacology* 47 (7): 1292–1303. https://doi.org/10.1038/s41386-021-01205-0.

Yamasaki, Miwako, Rieko Okada, Chihiro Takasaki, Shima Toki, Masahiro Fukaya, Rie Natsume, Kenji Sakimura, Masayoshi Mishina, Tetsuo Shirakawa, and Masahiko Watanabe. 2014. “Opposing Role of NMDA Receptor GluN2B and GluN2D in Somatosensory Development and Maturation.” *Journal of Neuroscience* 34 (35): 11534–48. https://doi.org/10.1523/JNEUROSCI.1811-14.2014.

Zeeman, Michael, Xiuping Liu, Oliver Zhang, and Jun Yan. 2021. “Role of N-Methyl-D-Aspartate Receptor Subunits GluN2A and GluN2B in Auditory Thalamocortical Long-Term Potentiation in Adult Mice.” *Neuroscience Letters* 761 (February): 136091. https://doi.org/10.1016/j.neulet.2021.136091.

Zhan, X. J., C. L. Cox, J. Rinzel, and S. Murray Sherman. 1999. “Current Clamp and Modeling Studies of Low-Threshold Calcium Spikes in Cells of the Cat’s Lateral Geniculate Nucleus.” *Journal of Neurophysiology* 81 (5): 2360–73. https://doi.org/10.1152/jn.1999.81.5.2360.

Zhang, De Xing, and William B. Levy. 1992. “Ketamine Blocks the Induction of LTP at the Lateral Entorhinal Cortex-Dentate Gyrus Synapses.” *Brain Research* 593 (1): 124–27. https://doi.org/10.1016/0006-8993(92)91273-H.

Zhang, L I, S Bao, and M M Merzenich. 2001. “Persistent and Specific Influences of Early Acoustic Environments on Primary Auditory Cortex.” *Nature Neuroscience* 4 (11): 1123–30. https://doi.org/10.1038/nn745.

Zhou, Xiaoming, Rogerio Panizzutti, Étienne de Villers-Sidani, Caroline Madeira, and Michael M. Merzenich. 2011. “Natural Restoration of Critical Period Plasticity in the Juvenile and Adult Primary Auditory Cortex.” *Journal of Neuroscience* 31 (15): 5625–34. https://doi.org/10.1523/JNEUROSCI.6470-10.2011.